PLANAR ARRAY ANTENNA DESIGN ANALYSIS VOLUME I

THESIS

Bradley P. Chrisman
Captain, USAF

AFIT/GE/ENG/89D-4

DEPARTMENT OF THE AIR FORCE
AIR UNIVERSITY
AIR FORCE INSTITUTE OF TECHNOLOGY

Wright-Patterson Air Force Base, Ohio

AFIT/GE/ENG/89D-4

PLANAR ARRAY ANTENNA
DESIGN ANALYSIS
VOLUME I

THESIS

Presented to the Faculty of the School of Engineering

of the Air Force Institute of Technology

Air University

In Partial Fulfillment of the

Requirements for the Degree of

Master of Science in Electrical Engineering

Bradley P. Chrisman, B.S.

Captain, USAF

December 1989

most important, I thank my wife Brenda and my daughter Andrea for their patience, understanding, and perseverance during those many hours I spent away studying or working on my thesis. Their encouragement is greatly appreciated, especially toward the end of the program where it counted the most.

Bradley P. Chrisman

Table of Contents

Volume II

List of Figures

List of Tables

Abstract

The purpose of this study was to develop a computer program that can assess the impact of small design perturbations on the performance of a planar array antenna of dipoles. The antenna designer can compare an array's theoretical performance standards with those of the perturbed array.

In the course of this study, an expression for the expected or average radiation pattern for the perturbed planar array was developed and used in the program. Translational errors in the positions of the elements, errors in the element's drive amplitude and phase, non-identical element patterns, and missing elements were accounted for in the expected radiation pattern.

The designer specifies the array design parameters and the tolerance data, then the program calculates the radiation pattern data, half-power beamwidths, and directivities for specified scan angles and frequency bandwidth for the design and expected arrays. The radiation pattern data can be plotted allowing side lobe comparison between the expected and design arrays.

The study confirmed five trends noted in earlier studies: (1) The rise in side lobe level due to random errors, for a given set of tolerances and number of elements, increased as the side lobe level was further suppressed. (2) For a given set of tolerances, pattern deterioration was

found to decrease as the array was enlarged. (3) For a given set of tolerances, pattern deterioration was less for a planar array of size L^2 than it was for a linear array of length L. (4) The side lobe level increase due to random errors did not depend on the scan angle. (5) Although not shown conclusively, but, in a qualitative sense, translational errors were found to cause the dominant effect with high element reliability.

The antenna designer can use the program to assess the effects of certain tolerances in designing the array. The designer can use the program as a tool for establishing a bound on the tolerances to achieve a certain side lobe level. Or, given the tolerances, the designer can adjust the size of the array until the desired side lobe level is achieved.

Preface

The purpose of this study was to develop a computer program that can assess the impact of small design perturbations on the performance of a planar array antenna. The antenna designer can compare theoretical design calculations for an array with those of the perturbed array.

Considerable work was spent validating each routine to ensure theoretical and expected results agreed with known examples found in the literature. The program calculates radiation pattern data, half-power beamwidths, and directivities for specified scan angles and frequency bandwidth for both the design array and expected array. The radiation pattern data can be plotted to allow a side lobe comparison between the design and expected arrays. This work should be continued, as additional routines could further enhance the effectiveness of this program.

In developing the theory and writing the program and thesis, I had a great deal of assistance from several individuals. I gratefully thank my faculty advisor Major H. H. Barksdale for his patience and invaluable suggestions that ultimately lead to the conclusion of this project. I also thank my committee members, Capt. G. T. Warhola and Dr. V. P. Pyati for their contributions to this effort. I am also indebted to the AFIT librarians for their professional assistance in locating several key documents that enabled me to undertake this project. Finally, and without a doubt,

PLANAR ARRAY ANTENNA DESIGN ANALYSIS

Volume I

I. Introduction

Background

One of the fundamental principles of array antenna theory is that the radiation pattern is determined by the amplitude and phase of the excitation currents over the array, interelement spacing, frequency of operation, and the choice of radiating elements. The antenna designer can, theoretically, specify the form of the currents across the array, the interelement spacings, and elements and expect the resulting radiation pattern to be as predicted. In practice, however, there will be unavoidable errors in the amplitude and phase of currents, the interelement spacing, and the individual element's radiation pattern so that the actual radiation pattern will differ from the theoretical. The agreement between the two depends on how well the desired distribution of the currents across the array, the interelement spacing, and the element's radiation pattern can be achieved.

Errors in an array antenna can be divided into two categories depending on whether they are predictable (systematic) or random (21:364; 22:227; 25:13). Chief among predictable errors is a phenomena known as mutual coupling. The signal emitted from any one element will induce a sympa-

thetic excitation in every other element, thus, altering the array's radiation pattern (25:13). Another example is the finite quantization of the phase produced by a digital phase shifter (22:227). The effects of such errors are predictable and the resulting radiation pattern can be computed by classical methods from a knowledge of the array design.

Random errors are caused by the accidental deviation of the array antenna parameters from their design value. An array antenna radiation pattern might differ from the desired pattern because of, (1) errors in the amplitude of the currents at each element, (2) errors in the phase of the current, (3) missing elements (due to catastrophic failure), (4) rotation of the radiating elements, (5) translational errors in the element location, and (6) errors in the radiation pattern of each element (22:228). Although they are small, they are ever-present and can limit the minimum side lobe level that can be achieved just as random noise limits the sensitivity of a radio receiver. In most radar systems, low side lobe levels are very important in minimizing the false target indications and jamming through the side lobes (4:21). Random errors can also cause a reduction in power gain, an error in the direction of the main beam, lower directivity, and deviations in other performance standards.

If errors in an existing antenna can be measured, the pattern can be calculated in the classical manner. However, one cannot predict the exact nature of random errors that

might be encountered in some particular antenna from a knowledge of its design. The actual existence of an antenna is required. It is possible, however, to predict in statistical terms the pattern behavior of a collection of antennas. The average value of the pattern and the standard deviation about the average are used to describe the antenna performance. The statistical description of random errors cannot be applied to any particular antenna but applies to the collection of similar antennas whose errors are described by the same statistical parameters (22:228).

In view of the preceding, the TAC/INTEL Division, Special Projects Systems Program Office, Deputy for Reconnaissance and Electronic Warfare Systems, Aeronautical Systems Division (ASD/RWZI) is currently sponsoring work in developing a computer program to predict an array's performance based on its design and a set of design tolerances.

Problem

The basic problem facing ASD/RWZI is evaluating the impact of systematic and random errors on the performance standards of a given planar array antenna design. This study will investigate the effects of random fluctuations on the performance characteristics of a planar array of dipole antennas and develop a FORTRAN computer program to predict the array's performance based on these random errors. The effects of random errors on an array's radiation pattern is well documented in the literature, however, a specific

program incorporating the effects of random errors on a particular array suitable for use in a system program office has not been developed. Therefore, this study should have direct application in a system program office to predict the effects of random errors on an array's performance.

Scope

This project will consider the effects of random fluctuations on the performance standards of planar arrays of dipole antennas. Predictable or systematic errors will not be considered. Rectangular arrays will be considered along with the more common forms of amplitude distributions across the array, i.e., uniform, binomial, Dolph-Chebyshev, and Taylor $\bar{n}$-parameter element weights. The array's performance standards include side lobe level, power gain, directivity, half-power beamwidth, bandwidth, and pointing angles.

Assumptions/Limitations

In order to make the problem of determining the effects of random errors on planar array performance tractable, several assumptions must be made.

1. The planar array will lie in the x-y plane.

2. All elements in a particular planar array will be the same.

3. The excitation coefficients and the positions of the elements actually have some random scatter about their

mean or expected values. These expected values may be regarded as averages, taken over a large number of different arrays, or they may be thought of as long-term time averages for a single array whose parameters very with time in a random fashion (11:119; 14:640-644; 21:365; 22:229).

4. Root-mean-square errors in element position are all small, compared to the wavelength, independent random variables which are normally distributed (Gaussian distribution) with zero means and respective variances $\overline{\gamma^2_{x,y,z}}$ (1:268;3:235-236; 11:116; 16:268; 20:175).

5. The mean-square phase and amplitude errors in the drive current at any element and the mean-square error in the element patterns are all taken to be independent of the errors in any other element, small, and normally distributed. The mean-square phase errors are small compared to pi (π) and the mean-square amplitude and element pattern errors are small compared to unity (1:267;16:269;22:229).

6. Antenna efficiency remains the same between the design antenna and the antenna with small perturbations, so that, from the relations:

$$G_{des} = eD_{des} \tag{1.1}$$

and

$$G_{ave} = eD_{ave} \tag{1.2}$$

we can use:

$$G_{ave}/G_{des} = D_{ave}/D_{des} \tag{1.3}$$

to determine the change in power gain once D_{ave} and D_{des} are calculated. G_{des} and D_{des} are the design power gain and directivity, respectively, and G_{ave} and D_{ave} are the power gain and directivity, respectively, determined from the expected or average radiation pattern due to errors in the design of the array.

Review of the Literature

Many authors have studied the effects of random errors on the radiation pattern of array antennas and developed expressions relating these errors to different performance characteristics of the antenna. The first comprehensive study was conducted by Ruze (21:364-380), who considered an equispaced linear array containing random errors in the exciting currents, and deduced the influence they would have on directivity and side lobe level. He used the restrictions that the magnitudes of all error currents be the same and that all phases of an error current be equally probable. He concluded that for a given current precision, low side lobes are more readily obtained with large antennas. Ashmead (2:81-92) extended Ruze's work by assuming that each error current was the same fraction of the corresponding unperturbed current, all phases still being equally probable. He presented a method for finding the mean side lobe suppression which may be obtained for any Chebyshev distribution. He showed that an over-design can actually result in loss of suppression of the side lobes as well as loss in

gain. Bailin and Ehrlich (3:235-241) took the problem one step further by considering the physical errors, namely inaccuracies in manufacturing, which cause random errors in the exciting currents. Applying statistical methods to the standard expression for the far field of a linear array, they were able to calculate the probability that a side lobe level will exceed a certain comparison value taken to be the mean plus the standard deviation of the magnitude of the field. Their results indicate there are two courses of action available to the designer in achieving the desired side lobe suppression. The first is to require very small tolerances in manufacture, however, this would be cost prohibitive, especially in making large arrays. The second course is to over-design the array by designing for an N-db side lobe level if an M-db level is required where N > M. The amount of over-design can be governed by the results presented in their paper, however, if the length of the array is fixed, the over-design will result in reduced aperture efficiency. Their work was furthered by O'Neill and Bailin (18:93-102) in a paper which establishes a set of standards based on the theory and the results of many calculations.

Gilbert and Morgan (14:637-663) studied the optimum design of discrete, directive antenna arrays of arbitrary geometrical configuration in space. They allowed the excitations and spatial positions of the elements comprising the

array to vary in a random fashion about their nominal values. They concluded that under certain conditions the expected power pattern of an array turns out to be the power pattern of the nominal array, plus a background power level which has the same dependence in direction as the pattern of a single element.

Cheng (7:145-147) analyzed small phase errors and derived several expressions relating phase errors to the maximum possible loss in antenna gain and half 3-db beamwidth when the peak value of the phase deviation is known. His expressions are derived for both rectangular and circular apertures.

Elliott (11:114-120) extended the problem to consider the effect of random constructional errors on the pattern of a two dimensional dipole antenna array. He showed that the most serious tolerance appears to lie in the translational positions of the dipoles and their angular (rotational) positions are relatively unimportant. Of secondary importance are the errors in the radiating currents. He derived an expression which relates side lobe level to these errors with representative calculations displayed in his examples. Several noteworthy results were obtained from his analysis: (1) the rise in side lobe level due to random errors is independent of scan angle, (2) the rise in side lobe level is less the larger the antenna, for a given tolerance and a given side lobe level, and (3) the rise in side lobe level

is more the lower the design side lobe level, for a given antenna size and a given tolerance.

Rondinelli (20:174-189) advanced the study for planar arrays by deducing the effects of random errors on beam pointing accuracy and on the average rise in side lobe level within a specified cone around the main beam. The complexity of the beam pointing problem is such that only a restricted solution was obtained. However, this complexity is greatly relieved when one's attention is confined to linear arrays, and Leichter (16:268-275) provided a solution for this case.

Allen (1:259-319) was concerned with several extensions of the theory of random error effects and a critical "second look" at some earlier results. First, Allen examined the potential sources of errors including the previously neglected effects of non-identical element factors and the possibility of catastrophic failures. He shows that all error effects can be characterized by these parameters: (a) The expected fraction of operating elements, (b) the total amplitude variance, and (c) the characteristic function of the element phase errors. Simple relationships are pointed out between the last two parameters and the corresponding statistics of the various errors possible in each element, under the assumption of independence of the various contributing sources.

Allen's derivation of the probability density function of the far-field followed, in which some of the restrictive assumptions of previous derivations are omitted. The derivation given is valid for any assumed distributions of the various error sources, with only the restrictions that the errors are essentially independent from element to element, and that the corresponding errors in different elements are samples of the same random variable. He shows that the pattern statistics may be markedly different in the principle lobe regions and in the side lobe regions and that two distinct probability density functions are generally necessary to satisfactorily describe the field everywhere.

Allen concludes with a brief review of the effects of random errors on side lobe levels, with emphasis on the error effects in regions where errors predominate the design pattern. Also, the expected reduction in the array's directivity due to small errors is derived.

Skolnik (22:227-233) discussed the effect of random errors on a planar array of isotropic elements. He included errors in the amplitude of the currents at each element, errors in the phase of the current, and the effect of missing elements (due to catastrophic failure). He derived an average power pattern that is the superposition of two terms. One term is the no-error power pattern multiplied by the square of the fraction of elements remaining and multiplied by a factor proportional to the phase error. The

second term depends on both the amplitude and the phase errors as well as on the fraction of elements remaining. He gives an expression for the reduction in gain based on the average power pattern.

Major Definitions

The array's performance standards are well documented in the current literature (4,23). The purpose of this section is to review the definitions that will be used to calculate an array's performance standards with and without random errors considered.

Side Lobe Level (SLL) is a measure of how well the power is concentrated into the main lobe; it is the ratio of the power pattern value of the side lobe peak to the pattern value of the main lobe (23:29-30):

$$SLL_{dB} = 20 \log|F(SLL)/F(MAX)| \qquad (1.4)$$

where $AF(\theta,\phi)$ is the normalized field pattern, $|F(MAX)|$ is the maximum value of the pattern magnitude at the angles θ,ϕ where the maximum occurs; and $|F(SLL)|$ is the pattern value of the maximum of the highest side lobe magnitude at its corresponding angles θ,ϕ. For a normalized field pattern $|F(MAX)| = 1$.

Directive Gain is a measure of how well an antenna radiates its power in a given direction and is defined as the ratio of the radiation intensity $H(\theta,\phi)$ in a certain direction to the average radiation intensity H_{ave} (23:34):

$$D(\theta,\phi) = H(\theta,\phi)/H_{ave} \tag{1.5}$$

where H_{ave} is defined as:

$$H_{ave} = \iint_{\Omega} H(\theta,\phi)\, d\Omega \tag{1.6}$$

and

$$d\Omega = \sin\theta\, d\theta\, d\phi \tag{1.7}$$

Equation (1.5) can be manipulated to yield an expression in terms of the normalized field pattern $F(\theta,\phi)$ (23:35):

$$D(\theta,\phi) = 4\pi |F(\theta,\phi)|^2/\Omega_A \tag{1.8}$$

where Ω_A is the antenna beam solid angle defined by:

$$\Omega_A = \iint_{\Omega} |F(\theta,\phi)|^2\, d\Omega \tag{1.9}$$

Directivity (D_0) is defined as the maximum value of directive gain or (23:36):

$$D_0 = 4\pi/\Omega_A \tag{1.10}$$

Power gain $G(\theta,\phi)$ of antenna in a given direction is defined as (4:43); "4π times the ratio of the radiation intensity in that direction to the net power accepted by the antenna from a connected transmitter." In general:

$$G(\theta,\phi) = 4\pi\ H(\theta,\phi)/P_{in} \tag{1.11}$$

where

$$H(\theta,\phi) = \text{radiation intensity} = |F(\theta,\phi)|^2 \tag{1.12}$$

and

$$P_{in} = \text{total input power} \tag{1.13}$$

However, for the purposes of this study, we will calculate the change in power gain based on Assumption number six and equation (1.3).

The half-power beamwidth (HPBW) is the angular separation of the points in the Θ_h and Ψ_h directions where the magnitude of the main beam of the power pattern equals one-half as illustrated in Figure 1. Hence, we have:

$$\Theta_h = |\theta_{HPleft} - \theta_{HPright}| \tag{1.14}$$

and

$$\Psi_h = |\Psi_{HPleft} - \Psi_{HPright}| \tag{1.15}$$

where θ_{HPleft} and $\theta_{HPright}$ are the points to the "left" and "right" of the main beam where:

$$|F(\theta,\phi)|^2 = \tfrac{1}{2} \tag{1.16}$$

Similarly for Ψ_{HPleft} and $\Psi_{HPright}$.

The bandwidth of an antenna is defined as (4:47) "the range of frequencies within which the performance of the antenna, with respect to some characteristic conforms to a specified standard." The bandwidth is calculated using:

$$\frac{\text{(upper frequency - lower frequency) x 100}}{\text{center frequency}} \tag{1.17}$$

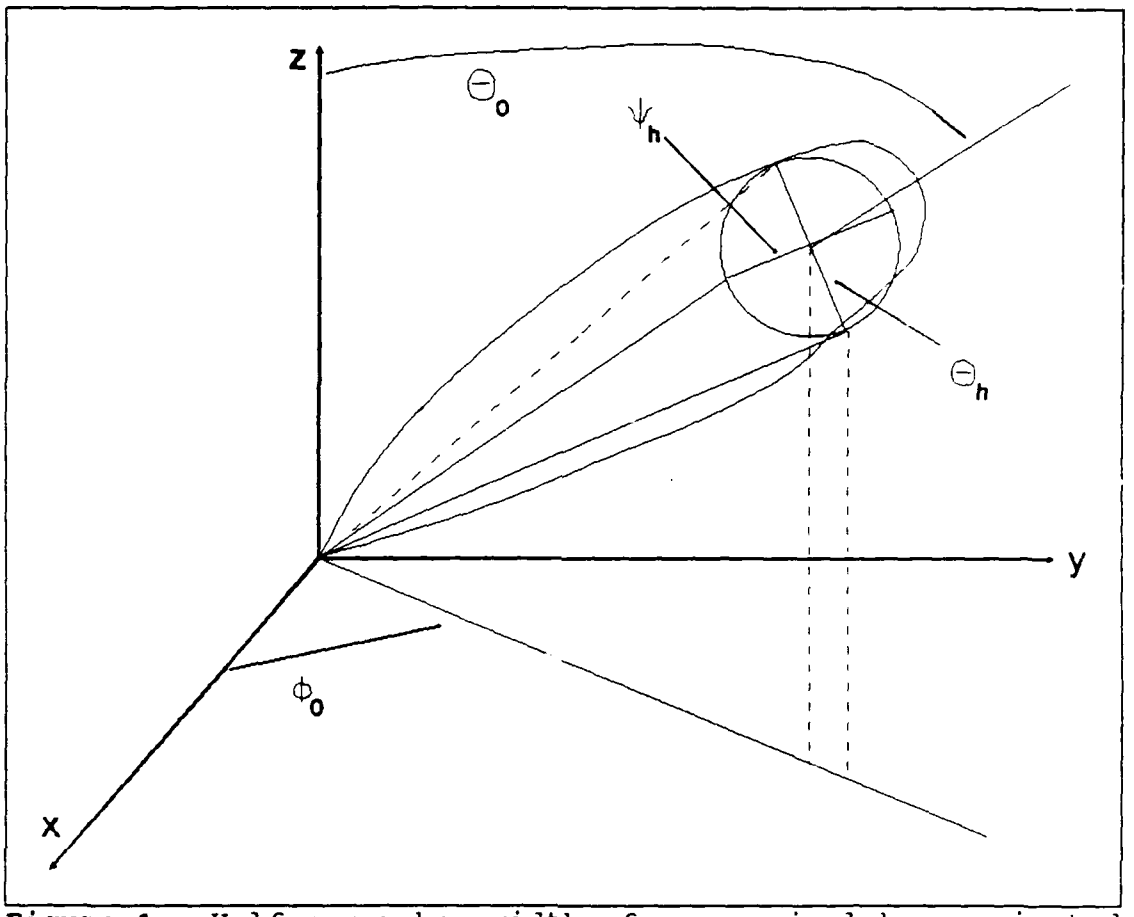

Figure 1. Half-power beamwidths for a conical beam oriented toward $\theta = \theta_0$, $\phi = \phi_0$.

Pointing angles are defined as the direction of maximum radiation. Much like bandwidth, as the pointing angles are varied from the design pointing angles, beamwidth, directivity, and other performance standards will change.

Approach

The main objective of this thesis is to apply the results from earlier studies on the effects of random errors on an array's radiation pattern and write a FORTRAN program incorporating these results to determine an array's perfor-

mance with errors. However, no one author has incorporated the effects of all random errors, identified in the Background section, into one expression.

Three expressions relating various random errors to an array's radiation pattern emerged from the literature review. Elliott (11:116) derived an expression for the average radiation pattern based on translational and rotational errors in the positions of dipoles and random errors in the exciting current of the dipoles. An expression derived by Skolnik (22:231), took into account errors in the amplitude and phase of the drive current at each isotropic element and missing elements (due to catastrophic failure). Finally, Allen (1:288) derived an expression for the average radiation pattern by considering non-identical element factors, translational errors in the positions of the elements, errors in the amplitude and phase of the drive currents of each element, and missing elements. Allen's expression was derived for a linear array, but can be extended to the planar array case quite easily. Allen's expression is the most comprehensive in terms of including all of the various random errors, except rotational errors which Elliott concluded are relatively unimportant. The expression for the average radiation pattern derived in this paper will include all the errors considered by Allen and will follow Skolnik's methodology in deriving the expression for a planar array.

Once the average array pattern is computed for a certain pointing angle and element excitations, it is a straightforward process to determine the random error effects on the array's various performance standards using equations (1.3) through (1.17).

The FORTRAN program will be written to allow the user to specify certain tolerances, excitation schemes, dimensions of the array, phase tapers, operating wavelength or frequency, and the bandwidth of operation. The user will input the antenna's tolerances found in the antenna's design specification or provided by the antenna design manufacturer. The program will then compute the array's design and expected performance standards using the various equations defined earlier.

The program will be tested against several of the authors' (1,2,3,7,11,18,20) findings in the literature. First, though, a rigorous evaluation of excitation coefficient routines will be conducted to ensure the program produces the proper amplitudes for the elements. This is easily done by plotting the data generated by the program and verifying that the pattern produced from the data matches what was called for in terms of side lobe level or expected pattern. Then, to ensure the program performs properly, the tolerances used by these authors in their tests will be used in this program to re-affirm their results and qualitative assessments.

Chapter II develops the theoretical radiation pattern for a planar array antenna of dipoles beginning with Maxwell's equations. In Chapter III, we will derive a statistical radiation pattern based on small, independent perturbations in the design, allowing us to calculate the deviations in performance standards. Chapter IV outlines the operation of the FORTRAN program and its use. Chapter V evaluates the program with various random errors against known results, both, quantitatively and qualitatively. Finally, Chapter VI provides the conclusions from this study and recommendations for future endeavors in planar array design analysis.

II. Array Antenna Fundamentals

In this chapter, we will investigate the properties of radiators which are grouped together to create an array. The factors which will be found to have a major influence on array performance are the spatial distribution and orientation of the individual radiators and their relative excitations in amplitude and phase. The goal of the ensuing analysis is to show the dependence of the radiation pattern on the aforementioned factors.

The analysis begins with a time harmonic statement of Maxwell's equations. The vector potential function and equations governing it are introduced; its solution given in terms of the source distribution. The power density of the radiated field is expressed in terms of the vector potential function, and is, thus, connected to the sources. The resulting integral can be used as the basis of synthesis or analysis.

Applying this integral to a system of discrete, identical radiators, the pattern is shown to be the product of two expressions: the element factor and array factor. The concept of a linear array is examined with consideration given to pattern shape and scanning the main beam.

The following analysis includes a section on pattern synthesis. The two kinds of pattern synthesis considered are the Dolph-Chebyshev and discretized Taylor $\bar{n}$-parameter methods. The specific theory behind these synthesis methods

is not presented, instead, the expressions used in the program to calculate the weights are presented. The theory behind these two methods is well documented in the literature (4,9,10,12,23,24) and need not be repeated in this paper.

The chapter concludes with the development of the radiation pattern when the elements are assumed to be spaced in a two dimensional matrix in a plane, which leads to planar array theory. Again pattern shape is discussed as well as the ability to scan the array in two angular coordinates.

Preliminaries

In order to begin our derivation of the planar array radiation pattern, we will need the time-harmonic Maxwell equations for linear, homogenous, isotropic mediums:

$$\nabla \times \mathbf{E} = -j\omega\mu\mathbf{H} \tag{2.1}$$

$$\nabla \times \mathbf{H} = j\omega\epsilon\mathbf{E} + \mathbf{J} \tag{2.2}$$

$$\nabla \cdot \mathbf{E} = \rho/\epsilon \tag{2.3}$$

$$\nabla \cdot \mathbf{H} = 0 \tag{2.4}$$

and the continuity equation:

$$\nabla \cdot \mathbf{J} = -j\omega\rho \tag{2.5}$$

where $\mathbf{J}$ is the source current density and ρ is the source charge density and $j = \sqrt{-1}$. The quantities $\mathbf{J}$ and ρ are constrained to the surface for perfect conductors since the internal electric fields are zero. Therefore, the field quantities $\mathbf{J}$ and ρ are actually written as $\mathbf{J}_s$ and ρ_s indica-

ting they are surface quantities. The permittivity and permeability are ϵ and μ, respectively. All fields (**E**, **H**, **J**, and ρ) are both spatial (x,y,z) and temporal (t) functions. The time dependence, $e^{j\omega t}$, is assumed for all fields and is suppressed throughout this paper.

Since the electric (**E**) and magnetic (**H**) fields are coupled in Maxwell's equations, we must solve the equations simultaneously to determine **E** and **H** from a given current distribution **J**. We can solve Maxwell's equations by introducing a vector potential **A** and a scalar potential Φ. These two potential functions serve to decouple Maxwell's equations, so that we can obtain the electric and magnetic fields solely as functions of the vector potential. We can find the electric field from (23:10):

$$\mathbf{E} = -j\omega\mu\mathbf{A} + \nabla(\nabla \cdot \mathbf{A})/j\omega\epsilon \tag{2.6}$$

or (13:3):

$$\mathbf{E} = (j\omega\epsilon)^{-1}(\nabla \times \nabla \times \mathbf{A}) \tag{2.7}$$

and the magnetic field from:

$$\mathbf{H} = \nabla \times \mathbf{A} \tag{2.8}$$

We find the vector potential **A** by solving the Helmholtz equation:

$$\nabla^2\mathbf{A} + \omega^2\mu\epsilon\mathbf{A} = -\mathbf{J} \tag{2.9}$$

The total solution to the Helmholtz equation (2.9) is (23:13):

$$\mathbf{A}(x,y,z) = \iiint_{V'}\left[\mathbf{J}(x',y',z')e^{-jkR}/4\pi R\right]dV' \tag{2.10}$$

The geometry is shown in Figure 2. The coordinate system shown is used to describe both the source point and the field point. The vector **r**(x,y,z) is the vector from the coordinate origin to the field point P. The vector **r'**(x',y',z') is the vector from the coordinate origin to the source point where the complex vector current density **J** is flowing as shown in Figure 2. In equation (2.10), $k = \omega(\mu_0\epsilon_0)^{1/2} = \omega/c = 2\pi/\lambda$ is the wave number, or free space propagation constant, $c = (\mu_0\epsilon_0)^{-1/2} = f\lambda$ is the velocity of light, λ is the wavelength, and f is the frequency. The distance from the source point to the field point is $R = |\mathbf{r} - \mathbf{r'}|$, and the volume (V') is chosen large enough to encompass all antenna sources, in our case the array.

Radiation Pattern

A radiation pattern is a graphical representation of the far field radiation properties of an antenna (23:17). Referring to Figure 2, R is given by:

$$R = \left[(x-x')^2 + (y-y')^2 + (z-z')^2\right]^{1/2} \qquad (2.11)$$

Converting the rectangular cartesian coordinates to spherical coordinates using, $x = r\sin\theta\cos\phi$, $y = r\sin\theta\sin\phi$, and $z = r\cos\theta$, we have:

$$R = \left[(r\sin\theta\cos\phi - x')^2 + (r\sin\theta\sin\phi - y')^2 + (r\cos\theta - z')^2\right]^{1/2} \qquad (2.12)$$

In order to simplify the expression for R, we can make use

of the binomial theorem and note, that if

$r >> r' = (x'^2 + y'^2 + z'^2)^{1/2}$, then we can write:

$$R \approx r - x'\sin\theta\cos\phi - y'\sin\theta\sin\phi - z'\cos\theta \qquad (2.13)$$

where we are disregarding any terms of higher order than r^{-1} for large r in the binomial expansion (13:4). In the denominator of (2.10) we let:

$$R \approx r \qquad (2.14)$$

However, in the phase term we must be more accurate and will

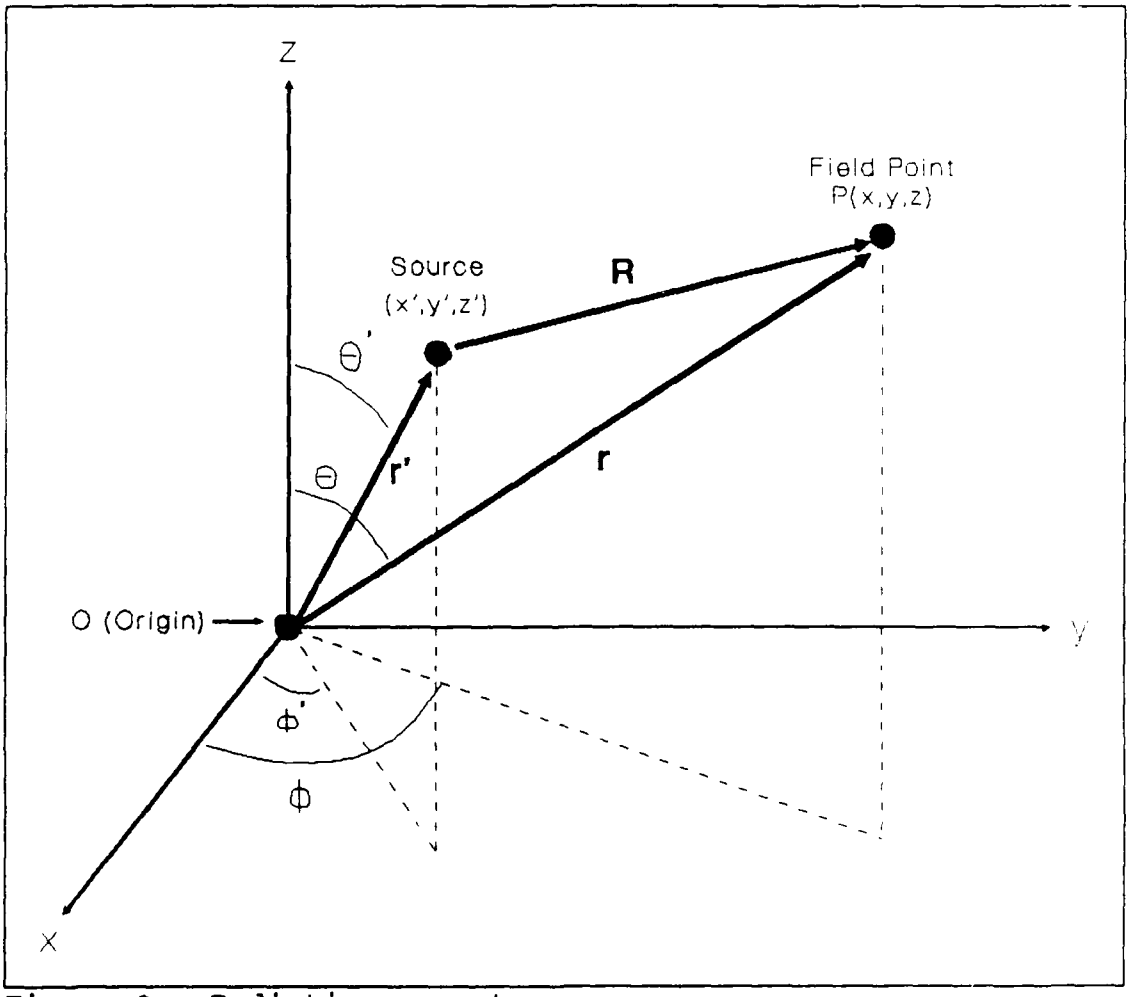

Figure 2. Radiation geometry

use (2.13). Now (2.10) becomes:

$$\mathbf{A}(x,y,z) = (e^{-jkr}/4\pi r) \iiint_{V'} \mathbf{J}(x',y',z')e^{j\Gamma}dx'dy'dz' \quad (2.15)$$

where

$$\Gamma = k(x'\sin\theta\cos\phi + y'\sin\theta\cos\phi + z'\cos\theta) \quad (2.16)$$

Simplifying equation (2.15) we have:

$$\mathbf{A}(x,y,z) = (e^{-jkr}/4\pi r)\mathbf{U}(\theta,\phi) \quad (2.17)$$

where:

$$\mathbf{U}(\theta,\phi) = \iiint_{V'} \mathbf{J}(x',y',z')e^{j\Gamma}dx'dy'dz' \quad (2.18)$$

is the unnormalized field pattern.

The factor $e^{-jkr}/4\pi r$ is recognized as representing an outward traveling spherical wave. Thus, $\mathbf{A}(x,y,z)$ is an outgoing spherical wave, with a directional weighting function $\mathbf{U}(\theta,\phi)$. As we will show, the radiation pattern can be expressed in terms of this weighting function (13:4).

To develop the radiation pattern, we must begin with equations (2.6) and (2.8). Performing the curl operations in spherical coordinates, and retaining only the terms in r^{-1} (called the radiation terms) we find (13:4):

$$\mathbf{H} = -jk\hat{\mathbf{r}} \times \mathbf{A} \quad (2.19)$$

and

$$\mathbf{E} = jk\eta\hat{\mathbf{r}} \times (\hat{\mathbf{r}} \times \mathbf{A}) = -jk\eta\mathbf{A}_T \quad (2.20)$$

where $\hat{\mathbf{r}}$ is a unit vector in the radial direction and $\eta = (\mu_o/\epsilon_o)^{1/2} = 377$ ohms, the free space impedance. $A_T = A_\theta\hat{\theta} + A_\phi\hat{\phi}$ is the transverse part of $\mathbf{A}$, where $\hat{\theta}$ and $\hat{\phi}$

are the unit vectors in the theta and phi directions, respectively. We can see that the radiated electric field differs from the transverse magnetic vector potential function by only a multiplicative constant (13:4).

The complex Poynting vector yields an average power density which we can write as:

$$\mathbf{P}(\theta,\phi) = \tfrac{1}{2}\mathrm{Re}(\mathbf{E} \times \mathbf{H}^*) \tag{2.21}$$

or

$$\mathbf{P}(\theta,\phi) = \hat{\mathbf{r}}\left[k^2\eta/(4\pi r)^2\right](\tfrac{1}{2}U_\theta U_\theta^* + \tfrac{1}{2}U_\phi U_\phi^*) \tag{2.22}$$

where $\mathbf{Q}^*$ or Q^* signifies the complex conjugate of the vector $\mathbf{Q}$ or scalar Q, respectively. The θ-polarized pattern or vertically polarized pattern associated with E_θ is given by:

$$P_{r,\theta}(\theta,\phi) = \tfrac{1}{2}\left[k^2\eta/(4\pi r)^2\right]|U_\theta(\theta,\phi)|^2 \tag{2.23}$$

and the ϕ-polarized pattern or horizontally polarized pattern associated with E_ϕ is given by (13:5):

$$P_{r,\phi}(\theta,\phi) = \tfrac{1}{2}\left[k^2\eta/(4\pi r)^2\right]|U_\phi(\theta,\phi)|^2 \tag{2.24}$$

In equations (2.23) and (2.24), the subscript r is used to denote the radial component of $\mathbf{P}$. Changing the spherical unit vectors to their cartesian counterparts via the relations:

$$\hat{\theta} = \hat{\mathbf{x}}\cos\theta\cos\phi + \hat{\mathbf{y}}\cos\theta\sin\phi + \hat{\mathbf{z}}\sin\theta \tag{2.25}$$

$$\hat{\phi} = -\hat{\mathbf{x}}\sin\phi + \hat{\mathbf{y}}\cos\phi \tag{2.26}$$

we can write the θ and ϕ components of $\mathbf{U}$ from equation (2.18) as:

$$U_\theta(\theta,\phi) = \iiint_{V'} [\cos\theta\cos\phi J_x(x',y',z') + \cos\theta\sin\phi J_y(x',y',z') + \sin\theta J_z(x',y',z')] \times \exp(j\Gamma)dx'dy'dz' \quad (2.27)$$

and

$$U_\phi(\theta,\phi) = \iiint_{V'} [-\sin\phi J_x(x',y',z') + \cos\phi J_y(x',y',z')] \times \exp(j\Gamma)dx'dy'dz' \quad (2.28)$$

Equations (2.27) and (2.28) are the key results of our development and form the basis of the pattern analysis and synthesis that follows (13:5). If we start with known current distributions, U_θ and U_ϕ can be determined from (2.27) and (2.28) and then used in (2.23) and (2.24) to deduce the radiation patterns. This is the analysis problem. Conversely, if desired patterns are specified, (2.27) and (2.28) become integral equations in the sought-for current distribution. This is the synthesis problem (10:30-31).

Linear Arrays

Next, we will develop the necessary equations for linear arrays with various excitation schemes, along with two of the more familiar pattern synthesis methods. We will consider arrays of discrete, identical elements, namely center fed dipoles. The dipoles will be assumed to have a sinusoidal current distribution. A discussion of the dipole

used in this study is in Appendix A. The formulation for linear arrays can be directly extended to planar arrays.

Arrays of Discrete, Identical Elements. Consider now an antenna consisting of M+1 identical discrete radiating elements. By identical, we mean that any two of the elements can be made congruent by a simple translation. We can select a reference point $P_i(x_i,y_i,z_i)$ in the i^{th} element, and find a point $P_j(x_j,y_j,z_j)$ which occupies the same position in the j^{th} element. This collection of M+1 reference points serves to describe the relative positions of the different elements. We then establish local coordinate systems centered at each of these reference points.

If we let $x_i' = x' - x_i$, $y_i' = y' - y_i$, and $z_i' = z' - z_i$, we can define any point $Q_i(x_i',y_i',z_i')$ in the i^{th} radiator, relative to its characteristic point $P_i(x_i,y_i,z_i)$ (10:115). This situation is depicted in Figure 3. Then for example, at any point in the i^{th} radiator:

$$\mathbf{J}_x(x',y',z') = \mathbf{J}_x(x_i+x_i',y_i+y_i',z_i+z_i') \qquad (2.29)$$

similarly, for any point in the j^{th} radiator:

$$\mathbf{J}_x(x',y',z') = \mathbf{J}_x(x_j+x_j',y_j+y_j',z_j+z_j') \qquad (2.30)$$

Since it is assumed that all elements are identical, and similarly oriented, if I_i is the complex total current at the terminals of the i^{th} radiator, and I_j is the complex total current at the terminals of the j^{th} radiator, it follows that, if $x_i' = x_j'$, $y_i' = y_j'$, $z_i' = z_j'$, then from

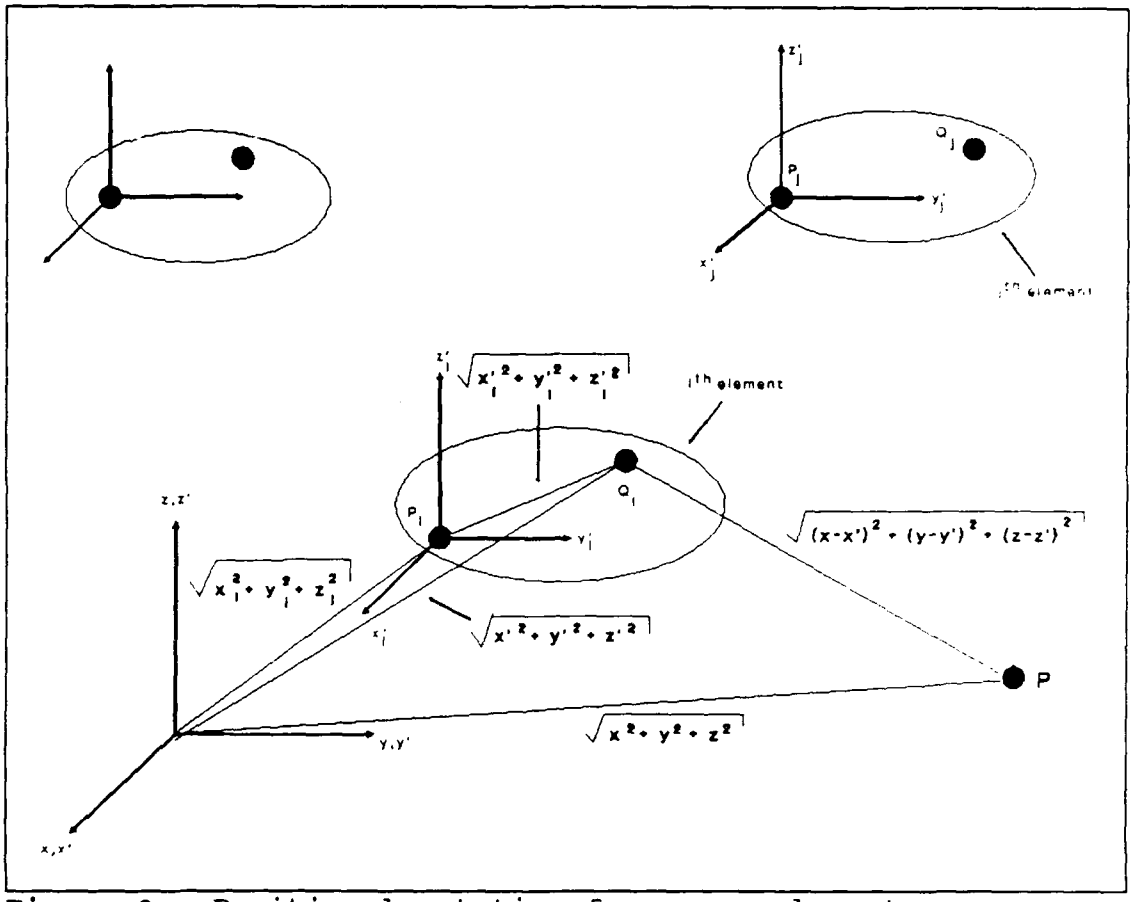

Figure 3. Positional notation for array elements

Elliott's work (13:7):

$$\frac{J_x(x_i+x_i',y_i+y_i',z_i+z_i')}{J_x(x_j+x_j',y_j+y_j',z_j+z_j')} = \frac{I_i}{I_j} \qquad (2.31)$$

because J_x is being determined at corresponding physical points in the two elements.

Elliott (13:6-8) has shown that by using (2.31), equation (2.28) can be written as:

$$U_\phi(\theta,\phi) = \sum_{i=0}^{M} (I_i/I_0)$$

$$X \exp[jk(x_i\sin\theta\cos\phi + y_i\sin\theta\sin\phi + z_i\cos\theta)]$$

$$X \iiint_{V_0'} [-\sin\phi J_x(x_0',y_0',z_0') + \cos\phi J_y(x_0',y_0',z_0')]$$

$$X \exp[jk(x_0'\sin\theta\cos\phi + y_0'\sin\theta\sin\phi + z_0'\cos\theta)]$$

$$X\, dx_0'dy_0'dz_0' \qquad (2.32)$$

In (2.32), the origin of the principle coordinates was chosen at the point $P_0(x_0,y_0,z_0)$, which will become the center of the array. We can rewrite (2.32) as (13:7-8):

$$U_\phi(\theta,\phi) = U_{\phi,a}(\theta,\phi)U_{\phi,e}(\theta,\phi) \qquad (2.33)$$

where

$$U_{\phi,a}(\theta,\phi) = \sum_{i=0}^{M} (I_i/I_0)$$

$$X \exp[jk(x_i\sin\theta\cos\phi + y_i\sin\theta\sin\phi + z_i\cos\theta] \qquad (2.34)$$

is the array factor for the ϕ component of **U** and:

$$U_{\phi,e}(\theta,\phi) = \iiint_{V_0'} [-\sin\phi J_x(x_0',y_0',z_0') + \cos\phi J_y(x_0',y_0',z_0')]$$

$$X \exp[jk(x_0'\sin\theta\cos\phi + y_0'\sin\theta\sin\phi + z_0'\cos\theta)]$$

$$X\, dx_0'dy_0'dz_0' \qquad (2.35)$$

is the element factor for the ϕ component of **U**. The element factor is the contribution to U_ϕ of all the currents in the first element. Because of the identical configuration and orientation of all elements, this contribution is the same for all other elements, except for the differences in posi-

tion and excitation. These later two contributions are accounted for by the array factor, equation (2.34) (13:8).

Similarly, we can rewrite (2.27) as:

$$U_\theta(\theta,\phi) = U_{\theta,a}(\theta,\phi)U_{\theta,e}(\theta,\phi) \tag{2.36}$$

where:

$$U_{\theta,a}(\theta,\phi) = \sum_{i=0}^{M} (I_i/I_0) \times \exp[jk(x_i\sin\theta\cos\phi + y_i\sin\theta\cos\phi + z_i\cos\theta)] \tag{2.37}$$

and:

$$U_{\theta,e}(\theta,\phi) = \iiint_{V_0'} [\cos\theta\cos\phi J_x(x_0',y_0',z_0') + \cos\theta\sin\phi J_y(x_0',y_0',z_0') - \sin\theta J_z(x_0',y_0',z_0')] \times \exp[jk(x_0'\sin\theta\cos\phi + y_0'\sin\theta\sin\phi + z_0'\cos\theta)] \times dx_0'dy_0'dz_0' \tag{2.38}$$

are the array factor and element factor, respectively, for the θ component of **U**. Equations (2.33) and (2.36) exhibit the principle of pattern multiplication (13:9).

Linear Arrays - Fundamental Considerations. We first let r_i be the distance from $P_0(x_0,y_0,z_0)$ to $P_i(x_i,y_i,z_i)$, with a line connecting P_0 to P_i having the direction cosines: $\cos\alpha_i$; $\cos\beta_i$; and $\cos\gamma_i$. Then, if all the elements lie along this common line, α, β, and γ are the same angles for every P_i. This forms a linear array (13:9). The array factor becomes:

$$U_a(\theta,\phi) = \sum_{m=0}^{M} (I_m/I_0)$$

$$X \exp[jkr_m(\cos\alpha\sin\theta\cos\phi + \cos\beta\sin\theta\sin\phi + \cos\gamma\cos\theta)] \quad (2.39)$$

Now if we change the increment to start at m = 1 and write $r_m = (m-1)d$, where d is the spacing between elements, (2.39) becomes:

$$U_a(\theta,\phi) = \sum_{m=1}^{M} (I_m/I_0)\ X \exp[jk(m-1)d(\cos\alpha\sin\theta\cos\phi + \cos\beta\sin\theta\sin\phi + \cos\gamma\cos\theta)] \quad (2.40)$$

We will let I_0 represent the magnitude of the excitation current at the center element of the array so all other I_m currents are normalized to the center element's current. Figure 4 shows the two array coordinate geometries for an even and odd number of elements.

Uniformly Excited Broadside Array. Consider a uniformly spaced array, placed along the x-axis with radiating elements at positions x_i=0, d, 2d, ···,Md. Along the x-axis, $\gamma = \beta = 90°$ and $\alpha = 0°$ so (2.40) becomes:

$$U_a(\theta,\phi) = \sum_{m=1}^{M} (I_m/I_0)\exp[j(m-1)kd_x\sin\theta\cos\phi] \quad (2.41)$$

If all the currents are equal and in-phase (2.41) becomes:

$$U_a(\theta,\phi) = \sum_{m=1}^{M} \exp[j(m-1)(kd_x\sin\theta\cos\phi)] \quad (2.42)$$

Naturally, if the entire radiation pattern were desired, we would have to multiply (2.42) by the element factor; how-

ever, for the time being, we will assume isotropic elements so that $U_e(\theta,\phi)$ =1 and $U_a(\theta,\phi)$ becomes our entire radiation pattern. Pattern plots along the xz-plane for an even and an odd number of elements at half-wavelength intervals are shown in Figures 5 and 6, respectively. If the interelement spacing is allowed to expand beyond one wavelength additional major lobes will appear known as grating lobes. This case is shown in Figure 7. Generally, it is undesirable to

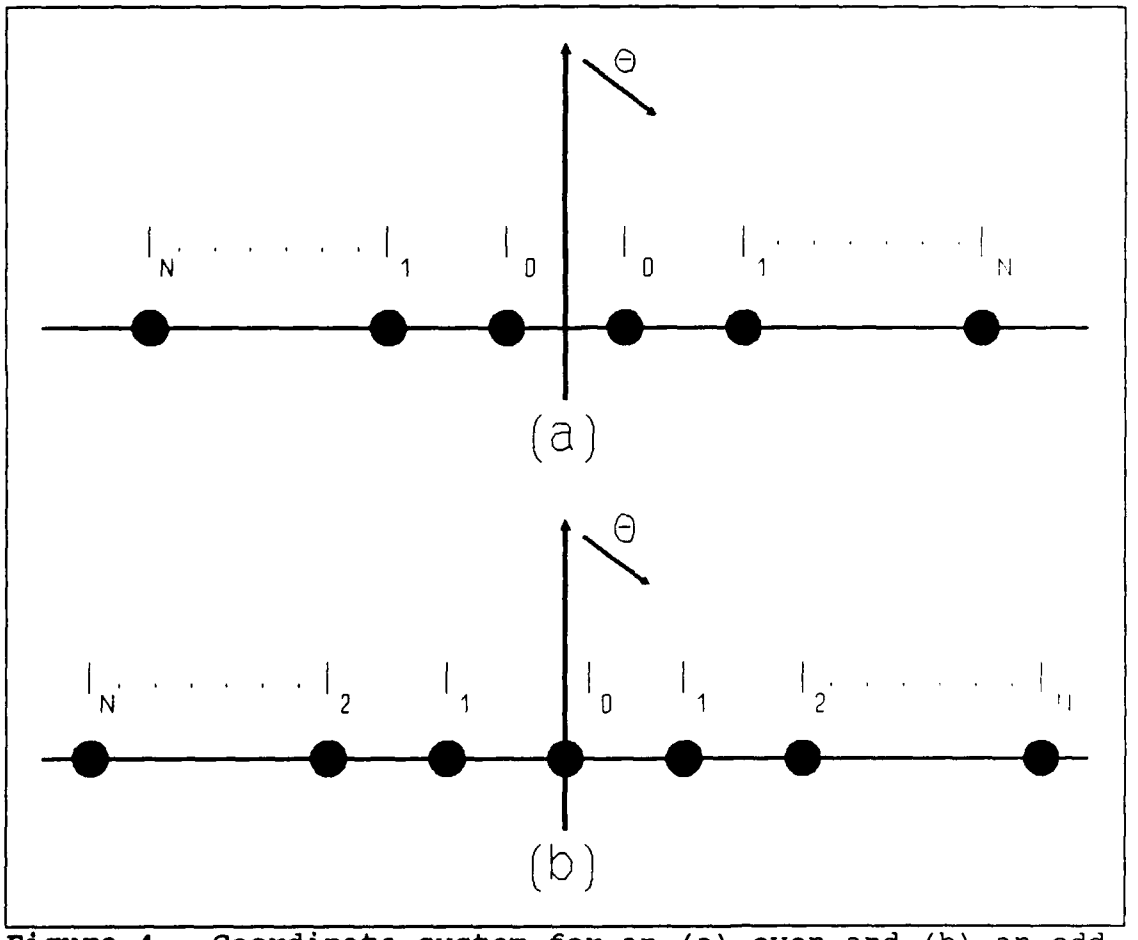

Figure 4. Coordinate system for an (a) even and (b) an odd number of array elements

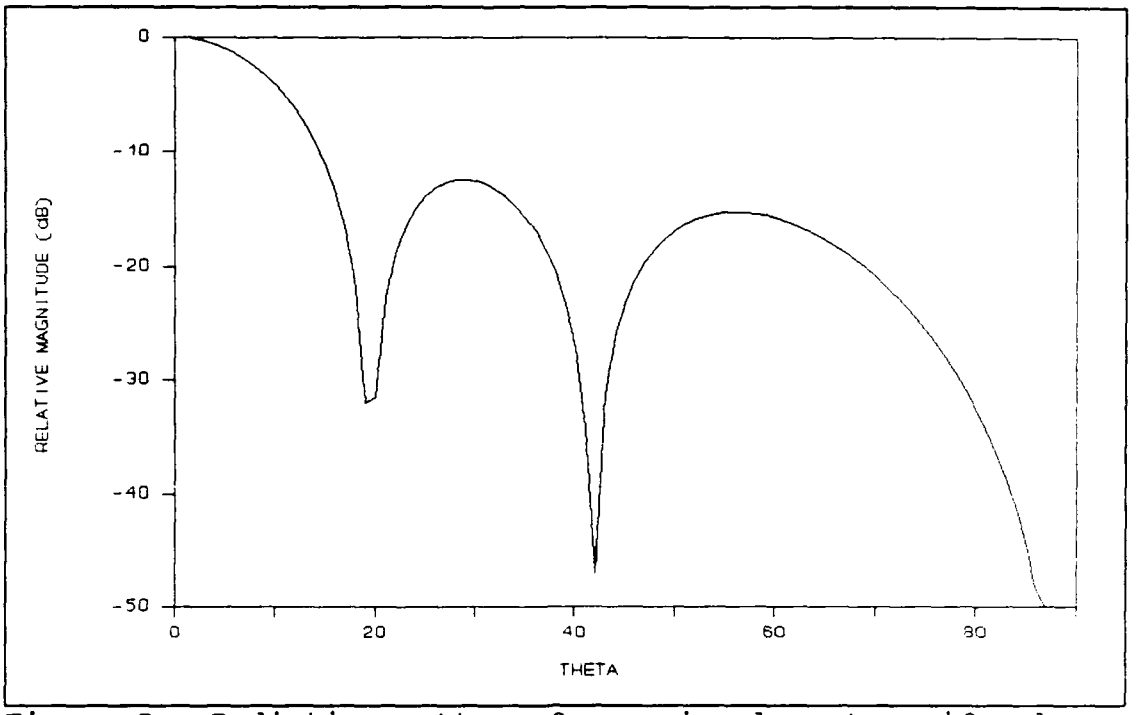

Figure 5. Radiation pattern for a six element, uniformly excited linear array with ½ wavelength interelement spacing

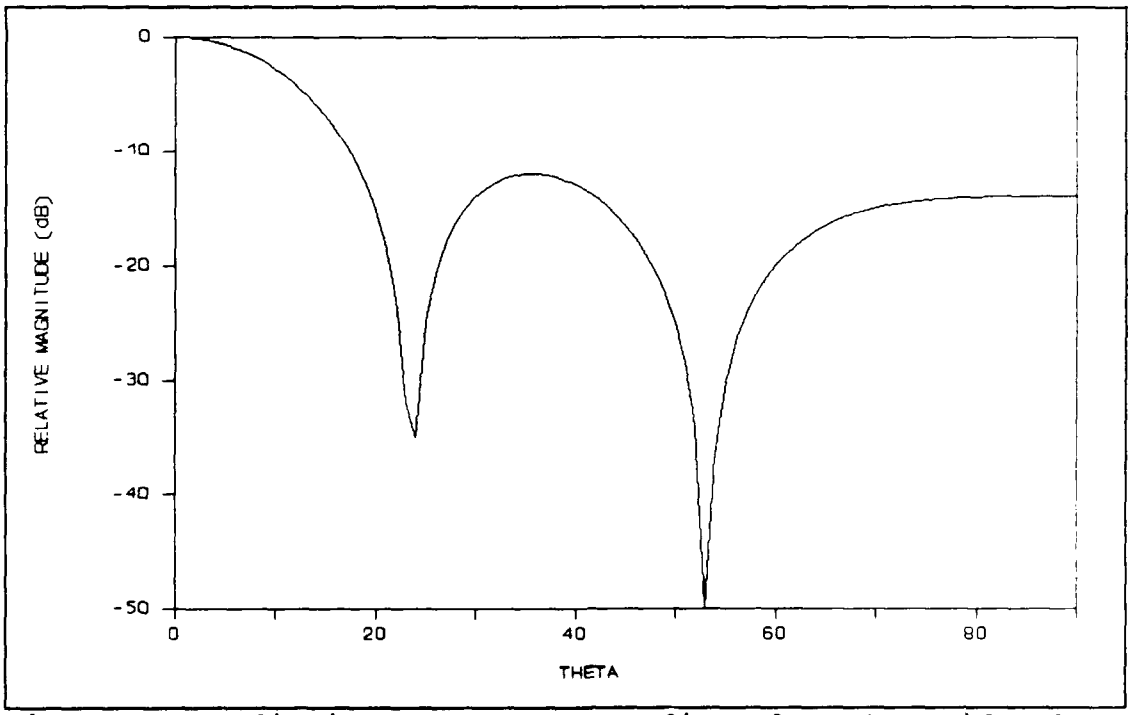

Figure 6. Radiation pattern for a five element, uniformly excited linear array with ½ wavelength interelement spacing

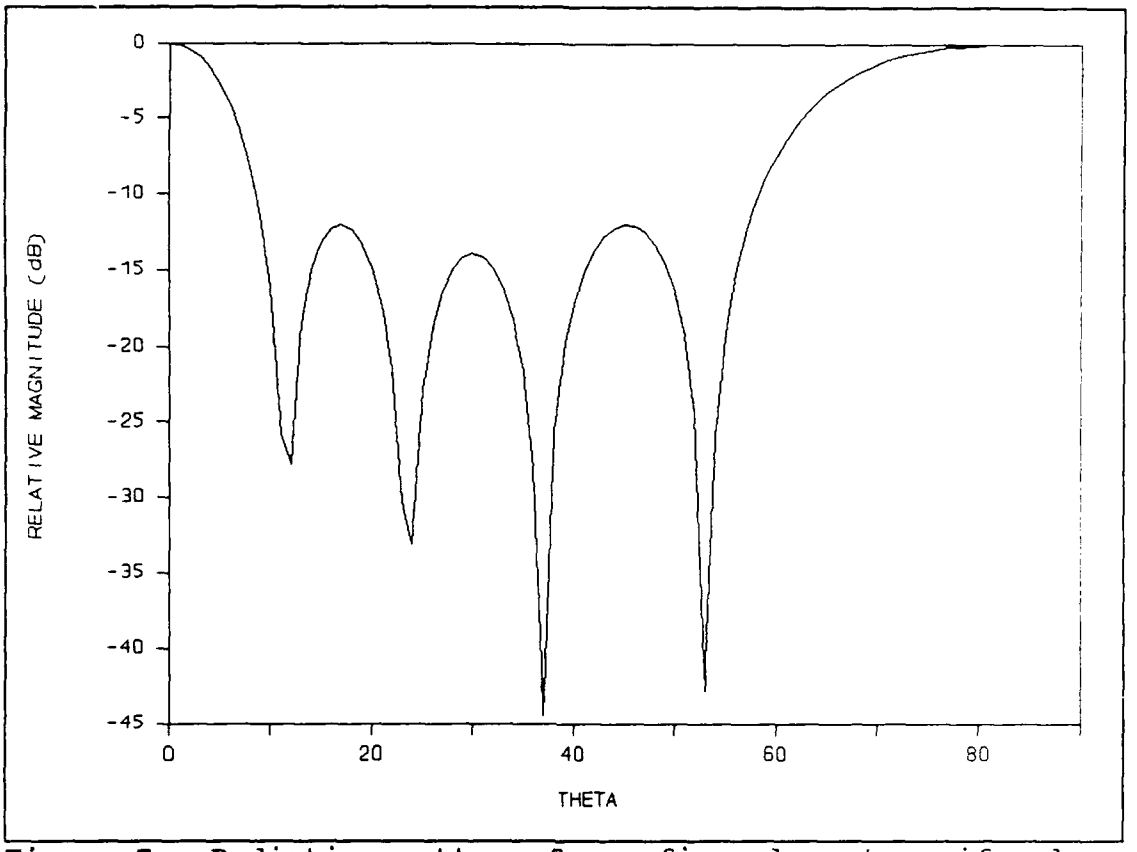

Figure 7. *Radiation pattern for a five element,* uniformly excited linear array with one wavelength interelement spacing showing the grating lobe at theta = 90°

have grating lobes and, as a result, most arrays are designed so that the interelement spacing is less than one wavelength (23:123).

Broadside Arrays with Tapered Excitation. Next, consider a uniformly spaced array placed along the x-axis so that (2.41) applies. Additionally, we will consider a tapered excitation with the assumption that the currents remain in-phase. With a tapered excitation, the center element (if an odd number of elements) or two center ele-

ments (if an even number of elements) receive the largest current with its neighbors receiving smaller currents towards the ends of the array where the end elements receive the smallest current (13:13-14).

One such tapered excitation scheme is the Binomial current distribution. To determine the excitation coefficients we can write the function $(1 + x)^{m-1}$ in a series using the binomial expansion:

$$(1+x)^{m-1} = 1 + (m-1)x + (m-1)(m-2)x^2/2! + (m-1)(m-2)(m-3)x^3/3! + \cdots, |x|<1 \quad (2.43)$$

where we let "m" be the number of elements in the array (4:243). If we apply this to a five element array and normalize to the center element the current distribution is: 1/6; 2/3; 1; 2/3; 1/6. For a six element array the distribution is: 1/10; 1/2; 1; 1; 1/2; 1/10. The array factor for both these cases plotted in the xz-plane is shown in Figures 8 and 9 for ½ wavelength interelement spacing. As we can see from Figures 8 and 9, the pattern is broader than the uniform array pattern (Figures 5 and 6) and the[illegible] side lobes.

Scanned Linear Array. Consider a uniform[illegible] array placed along the x-axis so that (2.41)[illegible] but assume the currents have equal ampli[illegible] a uniform progressive phase shift so that:

$$I_m = I_0 \exp[-j(m-1)[illegible] \quad (2.44)$$

where β_x is a constant, called the phase[illegible] factor

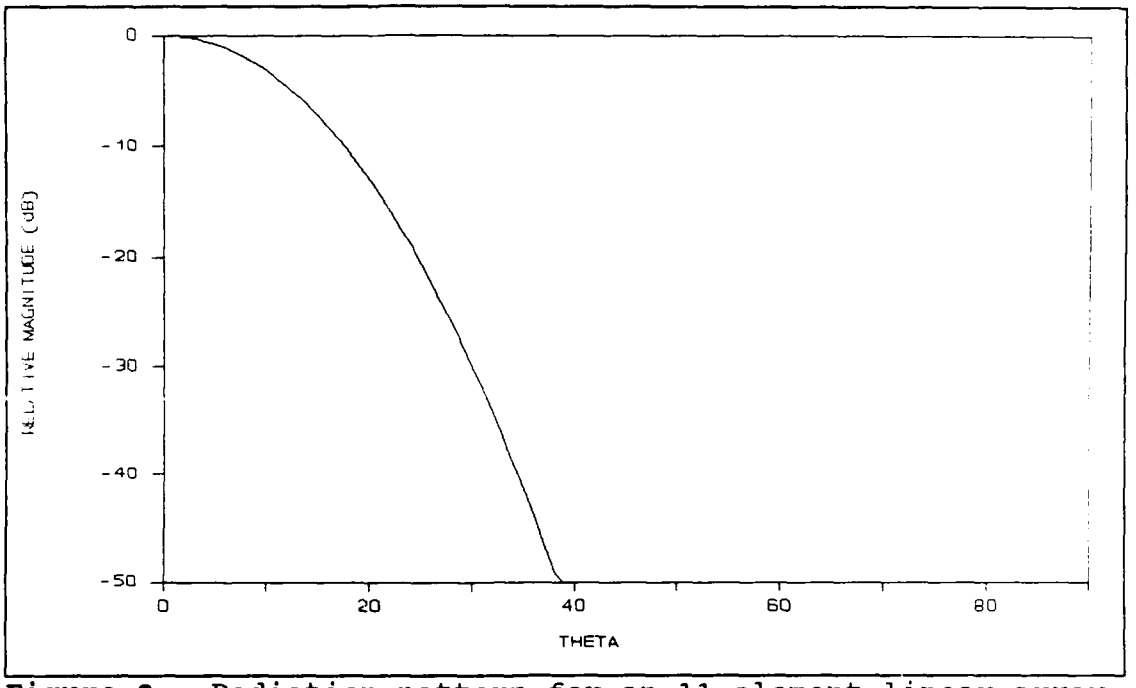

Figure 8. Radiation pattern for an 11 element linear array with a binomial current distribution and ½ wavelength inter-element spacing

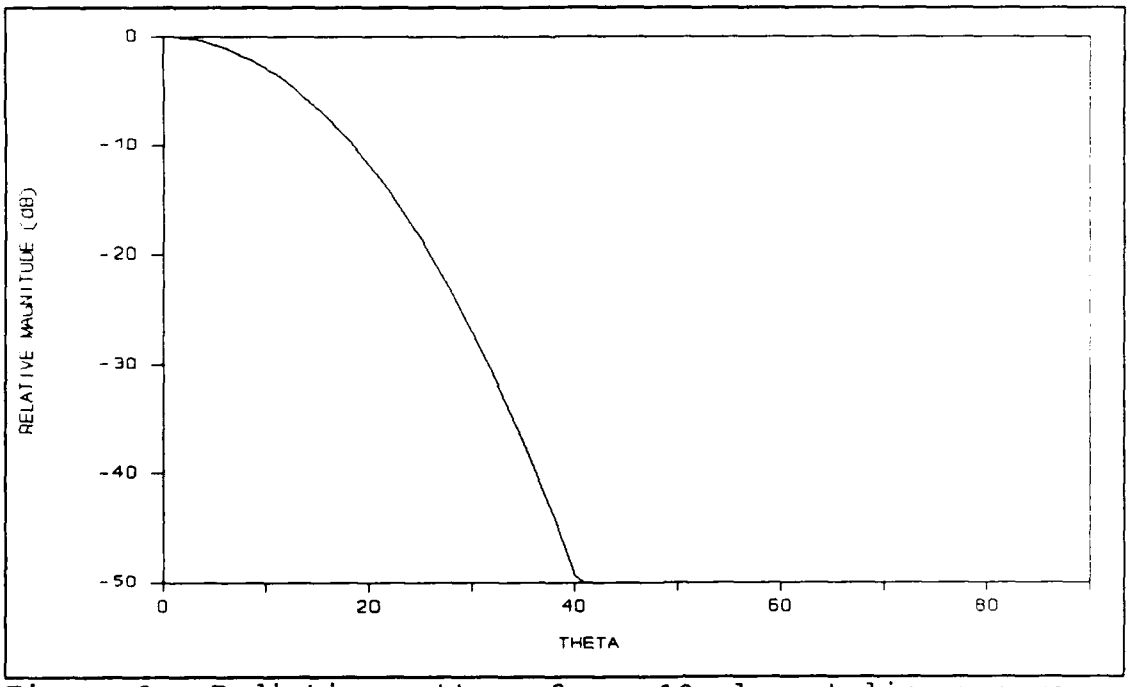

Figure 9. Radiation pattern for a 10 element linear array with a binomial current distribution and ½ wavelength inter-element spacing

(13:15). Equation (2.41) becomes:

$$U_a(\theta,\phi) = \sum_{m=1}^{M} \exp[j(m-1)(kd_x\sin\theta\cos\phi + \beta_x)] \qquad (2.45)$$

which differs from (2.41) only in a shift in origin. Equation (2.41) represented a beam aligned at $\theta=0°$, (2.45) allows the beam to align at $\theta=\theta_0$ where:

$$\beta_x = -kd\cos\theta_0 \qquad (2.46)$$

or

$$\theta_0 = \cos^{-1}(-\beta_x/kd) \qquad (2.47)$$

β_x can be used as a parameter to position the main beam in space. If β_x is varied, the beam will scan. Figure 10 shows the effect of scanning the main beam 40° from broadside for a uniformly excited linear array with ½ wavelength interelement spacing.

Pattern Synthesis. At times in array antenna design it is desired to achieve a narrow main beam accompanied by a low side lobe level. In this section, we will discuss the two most important narrow main beam, low side lobe methods: the Dolph-Chebyshev method for linear arrays and the Taylor line source method adapted for discrete arrays.

Dolph-Chebyshev Linear Array Method. Optimum beamwidth-side lobe level performance occurs when there are as many side lobes in the visible region ($0°\leq\theta\leq180°$) as possible and when they have the same level. In other words, for a specified beamwidth, the side lobe level would be as low as possible; or vice versa, for a specified side lobe

level the beamwidth would be as narrow as possible. Dolph (9:335-348) recognized that Chebyshev polynomials have this property and he applied them to the synthesis problem. The reader is encouraged to read Dolph's paper or the current literature (4,9,23) to gain an understanding of this method. In this paper, we are concerned with an efficient and accurate procedure for calculating the current values at each element in the array for a given side lobe level.

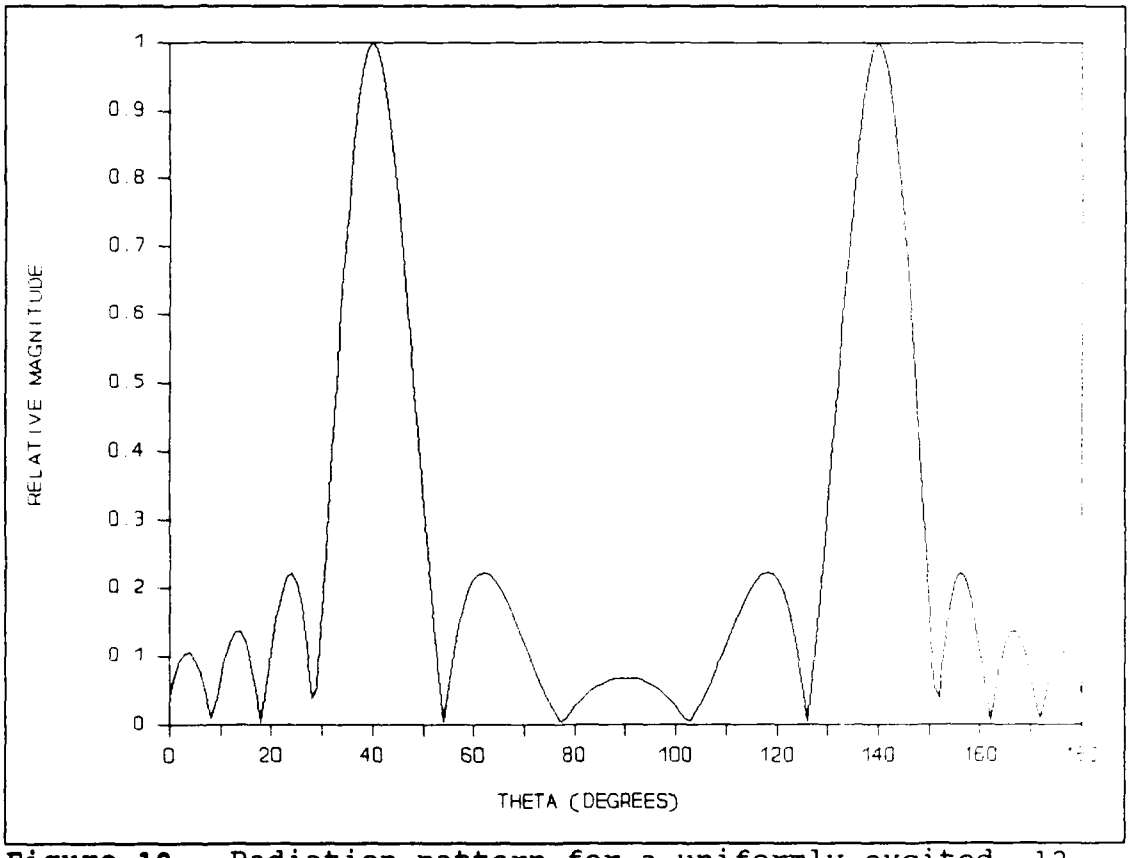

Figure 10. Radiation pattern for a uniformly excited, 12 element linear array with ½ wavelength interelement spacing, scanned at 40° from broadside

One such method for calculating the current values was presented by Bresler (5:951-952). Burns, Laxpati, and Shelton (6:884-887) evaluated several different programs for synthesizing low side lobe sum patterns for linear arrays in terms of run time and precision and concluded Bresler's nested product algorithm provided the best results, especially for larger arrays. As such, Bresler's algorithm is used in this paper.

Referring to the geometry in Figure 4, let S(dB)>0 be the desired side lobe ratio in decibels. Then:

$$S = 10^{S(dB)/20}, \tag{2.48}$$

and the variables x_0 and α are defined as:

$$x_0 = \cosh\left[(1/M-1)\cosh^{-1}(S)\right], \tag{2.49}$$

and

$$\alpha = 1 - 1/x_0^2 \tag{2.50}$$

If M is the total number of array elements, then the element weights are given by (19:72):

$$I_{N-n} = \begin{cases} (M-1)\alpha \cdot NP(n,\alpha,M) & \text{for } n = \begin{cases} 1,2,\ldots,N-1 & (M \text{ even}) \\ 1,2,\ldots,N & (M \text{ odd}) \end{cases} \\ 1 & \text{for } n = 0 \end{cases} \tag{2.51}$$

where $NP(n,\alpha,M)$ is the nested product:

$$NP(n,\alpha,M) = \sum_{m=1}^{n} \alpha^{n-m} \prod_{j=m}^{n} f_j^n \tag{2.52}$$

and

$$f_j^n = m(M-1-2n+j)/(n-j)(n+1-j) \tag{2.53}$$

and

$$f_n^n = 1 \qquad (2.54)$$

Figure 11 shows the radiation pattern of a Dolph-Chebyshev synthesized linear array with -26 dB side lobe suppression. Figure 12 shows the radiation pattern of a Dolph-Chebyshev synthesized linear array with -35 dB side lobe suppression.

Discretized Taylor $\bar{n}$-Parameter Linear Array Method. A second popular method for synthesizing a reduced side lobe pattern is the Taylor line source method adapted for arrays of discrete elements (4,10,24). This method differs from the Dolph-Chebyshev synthesis in that the beamwidth for a given side lobe level is not optimum (minimum), but, quite close to optimum. Similarly, for a given beamwidth, the resulting side lobe level will be larger than the optimum, but not by much. Another difference is the Taylor pattern side lobes decrease gradually away from the main beam, whereas, in Dolph-Chebyshev patterns the side lobes are all equal (10:162,19:77).

Taylor first perfected this method for continuous line sources noting the application to arrays of discrete elements (24:16-28). Since then, various authors have developed several approaches of applying Taylor's method to arrays (12:617-621,19:77-78,26:1089-1093). The two procedures used in this paper are the Null Matching method developed by Elliott and the Aperture Sampling method outlined by

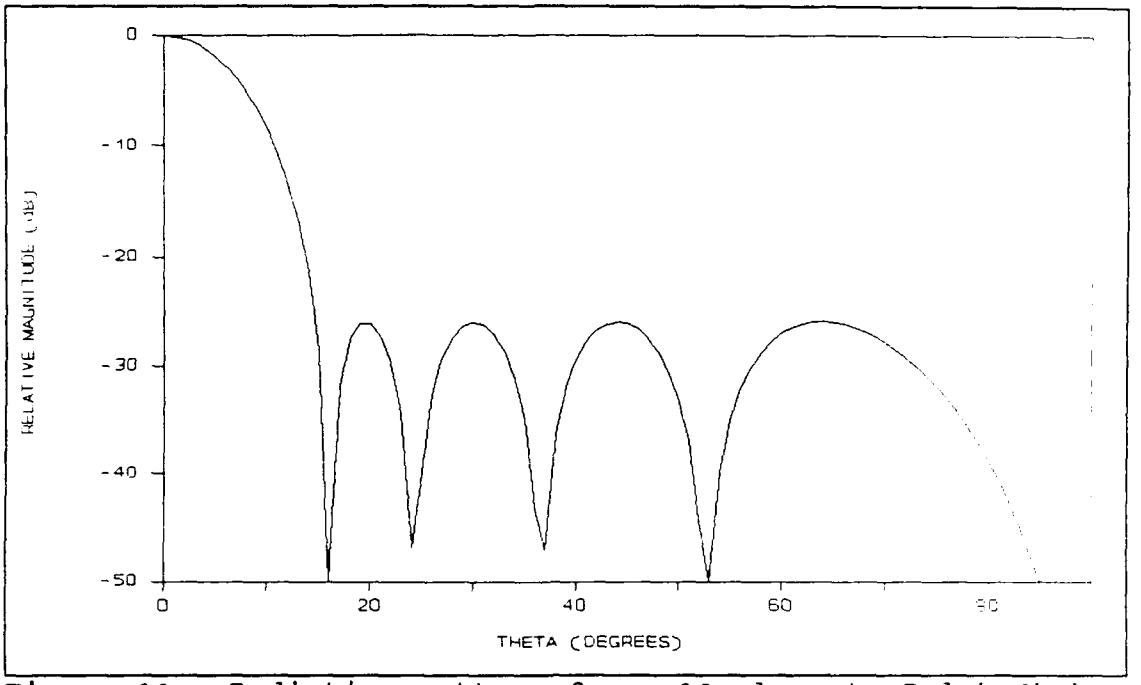

Figure 11. Radiation pattern for a 10 element, Dolph-Chebyshev synthesized linear array with ½ wavelength interelement spacing showing a -26 db side lobe level

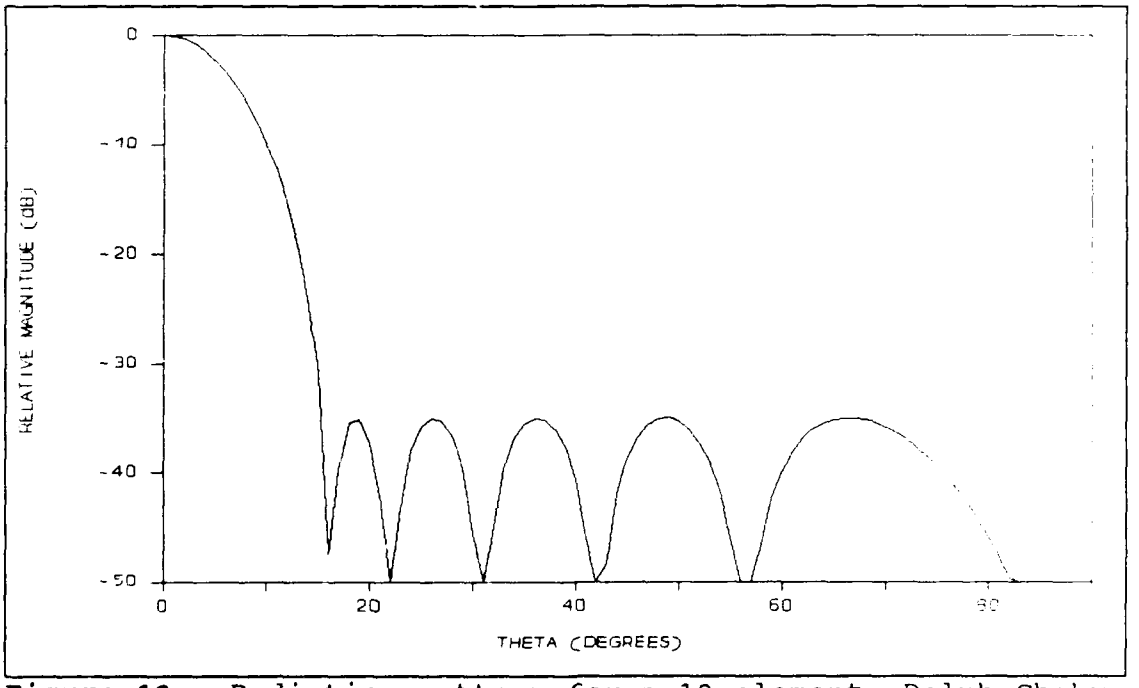

Figure 12. Radiation pattern for a 12 element, Dolph-Chebyshev synthesized linear array with ½ wavelength interelement spacing showing a -35 db side lobe level

Balanis (for line sources)(4:679-681) and implemented by Pozar for arrays of discrete elements.

To implement these two design methods, we consider an array of N+1 elements, spaced a distance d apart, modeled by a line source of length L=(N+1)d, so that the line source extends a distance d/2 past the ends of the array (19:77). The normalized Taylor line source for a broadside array is (4:679-681):

$$I(z) = (1/L)\left[1+2\sum_{p=1}^{\bar{n}-1} SF(p,A,\bar{n})\cos(2\pi pz/L)\right] \qquad (2.55)$$

where

$$SF(p,A,\bar{n}) = \begin{cases} \dfrac{[(\bar{n}-1)!]^2}{[(\bar{n}-1+p)!(\bar{n}-1-p)!]} \times \prod_{m=1}^{\bar{n}-1}\left[1-(\pi p/u_m)^2\right] & |p|<\bar{n} \\ 0 & |p|\geq\bar{n} \end{cases} \qquad (2.56)$$

is the space factor with $SF(-p,A,\bar{n}) = SF(p,A,\bar{n})$. The location of the nulls (u_m) are obtained using:

$$u_m = \begin{cases} \pm\pi\sigma\left[A^2+(m-\frac{1}{2})^2\right]^{1/2} & 1\leq n\leq\bar{n} \\ \pm m\pi & \bar{n}\leq n\leq\infty \end{cases} \qquad (2.57)$$

where

$$\sigma = \bar{n}/\left[A^2+(\bar{n}-\tfrac{1}{2})^2\right]^{1/2} \qquad (2.58)$$

and

$$A = (1/\pi)\cosh^{-1}S \qquad (2.59)$$

where S is defined by equation (2.48). The parameter $\bar{n}$ determines the number of close-in side lobes at the design

side lobe level and is chosen by the user. Small values of $\bar{n}$ yield source distributions which are maximum at the center and monotonically decrease toward the edges. In contrast, large values of $\bar{n}$ result in sources which are peaked simultaneously at the center and at the edges, and they yield sharper main beams.

Using the Aperture Sampling method, the N+1 element weights are computed as (19:78):

$$I_n = I(z_n) \tag{2.60}$$

where

$$z_n = -[(N/2)+1]d+nd, \quad n=1,2,3,\ldots,N+1 \tag{2.61}$$

We begin the Null Matching method by writing the pattern function f(w) of an N+1 element array in the Schelkunoff product form:

$$f(w) = \prod_{n=1}^{N} (w-w_n) \tag{2.62}$$

where $w = \exp(j\Psi)$, $\Psi = kd\sin\theta$, and $w_n = \exp(j2\pi u_n/(N+1))$. The values w_n are the nulls of f(w). In terms of the element weights, the pattern function is:

$$f(w) = w^N+I_N w^{N-1}+\ldots+I_1 \tag{2.63}$$

where we have used $I_{N+1} = 1$. We find the element weights I_n by equating (2.62) and (2.63). This will produce the desired Taylor pattern (19:78). Elliott points out that the Null Matching method is slightly more accurate for small arrays, however, for larger arrays, Pozar points out that the larger number of complex arithmetic operations required

may lead to reduced accuracy for this method (12:621,19:78).

Figures 13 and 14 show the radiation pattern of two Taylor synthesized linear arrays. The radiation pattern in Figure 13 is for a 19 element linear array with 0.7 wavelength interelement spacing, a design side lobe level of -20 db, and $\bar{n} = 6$, using the Null Matching method. Figure 14 shows the radiation pattern of a 41 element linear array with 0.5 wavelength interelement spacing, a design side lobe level of -25 db, and $\bar{n} = 6$, using the Aperture Sampling method. In both Figures, the first six innermost side lobes are at relatively the same level.

Before leaving the topic of Taylor synthesis, it is important to consider the criteria Taylor provides for choosing the appropriate value of $\bar{n}$. Taylor provides the details in his paper (24:23); summarizing, $\bar{n}$ must be chosen such that a unit increase in $\bar{n}$ does not increase σ as given in (2.58). This means that for a space factor $SF(p,A,\bar{n})$ with a design side lobe ratio of 0-20 db, $\bar{n}$ must be at least 2; for 25 db, $\bar{n}$ must be at least 3; for 30 db, $\bar{n}$ must be at least 4; for 35 db, $\bar{n}$ must be at least 5; and for 40 db, $\bar{n}$ must be at least 6. If $\bar{n}$ is increased sufficiently beyond the endpoint of the visible range, L/λ, all the visible lobes tend to become uniform. Such large values of $\bar{n}$ have the effect of supergaining the array, a phenomenon Taylor examines at length in his paper (24:23,24-26). One is encouraged to read Taylor's paper in order to gain a better

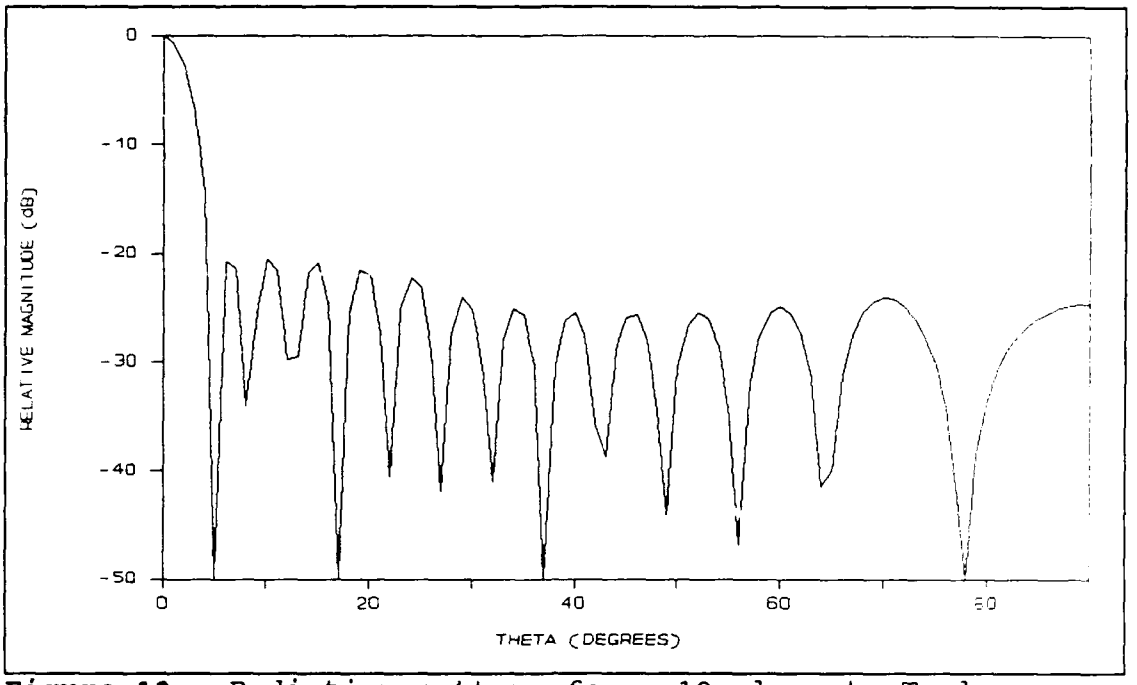

Figure 13. Radiation pattern for a 19 element, Taylor synthesized ($\bar{n}$=6) linear array with 0.7 wavelength inter-element spacing and a -20 db design side lobe level

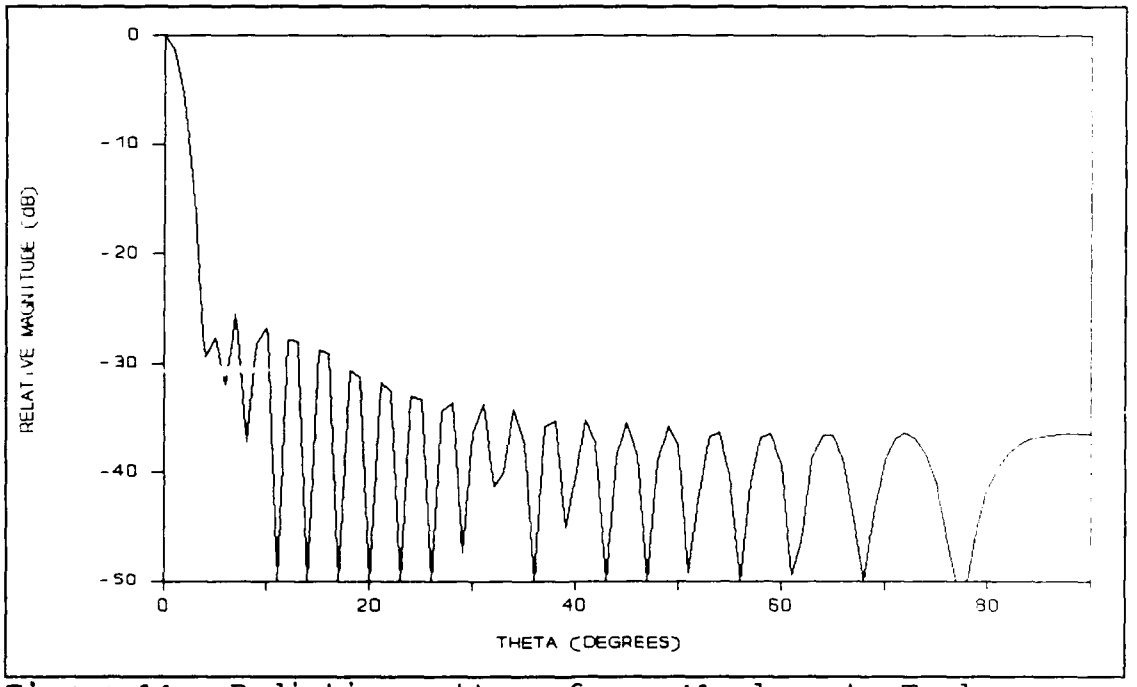

Figure 14. Radiation pattern for a 41 element, Taylor synthesized ($\bar{n}$=6) linear array with 0.5 wavelength inter-element spacing and a -25 db design side lobe level

understanding of this synthesis procedure and the choice of $\bar{n}$ and its effects on the pattern.

Planar Arrays.

Earlier, we developed the case of a linear array along the x-axis. Now, if we extend an additional line of radiators along the y-axis we form a rectangular or planar array. Planar arrays afford more symmetrical patterns with lower side lobes and the ability to scan the main beam toward any point in space.

Consider the geometry in Figure 15. If we have M elements along the x-axis the array factor is given by equation (2.45) or:

$$U_a(\theta,\phi) = \sum_{m=1}^{M} (I_m/I_{0x}) \exp[j(m-1)(kd_x \sin\theta\cos\phi+\beta_x)] \qquad (2.64)$$

where I_{0x} is the current of the center element if an odd number of elements or center elements if an even number of elements and we are removing the restriction that the currents have equal amplitudes in (2.45). Now, if we have N elements along the y-axis with an interelement spacing of d_y and a progressive phase shift β_y, equation (2.40) becomes:

$$U_a(\theta,\phi) = \sum_{n=1}^{N} (I_n/I_{0y}) \exp[j(n-1)(kd_y \sin\theta\sin\phi+\beta_y)] \qquad (2.65)$$

where I_{0y} is the current of the center element if an odd number of elements or center elements if an even number of elements and $\alpha=\gamma=90°$ and $\beta=0°$ in equation (2.40). Realizing we have normalized the current excitations to the center

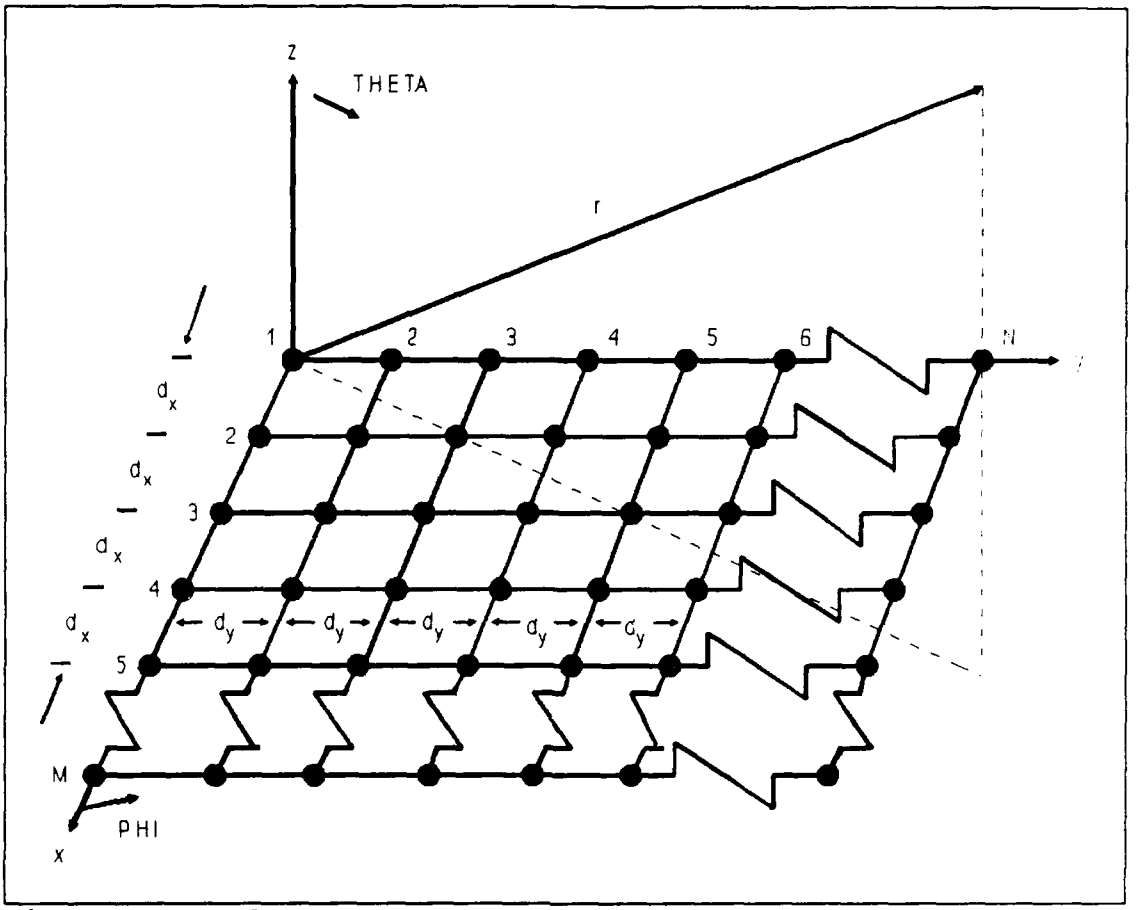

Figure 15. Planar array geometry

element (I_{0x} or I_{0y}) or two center elements, we will rewrite (I_m/I_{0x}) as I_{m1} and (I_n/I_{0y}) as I_{1n} to simplify the expressions. We can write the array factor for the planar array as (4:261):

$$U_a(\theta,\phi) = \sum_{n=1}^{N} I_{1n} \left[\sum_{m=1}^{M} I_{m1}\exp[j(m-1)(kd_x\sin\theta\cos\phi+\beta_x)] \right] X \exp[j(n-1)(kd_y\sin\theta\sin\phi+\beta_y)] \quad (2.66)$$

or

$$U_a(\theta,\phi) = S_{xM}S_{yN} \quad (2.67)$$

where

$$S_{xM} = \sum_{m=1}^{M} I_{m1}\exp[j(m-1)(kd_x\sin\theta\cos\phi+\beta_x)] \quad (2.68)$$

$$S_{yN} = \sum_{n=1}^{N} I_{1n}\exp[j(n-1)(kd_y\sin\theta\sin\phi+\beta_y)] \quad (2.69)$$

Looking at (2.68) and (2.69), the phases β_x and β_y are independent of each other and they could be adjusted such that the main beam of S_{xM} does not coincide with the main beam of S_{yN}. Usually, we require that the main beams of S_{xM} and S_{yN} coincide so that their maxima be directed toward the same direction. If we have one main beam directed along $\theta=\theta_0$ and $\phi=\phi_0$, the progressive phase shift between elements in the x- and y-directions must be equal to (4:263):

$$\beta_x = -kd_x\sin\theta_0\cos\phi_0 \quad (2.70)$$

$$\beta_y = -kd_y\sin\theta_0\sin\phi_0 \quad (2.71)$$

Finally, multiplying the array factor by the element factor for a dipole radiator (Appendix A) we obtain, in general:

$$U_\theta(\theta,\phi) = U_{\theta,e}(\theta,\phi)U_a(\theta,\phi) \quad (2.72)$$

or

$$U_\theta(\theta,\phi) = U_{\theta,e}(\theta,\phi)S_{xM}S_{ym} \tag{2.73}$$

where $U_{\theta,e}(\theta,\phi)$ is the element pattern of a dipole aligned along either the x-, y-, or z-axis, given in equations (A.12), (A.15), and (A.6), respectively, in Appendix A.

Summary

The first part of this chapter dealt with the derivation of the radiation pattern for antennas. Then we derived the radiation patterns for linear arrays with identical elements. At this point, we looked at how to scan the main beam by controlling the phase taper across the array. We also investigated different tapering schemes, namely, uniform, binomial, Chebyshev, and Taylor $\bar{n}$ parameter, for controlling the side lobe level and beamwidth. Finally, we developed the radiation pattern for a planar array in the xy-plane. In the next chapter, we will take into account small perturbations in the location of the array's elements, the element's drive amplitude and phase, and non-identical element factors and proceed to develop an average, or expected, radiation pattern for a planar array.

III. The Effects of Random Errors on the Array Pattern

This chapter deals with the effects of various random errors on the array pattern. We will derive the average, or expected, radiation pattern factor for a planar array following Skolnik's methodology (22:228-231). We will include translational errors in the positions of the elements, errors in the element's drive amplitude and phase, non-identical element patterns, and missing elements much as Allen did in deriving his average array pattern for a linear array (1:264-268). Rotational errors in the elements will not be considered since Elliott concluded they were relatively unimportant in the analysis of random errors (11:120). The expected radiation pattern for the planar array derived in this paper will have the same form as the expression derived by Allen (1:288) for the linear array. After deriving the expected radiation pattern we will develop an expression for the change in directivity due to random errors.

Sources of Errors Affecting Array Performance

We can write the no-error pattern factor of a planar array, taking into account the element factor, as:

$$U(\theta,\phi) = U_{\theta,e}(\theta,\phi) \sum_{m=1}^{M}\sum_{n=1}^{N} a_{mn} \times \exp\left[jk\left[(m-1)(\nu-\nu_0)+(n-1)(u-u_0)\right]\right] \qquad (3.1)$$

where:

$$\nu = kd_x \sin\theta \cos\phi \tag{3.2}$$

$$\nu_0 = kd_x \sin\theta_0 \cos\phi_0 \tag{3.3}$$

$$u = kd_y \sin\theta \sin\phi \tag{3.4}$$

$$u_0 = kd_y \sin\theta_0 \sin\phi_0 \tag{3.5}$$

and d_x and d_y are the interelement spacings in the x and y directions, respectively, and we are assuming the array is linearly phased to point the main beam in the direction θ_0, ϕ_0. The function $U_{\theta,e}(\theta,\phi)$ is the unnormalized element factor which is the average pattern of the array elements in the array environment.

Instead of actually realizing the field in equation (3.1), one would in practice obtain a field:

$$U(\theta,\phi) = \sum_{m=1}^{M}\sum_{n=1}^{N} U_{\theta,e;mn}(\theta,\phi) a'_{mn} \exp\left[-j(m-1)\nu_0\right]$$

$$X \exp\left[-j(n-1)u_0\right] \exp(\delta_{mn}) \exp(jk\mathbf{r}'_{mn}\cdot\hat{\mathbf{r}}) \tag{3.6}$$

where $U_{\theta,e;mn}(\theta,\phi)$ is the actual pattern of the mn^{th} element in its array environment, with respect to a coordinate system centered on the mn^{th} element. The quantity a'_{mn} represents the value of a_{mn} with error and δ_{mn} is the phase error of the mn^{th} element drive. The exponential expressing the phase delay of the elements at the far-field point is generalized to allow for mechanical error in antenna placement. The vector dot product is written in spherical coordinates as:

$$\mathbf{r}'_{mn} \cdot \hat{\mathbf{r}} = x_{mn}\sin\theta\cos\phi + y_{mn}\sin\theta\sin\phi + z_{mn}\cos\theta \tag{3.7}$$

where the "center of radiation" of the mn^{th} element is at x_{mn}, y_{mn}, z_{mn} (1:265).

Reduction of Errors to Pure Amplitude and Phase Errors

As we can see from equation (3.6), many errors manifest themselves as amplitude and phase errors. This is easily seen by recasting equation (3.6) in the form:

$$U(\theta,\phi) = U_{\theta,e}(\theta,\phi) \sum_{m=1}^{M}\sum_{n=1}^{N} b_{mn}(\theta,\phi)\exp[j\Psi_{mn}(\theta,\phi)]$$

$$X \exp\left[jk[(m-1)(\nu-\nu_0)+(n-1)(u-u_0)]\right] \qquad (3.8)$$

where for particular angles θ and ϕ, the apparent amplitude of the mn^{th} element is given by:

$$b_{mn}(\theta,\phi) = [U_{\theta,e;mn}(\theta,\phi)/U_{\theta,e}(\theta,\phi)]a'_{mn} \qquad (3.9)$$

and the apparent phase error term, $\Psi_{mn}(\theta,\phi)$, by:

$$\Psi_{mn}(\theta,\phi) = \delta_{mn} + k[x_{mn}-(m-1)d_x]\sin\theta\cos\phi$$

$$+ k[y_{mn}-(n-1)d_y]\sin\theta\sin\phi + kz_{mn}\cos\theta \qquad (3.10)$$

where $k = 2\pi/\lambda$.

Statistics of the Apparent Amplitude Error. We can write the element factor of the mn^{th} element for particular angles θ and ϕ as:

$$U_{\theta,e;mn}(\theta,\phi) = U_{\theta,e}(\theta,\phi)[1 + \mu_{mn}(\theta,\phi)] \qquad (3.11)$$

where the $\mu_{mn}(\theta,\phi)$ are samples of a random variable and are assumed to be normally distributed with a zero mean and variance $\sigma_\mu^2(\theta,\phi)$.

The amplitude error of the drive to the mn^{th} element is handled in a similar manner by assigning a random component, Δ_{mn}, to the drive amplitude. This is assigned in a multiplicative manner as (1:267):

$$a'_{mn} = (1 + \Delta_{mn})a_{mn} \tag{3.12}$$

where the Δ_{mn} are samples of a random variable and are assumed to be normally distributed with a zero mean and variance σ_Δ^2.

Adding a reliability factor, r_{mn}, we can write:

$$a'_{mn} = r_{mn}(1 + \Delta_{mn})a_{mn} \tag{3.13}$$

where $r_{mn} = 1$ with a probability P, and zero with probability $1 - P$. Finally, we can write (1:267):

$$b_{mn} = [1 + \mu_{mn}(\theta,\phi)][1 + \Delta_{mn}]r_{mn}a_{mn} \tag{3.14}$$

With these assumptions, we can write the mean and mean-square of the mn^{th} element's apparent amplitude as:

$$\overline{b_{mn}}(\theta,\phi) = a_{mn}P \tag{3.15}$$

and

$$\overline{b_{mn}^2}(\theta,\phi) = Pa_{mn}^2(1 + \sigma_\mu^2(\theta,\phi) + \sigma_\Delta^2 + \sigma_\mu^2(\theta,\phi)\sigma_\Delta^2) \tag{3.16}$$

Separating the catastrophic failure from the Δ_{mn} factor, the variances in the μ and Δ cross product term will be much less than unity in practice and their product can be ignored in (3.16) without much loss of accuracy (1:267). Letting:

$$\sigma_A^2(\theta,\phi) \approx \sigma_\mu^2(\theta,\phi) + \sigma_\Delta^2 \tag{3.17}$$

we can write equation (3.16) as:

$$\overline{b_{mn}^2}(\theta,\phi) = Pa_{mn}^2[1 + \sigma_A^2(\theta,\phi)] \tag{3.18}$$

where $\sigma_A^2(\theta,\phi)$ is the amplitude variance.

Statistics of the Apparent Phase Error. In finding the expected power pattern we will be taking the complex conjugate of equation (3.10), multiplying the result by equation (3.10), and then finding the average denoted by an overbar, such that:

$$\begin{aligned}\overline{\exp[j[\Psi_{mn}(\theta,\phi) - \Psi_{pq}(\theta,\phi)]]} &= \overline{\exp[j(\delta_{mn} - \delta_{pq})]} \\ &\times \overline{\exp[jk(x_{mn} - x_{pq})\sin\theta\cos\phi]} \\ &\times \overline{\exp[jk(y_{mn} - y_{pq})\sin\theta\sin\phi]} \\ &\times \overline{\exp[jk(z_{mn} - z_{pq})\cos\theta]}\end{aligned} \tag{3.19}$$

where it is assumed that δ_{mn}, δ_{pq}, x_{mn}, x_{pq}, y_{mn}, y_{pq}, z_{mn}, and z_{pq} are all statistically independent random variables (22:229).

Assuming that the phase error δ (we have dropped the subscripts for simplicity) is described by the gaussian probability density function with zero mean (22:230):

$$p_1(\delta) = [1/(2\pi\overline{\delta^2})^{1/2}]\exp[-\delta^2/(2\overline{\delta^2})] \tag{3.20}$$

where $\overline{\delta^2}$ is the variance (generally denoted σ^2) or mean-square value of the deviation about the average, which

average here is zero. The probability density function $p_1(\delta)$, when multiplied by the infinitesimal $d\delta$, gives the probability of finding the variable δ between the values of δ and $\delta + d\delta$. The gaussian probability density function is chosen because it is a good description of many types of errors that occur in practice (22:230). The gaussian assumption will be asymptotically true if the phase error δ is due to a number of causes and such errors are small so that a linear relation exists between the cause of the phase error and the error itself (22:230). By asymptotic, it is meant that as the sample size is increased, the dispersion in the associated sampling distribution of the mean decreases, reflecting the increased clustering of the sample means such that the gaussian distribution is obtained (18:302).

Let $y = \delta_{mn} - \delta_{pq}$ so that the problem becomes that of finding the average value of e^{jy}. From the definition of the average value we have (22:230):

$$\overline{\exp(jy)} = \int_{-\infty}^{\infty} \exp(jy)p(y)dy \qquad (3.21)$$

where p(y) is the probability density function for the variable y. The probability density function for δ is given by equation (3.20) and is needed in determining p(y). The variable y is a function of two independent variables δ_{mn} and δ_{pq} (we have defined them to be independent so long as

$m \neq p$, $n \neq q$). The joint probability density function for the two independent variables is the product of the individual variable's densities (22:230):

$$p(\delta_{mn}, \delta_{pq}) = p_1(\delta_{mn})p_1(\delta_{pq}) = p_1(y+\delta_{pq})p_1(\delta_{pq}) \qquad (3.22)$$

By substituting $p_1(\delta)$ given in equation (3.20) into the integral for p(y), we find the average value of e^{jy} to be (22:230):

$$\overline{\exp(jy)} = \int_{-\infty}^{\infty} \cos(y)p(y)dy + j \int_{-\infty}^{\infty} \sin(y)p(y)dy \qquad (3.23)$$

The second term is zero, provided the integral exists, since an odd function integrated from $-\infty$ to $+\infty$ is zero (sin(y) is an odd function, p(y) is an even function). Substituting the PDF of equation (3.20) into (3.23) and using (8:201)

$$\int_0^{\infty} \exp(-a^2x^2)\cos(2px)dx = [\pi^{1/2}/(2a)]\exp(-p^2/a^2) \qquad (3.24)$$

to perform the integration on the first integral, we find (22:230):

$$\overline{\exp(jy)} = \overline{\cos(y)} = \exp(-\overline{\delta^2}) \qquad (3.25)$$

Following a similar procedure for the second term averaged in equation (3.19), using (3.24), we find:

$$\overline{\exp[jk(x_{mn}-x_{pq})\sin\theta\cos\phi]} = \overline{\exp(jk\gamma_x\sin\theta\cos\phi)}$$

$$= \exp\left[\overline{\gamma_x^2}k^2\sin^2(\theta)\cos^2(\phi)\right] \qquad (3.26)$$

Similarly:

$$\overline{\exp(jk\gamma_y \sin\theta \sin\phi)} = \exp\left[\overline{\gamma_y^2} k^2 \sin^2(\theta)\sin^2(\phi)\right] \quad (3.27)$$

and:

$$\overline{\exp(jk\gamma_z \cos\theta)} = \exp\left[\overline{\gamma_z^2} k^2 \cos^2(\theta)\right] \quad (3.28)$$

where $\gamma_y = y_{mn} - y_{pq}$ and $\gamma_z = z_{mn} - z_{pq}$.

Power Pattern

The power, or radiation, pattern is:

$$|U(\theta,\phi)|^2 = U(\theta,\phi)U^*(\theta,\phi)$$

$$= U_{\theta,e}^2(\theta,\phi) \sum_{m=1}^{M}\sum_{n=1}^{N}\sum_{p=1}^{M}\sum_{q=1}^{N} b_{mn}(\theta,\phi) b_{pq}^*(\theta,\phi)$$

$$X \exp\left[j\left[\Psi_{mn}(\theta,\phi) - \Psi_{pq}(\theta,\phi)\right]\right]$$

$$X \exp[j(m-p)(\nu-\nu_0)]\exp[j(n-q)(u-u_0)] \quad (3.29)$$

Substituting equation (3.14) for $b_{mn}(\theta,\phi)$ and a similar expression in terms of p and q for $b_{pq}^*(\theta,\phi)$ into (3.29) we get:

$$|U(\theta,\phi)|^2 = U^2_{\theta,e}(\theta,\phi)$$

$$X \sum_{m=1}^{M}\sum_{n=1}^{N}\sum_{p=1}^{M}\sum_{q=1}^{N}{}' \left[[1 + \mu_{mn}(\theta,\phi)](1 + \Delta_{mn}) r_{mn} a_{mn}\right]$$

$$X \left[[1 + \mu_{pq}(\theta,\phi)](1 + \Delta_{pq}) r_{pq} a^*_{pq}\right]$$

$$X \exp\left[j[\Psi_{mn}(\theta,\phi) - \Psi_{pq}(\theta,\phi)]\right]$$

$$X \exp\left[j[(m - p)(\nu - \nu_0) + (n - q)(u - u_0)]\right] \tag{3.30}$$

This power pattern is a random quantity since r, Δ, μ, and Ψ are random variables. Now, we want to obtain the average power pattern. To start, we must separate the summation into two parts by separating those terms in which $m = p$, $n = q$ from the remaining terms in which $m \neq p$, $n \neq q$. This is done so we can apply an axiom in probability theory which states that the mean of a product of statistically independent random variables is equal to the product of the means of these random variables. The variables Δ_{mn}, Δ_{pq}, $\mu_{mn}(\theta,\phi)$, $\mu_{pq}(\theta,\phi)$, $\Psi_{mn}(\theta,\phi)$, $\Psi_{pq}(\theta,\phi)$ are independent if and only if $m \neq p$, $n \neq q$ (22:229).

Considering only those terms in the power pattern which are statistically independent and applying the aforementioned axiom yields:

$$\overline{|U(\theta,\phi)|^2_{m\neq p,n\neq q}} = U^2_{\theta,e}(\theta,\phi)P^2 \sum_{\substack{m=1\\(m\neq p,n\neq q)}}^{M}\sum_{n=1}^{N}\sum_{p=1}^{M}\sum_{q=1}^{N} a_{mn}a^*_{pq}$$

$$X\ \overline{\exp[(\delta_{mn}-\delta_{pq}) + k(x_{mn}-x_{pq})\sin\theta\cos\phi}$$

$$+ \overline{k(y_{mn}-y_{pq})\sin\theta\sin\phi + k(z_{mn}-z_{pq})\cos\theta]}$$

$$X\ \exp[j(m - p)(\nu - \nu_0)]$$

$$X\ \exp[j(n - q)(u - u_0)] \qquad (3.31)$$

where

$$\overline{b_{mn}} = Pa_{mn} \qquad (3.15)$$

and

$$\overline{b^*_{pq}} = Pa^*_{pq} \qquad (3.32)$$

have been used. In obtaining equation (3.31) we assumed Δ_{mn} and $\mu_{mn}(\theta,\phi)$ are zero mean and that $r_{mn} = P$ (22:230). Substituting equations (3.25), (3.26), (3.27), and (3.28) into equation (3.31), we can write:

$$\overline{|U(\theta,\phi)|^2_{m\neq p,n\neq q}} = U^2_{\theta,e}(\theta,\phi)P^2 \sum_{\substack{m=1\\(m\neq p,n\neq q)}}^{M}\sum_{n=1}^{N}\sum_{p=1}^{M}\sum_{q=1}^{N} a_{mn}a^*_{pq}$$

$$X\ \exp(-\overline{\delta^2})\ \exp(-\overline{\gamma_x^2}k^2\sin^2\theta\cos^2\phi)$$

$$X\ \exp(-\overline{\gamma_y^2}k^2\sin^2\theta\sin^2\phi)\ \exp(-\overline{\gamma_z^2}k^2\cos^2\theta)$$

$$X\ \exp[j(m - p)(\nu - \nu_0)]$$

$$X\ \exp[j(n - q)(u - u_0)] \qquad (3.33)$$

Now for the terms m =p and n = q, we find:

$$\overline{|U(\theta,\phi)|^2_{m=p,n=q}} = U^2_{\theta,e}(\theta,\phi) \sum_{m=1}^{M} \sum_{n=1}^{N} \overline{b^2_{mn}(\theta,\phi)} \qquad (3.34)$$

where $\overline{b^2_{mn}(\theta,\phi)}$ is given by equation (3.18). We can write equation (3.34) as:

$$\overline{|U(\theta,\phi)|^2_{m=p,n=q}} = U^2_{\theta,e}(\theta,\phi) P\left[1 + \sigma^2_A(\theta,\phi)\right] \sum_{m=1}^{M}\sum_{n=1}^{N} a^2_{mn} \qquad (3.35)$$

The average power pattern is the sum of the m ≠ p, n ≠ q and m =p, n =q terms (22:231):

$$\begin{aligned}\overline{|U(\theta,\phi)|^2} &= U^2_{\theta,e}(\theta,\phi) P^2 \exp(-\overline{\delta^2}) \\ &\quad X \exp\left[-k^2 (\overline{\gamma^2_x}\sin^2\theta\cos^2\phi + \overline{\gamma^2_y}\sin^2\theta\sin^2\phi + \overline{\gamma^2_z}\cos^2\theta)\right] \\ &\quad X \sum_{\substack{m=1 \\ (m\neq p,n\neq q)}}^{M}\sum_{n=1}^{N}\sum_{p=1}^{M}\sum_{q=1}^{N} a_{mn}a^*_{pq} \\ &\quad X \exp\left[j\left[(m-p)(\nu-\nu_0) + (n-q)(u-u_0)\right]\right] \\ &\quad + U^2_{\theta,e}(\theta,\phi)\left[1 + \sigma^2_A(\theta,\phi)\right] \sum_{m=1}^{M}\sum_{n=1}^{N} a^2_{mn} \qquad (3.36)\end{aligned}$$

In order to simplify matters, we will let:

$$\begin{aligned}\Psi_{AP}(\theta,\phi) &= \exp\left[-\left[\overline{\delta^2} + k^2(\overline{\gamma^2_x}\sin^2\theta\cos^2\phi\right.\right. \\ &\qquad \left.\left. + \overline{\gamma^2_y}\sin^2\theta\sin^2\phi + \overline{\gamma^2_z}\cos^2\theta)\right]\right] \qquad (3.37)\end{aligned}$$

Adding the terms m = p and n = q to the first summation and subtracting them as separate terms, so as not to include them twice, the average power pattern becomes (22:231):

$$\overline{|U(\theta,\phi)|^2} = P^2\ \Psi_{AP}(\theta,\phi)\ U^2_{\theta,e}(\theta,\phi)$$

$$X \sum_{m=1}^{M}\sum_{n=1}^{N}\sum_{p=1}^{M}\sum_{q=1}^{N} a_{mn}a^*_{pq}$$

$$X\ \exp\Big[j\big[(m-p)(\nu-\nu_0) + (n-q)(u-u_0)\big]\Big]$$

$$+ U^2_{\theta,e}(\theta,\phi)\Big[\big[1+\sigma^2_A(\theta,\phi)\big]P - P^2\Psi_{AP}(\theta,\phi)\Big]$$

$$X \sum_{m=1}^{M}\sum_{n=1}^{N} a^2_{mn} \qquad (3.38)$$

Simplifying, we find:

$$\overline{|U(\theta,\phi)|^2} = P^2\ \Psi_{AP}(\theta,\phi)\ |U_0(\theta,\phi)|^2 + U^2_{\theta,e}(\theta,\phi)$$

$$X\ \Big[\big[1+\sigma^2_A(\theta,\phi)\big]P - P^2\Psi_{AP}(\theta,\phi)\Big]\sum_{m=1}^{M}\sum_{n=1}^{N} a^2_{mn} \qquad (3.39)$$

Equation (3.39) is the sought for result of our analysis. This equation has the same form as Allen's equation (82) for a linear array (1:288). The effect of random errors is to produce an average power pattern that is the superposition of two terms. The first term is the no-error power pattern multiplied by the fraction of the elements remaining and the apparent phase error. The second term depends on the apparent amplitude and phase errors and the fraction of elements remaining and is directional only by the element factor and the terms in the apparent phase error.

Random Error Effects on Array Directivity

In order to predict the effect of random errors on the array's directivity, it is useful to formulate the average power pattern of the array normalized to a no-error peak value of unity (1:287). Then, by definition, the average power pattern is:

$$\overline{P(\theta,\phi)} = \overline{U(\theta,\phi)U^{*}(\theta,\phi)} = \overline{|U(\theta,\phi)|^{2}} \qquad (3.40)$$

where $\overline{|U(\theta,\phi)|^{2}}$ is given by equation (3.39). In preparation for what follows, in equation (3.39) let:

$$A(\theta,\phi) = 1 + \sigma_{A}^{2}(\theta,\phi) - P\Psi_{AP}(\theta,\phi) \qquad (3.41)$$

so that equation (3.39) becomes:

$$\overline{|U(\theta,\phi)|^{2}} = P^{2}\Psi_{AP}(\theta,\phi)|U_{0}(\theta,\phi)|^{2} + U_{\theta,e}^{2}(\theta,\phi)P\,\bar{A}(\theta,\phi)\sum_{m=1}^{M}\sum_{n=1}^{N} a_{mn}^{2} \qquad (3.42)$$

Now, for the directivity calculation the absolute value of $\overline{|U(\theta,\phi)|^{2}}$ is immaterial, so we can divide equation (3.42) by $P^{2}\Psi_{AP}(\theta,\phi)$ and use the form (1:287):

$$\overline{|U(\theta,\phi)|^{2}} = |U_{0}(\theta,\phi)|^{2} + \left[U_{\theta,e}^{2}(\theta,\phi)/P\right]\epsilon^{2}(\theta,\phi)\sum_{m=1}^{M}\sum_{n=1}^{N} a_{mn}^{2} \qquad (3.43)$$

where:

$$\epsilon^{2}(\theta,\phi) = A(\theta,\phi)/\Psi_{AP}(\theta,\phi) \qquad (3.44)$$

If we define a no-error efficiency (η) of the array amplitude taper as (1:274-275):

$$\eta = \left[\sum_{m=1}^{M}\sum_{n=1}^{N} a_{mn}\right]^2 / \left[MN \sum_{m=1}^{M}\sum_{n=1}^{N} a_{mn}^2\right] \tag{3.45}$$

we will obtain (1:288):

$$\sum_{m=1}^{M}\sum_{n=1}^{N} a_{mn}^2 = \left[\sum_{m=1}^{M}\sum_{n=1}^{N} a_{mn}\right]^2 / (\eta MN) \tag{3.46}$$

and:

$$\sum_{m=1}^{M}\sum_{n=1}^{N} a_{mn}^2 = |U_0(\theta_0,\phi_0)|^2 / U_{\theta,e}^2(\theta_0,\phi_0)\eta MN \tag{3.47}$$

so that:

$$|U_0(\theta_0,\phi_0)|^2 = \left[U_{\theta,e}^2(\theta_0,\phi_0)\right]\left[\sum_{m=1}^{M}\sum_{n=1}^{N} a_{mn}\right]^2 \tag{3.48}$$

Therefore, we can write equation (3.43) as (1:288):

$$\overline{|U(\theta,\phi)|^2} = |U_0(\theta,\phi)|^2 + |U_0(\theta_0,\phi_0)|^2 \times \left[\left[U_{\theta,e}^2(\theta,\phi)\epsilon^2(\theta,\phi)\right] / \left[U_{\theta,e}^2(\theta_0,\phi_0)\eta MNP\right]\right] \tag{3.49}$$

Allen states that:

> We have previously seen that the percentage pattern error near the beam maximum is trivial, or else the Central Limit Theorem is not applicable. Further, if the array is large and the correlation interval of the far-field is small, we would expect that the total radiated power would vary minutely from the average for nearly all such arrays. Thus, one would expect that a directivity value derived using (84) as the actual power density distribution over all space would be a satisfactory approximation. (1:288)

Allen is speaking from the context of his paper where he has shown that the percentage pattern error near the main beam

is trivial. The equation number (84) is the same, in form, as equation (3.49) presented in this paper.

The main beam directivity is given by:

$$D(\theta_0,\phi_0) = 4\pi|U(\theta_0,\phi_0)|^2 / \iint_{\substack{All\\Space}}|U(\theta,\phi)|^2 d\Omega \qquad (3.50)$$

where:

$$d\Omega = \sin\theta d\theta d\phi \qquad (3.51)$$

Substituting equation (3.49) into (3.50), we find:

$$D(\theta_0,\phi_0) = 4\pi|U_0(\theta_0,\phi_0)|^2 \div \left[\iint |U_0(\theta,\phi)|^2 d\Omega + \left[|U_0(\theta,\phi)|^2 / \eta MNP \right] X \iint \epsilon^2(\theta,\phi) \left[U^2_{\theta,e}(\theta,\phi) / U^2_{\theta,e}(\theta_0,\phi_0) \right] d\Omega \right] \qquad (3.52)$$

In deriving (3.52) it was assumed that the statistical side lobe level can be neglected compared to the peak intensity so that the second term in (3.49) can be disregarded in the numerator of (3.52)(1:288;22:233). We can denote the no-error directivity as $D_0(\theta_0,\phi_0)$ and divide numerator and denominator of equation (3.52) by $4\pi|U_0(\theta_0,\phi_0)|^2$ and we have:

$$D(\theta_0,\phi_0) = \left[\left[1/D_0(\theta_0,\phi_0) \right] + (1/4\pi\eta MNP) X \iint \epsilon^2(\theta,\phi) \left[U^2_{\theta,e}(\theta,\phi) / U^2_{\theta,e}(\theta_0,\phi_0) \right] d\Omega \right]^{-1} \qquad (3.53)$$

Before we proceed, let us consider the angle dependence of $\epsilon^2(\theta,\phi)$. We remember that $A(\theta,\phi)$ depends upon $\sigma_A^2(\theta,\phi)$ which contains two terms:

$$\sigma_A^2(\theta,\phi) \approx \sigma_\mu^2(\theta,\phi) + \sigma_\perp^2 \qquad (3.17)$$

The term σ_Δ^2 is angle invariant. However, note that the term $\sigma_\mu^2(\theta,\phi)$, the element factor variance about its average, may vary with angle and may well become larger, as $U_{\theta,e}(\theta,\phi)$ becomes small (in the side lobe region of the element) (1:289). Now we need to examine the angle dependence of $\Psi_{AP}(\theta,\phi)$:

$$\Psi_{AP}(\theta,\phi) = \exp\left[-\left[\overline{\delta^2} + k^2\left(\overline{\gamma_x^2}\sin^2\theta\cos^2\phi + \overline{\gamma_y^2}\sin^2\theta\sin^2\phi + \overline{\gamma_z^2}\cos^2\theta\right)\right]\right] \qquad (3.37)$$

where, again, $\overline{\gamma_x^2}$, $\overline{\gamma_y^2}$, and $\overline{\gamma_z^2}$ are the variances in element radiation center location. Allen notes that, if all the variances are roughly equal, then the angle dependence of $\Psi_{AP}(\theta,\phi)$ vanishes and we can write (1:289):

$$\Psi_{AP} = \exp\left[-(\delta^2 + k^2\overline{\gamma_x^2})\right] \qquad (3.54)$$

All the angular dependence of ϵ^2 has now been considered.

Thus, $\epsilon^2(\theta,\phi)$ is only weakly angle dependent (1:289) and we can write (1:289):

$$\begin{aligned}(1/4\pi)\iint\left[U_{\theta,e}^2(\theta,\phi)/U_{\theta,e}^2(\theta_0,\phi_0)\right]d\Omega &= \left[4\pi U_{\theta,e}^2(\theta_0,\phi_0)/\iint U_{\theta,e}^2(\theta,\phi)\,d\Omega\right]^{-1} \\ &= \left[d(\theta_0,\phi_0)\right]^{-1} \qquad (3.55)\end{aligned}$$

where $d(\theta_0,\phi_0)$ is the element directivity in the θ_0,ϕ_0 direction. Hence:

$$D(\theta_0,\phi_0) = \left[1/D_0(\theta_0,\phi_0) + \epsilon^2/\left[d(\theta_0,\phi_0)\eta MNP\right]\right]^{-1} \quad (3.56)$$

Allen states we can write the no-error array directivity as (1:289):

$$D_0(\theta_0,\phi_0) = d(\theta_0,\phi_0)\eta MN \quad (3.57)$$

assuming an array with at least 25 elements (1:208). Thus we can write our final result as (1:290):

$$D(\theta_0,\phi_0) = D_0(\theta_0,\phi_0)\left[1 + (\epsilon^2/P)\right]^{-1} \quad (3.58)$$

Summary

We have derived the average radiation pattern for a planar array to include translational errors in the positions of the elements, errors in the element's drive amplitude and phase, and the probability of the average fractional number of elements that remain operating. We have also considered the effects of non-identical element patterns on the overall radiation pattern. We saw that the average radiation pattern consists of two terms. One term is the no-error radiation pattern of the array modified by the square of the fraction of elements remaining and by a factor proportional to the apparent phase error. The second term depends on both the apparent amplitude and phase errors, the fraction of elements remaining, and the element pattern factor. It also depends on the array's excitation. Lastly, we derived an expression showing the effects of random errors on the array's directivity. In Chapter IV, we will

convert the theory of this chapter and Chapter II into FORTRAN code in order to rapidly assess the effects of random errors on certain performance characteristics of the array under consideration.

IV. Program Mechanics

The main objective of this project was to write a FORTRAN program that emulates the theory of the last two chapters, whereby, the antenna designer or program manager can assess the performance of their array antenna based on the theoretical design and the actual design with tolerances. This chapter explains the program that was written to perform the analysis. We begin the chapter with the overall layout of the program, followed by the program development and validation. We will specifically look at what was used to calculate a particular performance standard or obtain data points for a pattern plot.

Program Layout

The software written for this project consists of one main program and 27 subprograms. A list of the programs is in Appendix B. The main program (PARRAY.FOR) controls the order of processing while the other subprograms perform all the calculations. The program is intended to be user friendly, efficient, general enough to consider all types of arrays, and to run on a personal computer. However, there were two compromises involved in writing the program. The first compromise was between efficiency and being general enough to consider all design cases that could arise. We will get to some specific cases a little later in the chapter. The second compromise involves the FORTRAN language

and creating a user friendly program. Through the course of the program the user is prompted to enter certain data. Some of this data is entered as integers (numbers without decimals) and some as real numbers (numbers with decimals). If a real number is entered when an integer is asked for, the program terminates with a DOS run time error. So, care must be used when entering data. The program does specify what type of number to enter. Also, along the lines of being user friendly, each time the user enters a datum, that datum is returned by the program for the user to verify before proceeding. This ensures that the user has input the right number or action so that time is not wasted calculating performance standards for erroneous data. Now we will take a look at the overall layout of the program.

The program can be broken down into five parts. The first part consists of the data entry routines. The user inputs the center operating frequency or wavelength and the bandwidth of operation and the number of elements, interelement spacing, and type of pattern synthesis in the x- and y-directions of the planar array. The user also selects the type of array element to be used and its orientation and length if required. Finally, the user inputs all of the tolerance data for the expected array. The second part of the program consists of the pattern calculation routines. In this part, the program calculates the data points to allow plotting the design and expected array patterns at a

later time, if so requested. The data points for the patterns in the xz- and yz-planes can be calculated for both the design and expected arrays at the upper, center, and lower frequencies of the specified bandwidth. In all, twelve files can be produced. The user can import these ASCII files into any plotting routine, and once plots are made, can compare side lobe levels of the design array pattern to those of the expected array pattern. As previously alluded to, the user does have a choice as to which frequencies of the bandwidth the pattern data points are calculated. The third part of the program consists of the half-power beamwidth calculation routines. Before any calculations are made, however, the program prompts the user to enter the initial scan angles. After the scan angles are entered and verified, the half-power beamwidths for the design and expected arrays are calculated at the upper, center, and lower frequencies of the bandwidth. The fourth part of the program contains the directivity calculation routines. The directivities of the design array and the change in directivity due to errors for the expected array are calculated at the upper, center, and lower frequencies of the bandwidth. The last part of the program sends all data compiled to an output file and prompts the user on whether to continue for new scan angles. If the user elects to recompute the beamwidths and directivities for new scan angles, the program returns to the third part and the pro-

cess begins again. Otherwise, the program terminates. In the next section, we will discuss the specifics of how certain standards and data are calculated.

Program Development

In this section we will discuss the development of the main program and the subprograms and will list the routine names as they are covered. It is important at this point to recall that the array lies in the xy-plane with one side of the array extending down the positive x-axis and the other side down the positive y-axis as shown in Figure 15. The first element in either the x- or y-direction lies at the origin. Let us begin by looking at the first part of the program, the data entry and element excitation routines.

Part 1 - Data Entry and Element Excitation Routines.

The program (PARRAY.FOR) begins by asking for the center operating frequency or wavelength. The frequency is entered in hertz and the wavelength in centimeters. Also, all responses to the program prompts are returned for the user to verify to ensure the proper data was entered. Next, the user is asked to enter the bandwidth of operation. The bandwidth of operation is as defined Chapter I. If the user elects to enter frequencies, there is no problem. ver, if wavelengths are chosen, then the user must understand that the wavelength bandwidth is not the same as the frequency bandwidth. The user must also understand that the lower wavelength gives the upper frequency and the upper

wavelength gives the lower frequency. Again, the user is asked to verify the bandwidth, either in frequencies or wavelengths. The next step is to enter the array specifications in the x-direction. First, the user enters the number of elements in the x-direction followed by the interelement spacing. Then the user selects the type of excitation scheme desired. The choices are: (1) Dolph-Chebyshev synthesis (CHEBY.FOR), (2) Taylor $\bar{n}$-parameter synthesis (TAYLOR.FOR), (3) User Defined current distribution (USRDEF.FOR), (4) Binomial current distribution (BINOML.FOR), and (5) Uniform current distribution (UNIFRM.FOR). Each one of these excitation schemes, except of course the user defined scheme, was discussed at length in Chapter II. The respective equations from Chapter II were implemented for the Dolph-Chebyshev and Taylor $\bar{n}$-parameter synthesis methods and the Binomial and Uniform current distribution schemes. If one of these four schemes does not suit the user, then the user defined scheme will allow the user to input the element weights. If the Dolph-Chebyshev synthesis method is chosen, the user must enter the desired side lobe level. Recalling the theory of Chapter II, the side lobe level is entered as a positive number (in decibels) and CHEBY.FOR does check to see that it is a positive number. If the Taylor $\bar{n}$-parameter synthesis method is chosen, the user must enter the $\bar{n}$-parameter and the desired side lobe level. The user is given an appropriate range for

$\bar{n}$ based on the array's length and operating wavelength for reasons explained in Chapter II. After $\bar{n}$ is entered and verified the desired side lobe level is entered following the guidelines in Chapter II, Discretized Taylor $\bar{n}$-parameter Linear Array Method section. After the weights are calculated the user will have to decide whether to use the aperture sampling weights or the null matching weights. Guidelines for deciding which weights to use are located in Chapter 2. The binomial and uniform current distribution routines are automatic. If the user selects the user defined routine, then the element weights are entered one at a time beginning at the origin and progressing down the x-axis to the end of the array. Finally, this program can analyze linear arrays. Therefore, if the number of elements in the x-direction equals one, the program skips directly to the uniform current distribution routine. Now if there are two elements in the x-direction, then the program prompts the user for the distance between them, then skips directly to the uniform current distribution routine. This entire process is repeated for the y-direction.

After the array specifications are entered, PARRAY.FOR calls the element data routine (ELDATA.FOR). Here, the user is asked to select the type of element to be used in the array. The user has four choices: (1) a dipole oriented in the x-direction, (2) a dipole oriented in the y-direction, (3) a dipole oriented in the z-direction, and (4) an isotro-

pic element. If a dipole is selected, the user is asked to enter the dipole's length in centimeters.

After ELDATA.FOR returns control to PARRAY.FOR, PARRAY.FOR calls the error data routine (ERDATA.FOR). In this routine, the user is prompted for the array tolerance data. The user first enters the RMS amplitude error. Referring to equation (3.17) this is the term "σ_Δ" which is the standard deviation while the term "σ_Δ^2" is the variance or mean square value. Next, the user enters the RMS phase error in degrees. This term is converted to become the term "$\overline{\delta^2}$" in equation (3.37). Then in succession, the user enters the RMS error in the x, y, and z placement of the element. These three terms become $\overline{\gamma_x^2}$, $\overline{\gamma_y^2}$, and $\overline{\gamma_z^2}$, respectively, in equation (3.37). Next, the user enters the RMS element pattern error in decibels which is the term $\sigma_\mu(\theta,\phi)$ in equation (3.17). Lastly, the user enters the fraction of elements actually operating in the array. After all data is entered and verified, control is once again returned to PARRAY.FOR.

Part 2 - Radiation Pattern Calculations. The second part of the program deals with generating the pattern plots for the design and expected arrays. There are six routines involved in this part of the program.

The data for the design radiation pattern plots are generated by the routine DESRP.FOR. DESRP.FOR repeatedly calls the subroutine PARFAC.FOR and the function ELFAC.FOR

to calculate each data point in the pattern. PARFAC.FOR implements equation (2.73) while ELFAC.FOR implements equation (A.6), (A.12), or (A.15) depending on the orientation of the dipole. Obviously, if an isotropic element is used, then ELFAC.FOR returns a value of 1.0 for each angle. The routine DESRP.FOR calculates data points for the pattern in the upper xz-plane from ϕ=180°, θ=90° to ϕ=0°, θ=90°. This gives the radiation pattern due to elements along the x-axis. Data points for a pattern in the upper yz-plane are also calculated giving the radiation pattern due to the elements along the y-axis. The routine DESRP.FOR also gives the user the ability to scan the main beam in the theta direction in both the xz- or yz-planes. The program automatically sets ϕ_0 to 0° for the xz-plane pattern and to 90° for the yz-plane pattern.

The data calculated for the expected radiation pattern plots are generated by the routine AVERP.FOR. AVERP.FOR repeatedly calls the subroutine EXPRPF.FOR to calculate each data point for the pattern. The routine EXPRPF.FOR implements equation (3.39). EXPRPF.FOR repeatedly calls PARFAC.FOR and ELFAC.FOR to calculate the no error pattern in equation (3.39). AVERP.FOR follows the same process as DESRP.FOR.

The user is given the option of generating up to 12 different sets of data to later produce 12 separate plots. The user is asked if data points for the design and expected

radiation patterns are desired at the center frequency or wavelength of the operating band. If requested, four sets of data are generated, two sets for the design pattern (xz- and yz-planes) and two sets for the expected pattern (xz- and yz-planes). After these data sets are calculated, the user is asked if data sets are wanted for the lower frequency and then the upper frequency of the bandwidth. The names of the 12 files generated and their descriptions are shown below.

Filename	Description
DESRP1X.DAT	Design radiation pattern data at the center frequency along the x-axis
DESRP2X.DAT	Design radiation pattern data at the upper frequency along the x-axis
DESRP3X.DAT	Design radiation pattern data at the lower frequency along the x-axis
DESRP1Y.DAT	Design radiation pattern data at the center frequency along the y-axis
DESRP2Y.DAT	Design radiation pattern data at the upper frequency along the y-axis
DESRP3Y.DAT	Design radiation pattern data at the lower frequency along the y-axis
EXPRP1X.DAT	Expected radiation pattern data at the center frequency along the x-axis

Filename	Description
EXPRP2X.DAT	Expected radiation pattern data at the upper frequency along the x-axis
EXPRP3X.DAT	Expected radiation pattern data at the lower frequency along the x-axis
EXPRP1Y.DAT	Expected radiation pattern data at the center frequency along the y-axis
EXPRP2Y.DAT	Expected radiation pattern data at the upper frequency along the y-axis
EXPRP3Y.DAT	Expected radiation pattern data at the lower frequency along the y-axis

The data stored in each file is normalized to the pattern maximum. Also, the data stored in the design and expected radiation pattern data files is for the normalized pattern factor squared or $|F(\theta,\phi)|^2$.

Part 3 - Design and Expected Beamwidth Calculations. Generally, the task of finding the beamwidth of planar arrays is quite difficult. However, with a computer this task can be greatly simplified as we will show directly. This method is accurate for any array scanned in any direction.

We will assume that the maximum of the main beam is scanned in a direction toward θ_0,ϕ_0. To define the beamwidth two planes within the main beam are chosen. One plane is the elevation plane defined by the angle $\phi = \phi_0$; the other plane is perpendicular to it and contains the origin

of the coordinate system. The corresponding half-power beamwidth of each plane is designated, respectively, by Θ_h and Ψ_h as shown in Figure 1 (4:270).

The easiest way to calculate the respective beamwidths is by defining a new coordinate system to align with the direction of the main beam, such that, the z-axis is once again aligned along the boresight of the main beam as it would be for a broadside array. We wish to express the spherical angles θ and ϕ in terms of θ' and ϕ' with the pointing angles θ_0 and ϕ_0 supplied by the user. This geometry is shown in Figure 16. The angles θ_0 and ϕ_0 are Eulerian angles that produce two rotations in the cartesian coordinate system to align a new primed cartesian coordinate system along the main beam (15:107-109). Once this translation takes place, the pattern cuts can be taken in the x'z'- and y'z'-planes to obtain Θ_h and Ψ_h. First consider the relationships between the coordinates (x,y,z) and (x_1,y_1,z_1). The (x_1,y_1,z_1) coordinate system is the (x,y,z) system rotated ϕ_0 about the z-axis so:

$$x = x_1\cos\phi_0 - y_1\sin\phi_0 \tag{4.1}$$

$$y = x_1\sin\phi_0 + y_1\cos\phi_0 \tag{4.2}$$

$$z = z_1 \tag{4.3}$$

This step is depicted in Figure 17(a). We can express (4.1), (4.2), and (4.3) in matrix form as:

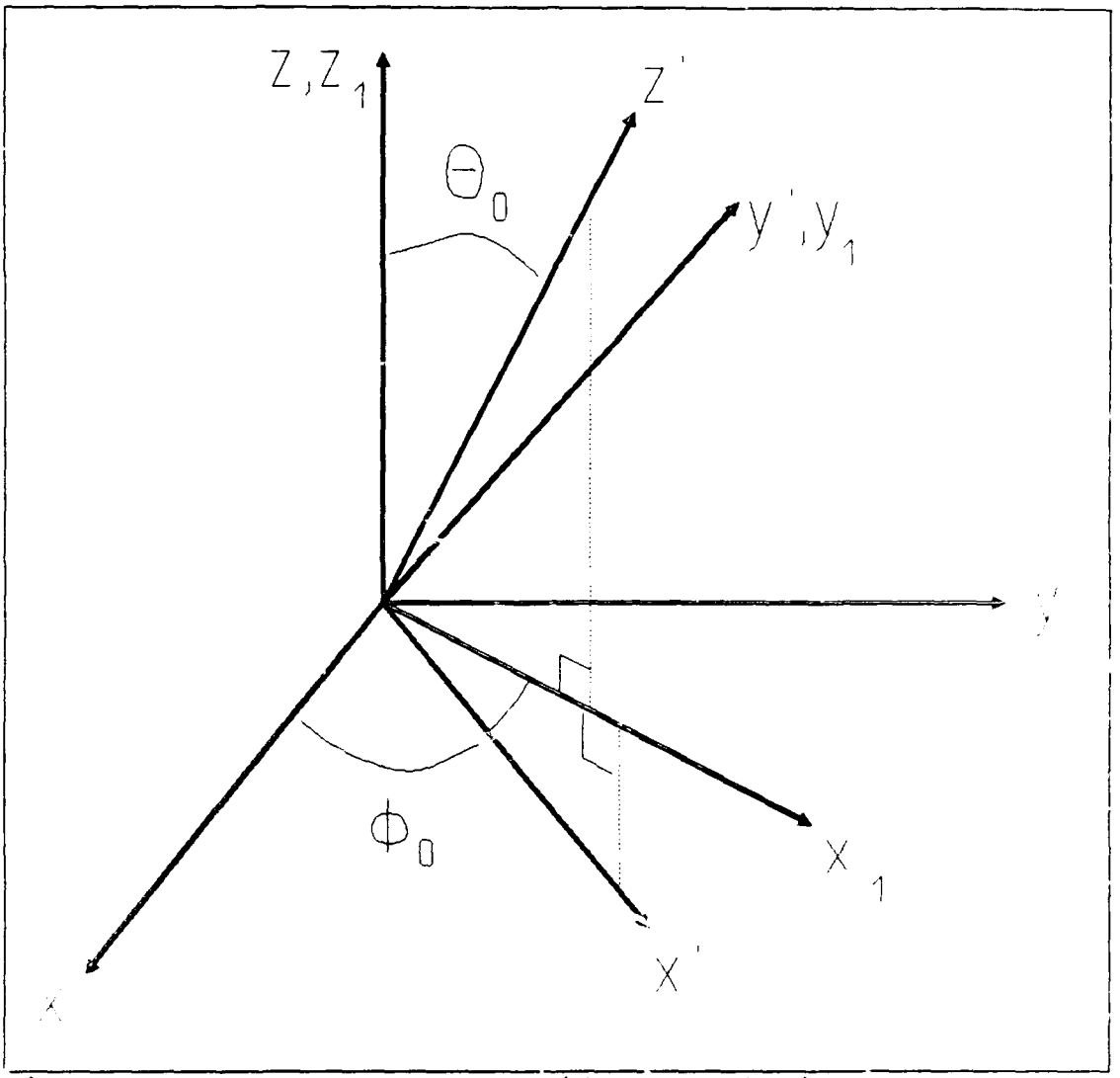

Figure 16. Geometry for beamwidth calculations

$$\begin{bmatrix} x \\ y \\ z \end{bmatrix} = \begin{bmatrix} \cos\phi_0 & -\sin\phi_0 & 0 \\ \sin\phi_0 & \cos\phi_0 & 0 \\ 0 & 0 & 1 \end{bmatrix} \begin{bmatrix} x_1 \\ y_1 \\ z_1 \end{bmatrix} \qquad (4.4)$$

Now consider the relationships between the coordinates (x_1, y_1, z_1) and (x', y', z'). The (x', y', z') coordinate system is the (x_1, y_1, z_1) system rotated θ_0 about the y_1 axis. So:

$$x_1 = x'\cos\theta_0 + z'\sin\theta_0 \tag{4.5}$$

$$y_1 = y' \tag{4.6}$$

$$z_1 = -x'\sin\theta_0 + z'\cos\theta_0 \tag{4.7}$$

This translation is depicted in Figure 17(b). We can write equations (4.5), (4.6), and (4.7) in matrix form as:

$$\begin{bmatrix} x_1 \\ y_1 \\ z_1 \end{bmatrix} = \begin{bmatrix} \cos\theta_0 & 0 & \sin\theta_0 \\ 0 & 1 & 0 \\ -\sin\theta_0 & 0 & \cos\theta_0 \end{bmatrix} \begin{bmatrix} x' \\ y' \\ z' \end{bmatrix} \tag{4.8}$$

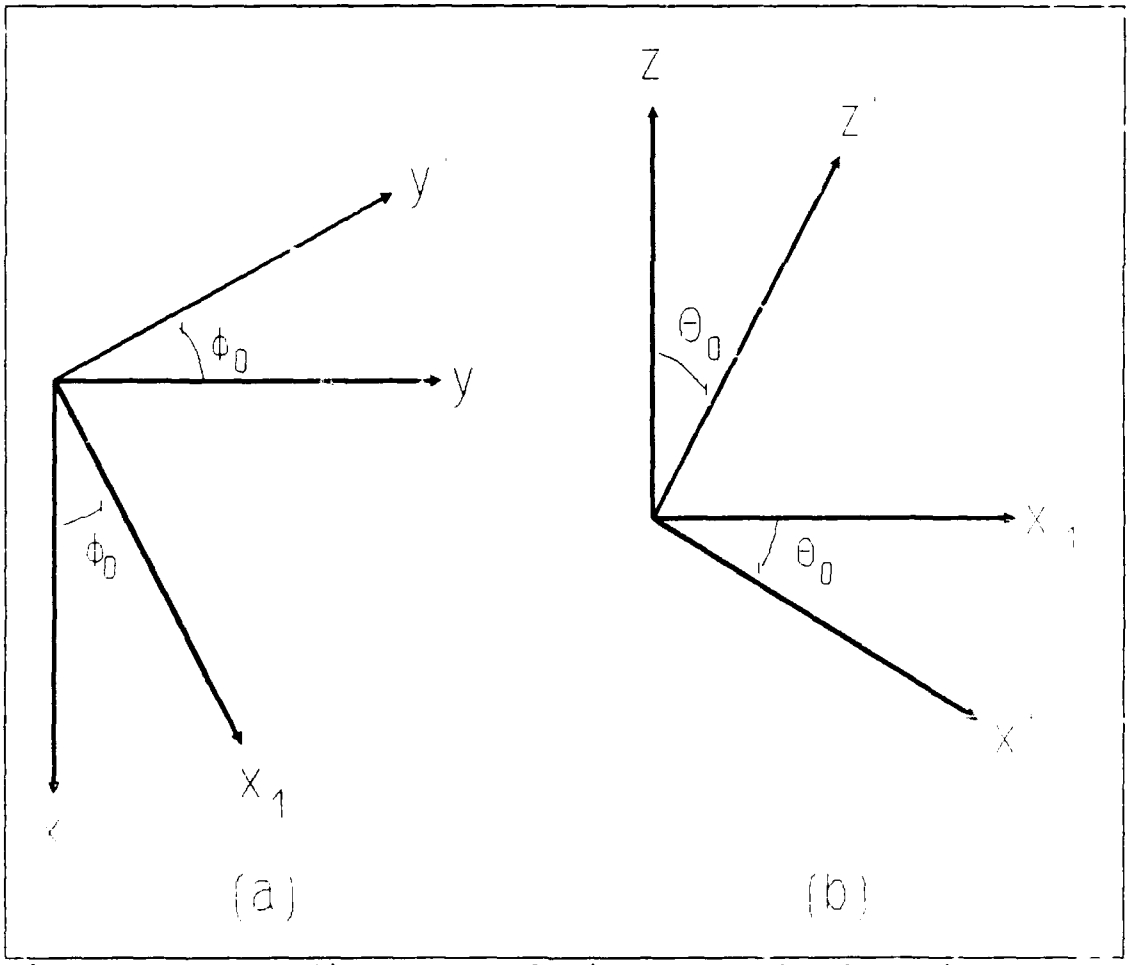

Figure 17. Coordinate translation steps for beamwidth calculations

Combining equations (4.4) and (4.8) yields:

$$\begin{bmatrix} x \\ y \\ z \end{bmatrix} = \begin{bmatrix} \cos\phi_0\cos\theta_0 & -\sin\phi_0 & \cos\phi_0\sin\theta_0 \\ \sin\phi_0\cos\theta_0 & \cos\phi_0 & \sin\phi_0\sin\theta_0 \\ -\sin\theta_0 & 0 & \cos\theta_0 \end{bmatrix} \begin{bmatrix} x' \\ y' \\ z' \end{bmatrix} \quad (4.9)$$

Now consider a vector of length R drawn from the origin to a point in space. The point has the coordinates:

$$\begin{aligned} x &= R\sin\theta\cos\phi \\ y &= R\sin\theta\sin\phi \\ z &= R\cos\theta \end{aligned} \quad (4.10)$$

in the (x,y,z) system and:

$$\begin{aligned} x' &= R\sin\theta'\cos\phi' \\ y' &= R\sin\theta'\sin\phi' \\ z' &= R\cos\theta' \end{aligned} \quad (4.11)$$

in the (x',y',z') coordinate system. Substituting (4.10) and (4.11) into (4.9) and cancelling the R's gives:

$$\begin{bmatrix} \sin\theta\cos\phi \\ \sin\theta\sin\phi \\ \cos\theta \end{bmatrix} = \begin{bmatrix} \cos\phi_0\cos\theta_0 & -\sin\phi_0 & \cos\phi_0\sin\theta_0 \\ \sin\phi_0\cos\theta_0 & \cos\phi_0 & \sin\phi_0\sin\theta_0 \\ -\sin\theta_0 & 0 & \cos\theta_0 \end{bmatrix} \begin{bmatrix} \sin\theta'\cos\phi' \\ \sin\theta'\sin\phi' \\ \cos\theta' \end{bmatrix} \quad (4.12)$$

which gives:

$$\begin{aligned} \sin\theta\cos\phi = {} & \sin\theta'(\cos\phi_0\cos\theta_0\cos\phi' - \sin\phi_0\sin\phi') \\ & + \cos\phi_0\sin\theta_0\cos\theta' \end{aligned} \quad (4.13)$$

$$\begin{aligned} \sin\theta\sin\phi = {} & \sin\theta'(\sin\phi_0\cos\theta_0\cos\phi' + \cos\phi_0\sin\phi') \\ & + \sin\phi_0\sin\theta_0\cos\theta' \end{aligned} \quad (4.14)$$

$$\cos\theta = -\sin\theta_0\sin\theta'\cos\phi' + \cos\theta_0\cos\theta' \qquad (4.15)$$

Now the expressions for $\sin\theta\cos\phi$, $\sin\theta\sin\phi$, and $\cos\theta$ in terms of θ_0, ϕ_0, θ', and ϕ' are substituted into the routines PARFAC.FOR, ELFAC.FOR, and EXPRPF.FOR to create the routines PARFEA.FOR, ELEFEA.FOR, and ERPFEA.FOR for use in the half-power beamwidth calculations.

To calculate the half-power beamwidths for the design pattern, PARRAY.FOR calls DBWDTH.FOR. Now consider the (x',y',z') coordinate system and the x'z'-plane. DBWDTH.FOR begins by searching for the value $(1/2)^{1/2}$ where ϕ' is equal to 180° by varying θ'in one degree increments until the magnitude of the pattern is equal to or just less than $(1/2)^{1/2}$. If the magnitude is equal to $(1/2)^{1/2}$ the angle is stored as θ' left and the routine begins searching where ϕ' is equal to 0°. If the magnitude of the pattern is just less than $(1/2)^{1/2}$ then that angle and the one just prior are sent to a routine that solves for the half-power point using a Regula Falsi root finding algorithm (REGFAL.FOR). This algorithm finds the angle to within a tolerance of $1.0(10^{-7})$ of $(1/2)^{1/2}$. The angle coming out of the regula falsi routine is stored as θ' left. The process is repeated for $\phi' = 0°$ and this angle stored in θ' right. Then Θ_h is found by adding θ' left to θ' right. A similar process is followed in finding Ψ_h. ϕ' is set to 270° and θ' varied in degree increments until the magnitude is equal to or just less than $(1/2)^{1/2}$. The root finding algorithm is called if the magni-

tude does not equal $(1/2)^{1/2}$ and a value returned for ψ left. The same process is followed in finding ψ right where ϕ' equals 90°. The beamwidth Ψ_h is found by adding ψ left and ψ right.

To find the half-power beamwidths for the expected pattern, PARRAY.FOR calls EBWDTH.FOR. The same process is followed here that was followed for finding the design beamwidths.

The design and expected beamwidths are calculated for the upper, center, and lower frequencies of the bandwidth. This routine takes longer to run than any other routine in the program since the coordinate translation significantly increases the complexity of the computations made by the program.

Part 4 - Directivity Calculations. Calculating the directivity for any given array is the only area in the program where a compromise between efficiency and being general was made. In order to be absolutely general, we would have to calculate the directivity by equation (1.10). However, numerically evaluating the double integral involved in (1.10), to any degree of accuracy, would mean the use of an integration routine with compensation. Using this type of scheme would involve a significant amount of computer time, especially on a personal computer. Instead, there is an approximation for directivity which is accurate for reasonable excitation schemes.

The directivity of a planar array can be calculated using (10:206):

$$D_0 = \pi \cos\theta_0 D_x D_y \qquad (4.16)$$

where D_x and D_y are the directivities of two broadside arrays in the x and y directions, respectively. The assumptions made in using (4.16) are; (1) the element pattern is such to eliminate the total pattern in the half space $\theta > \pi/2$ but is broad enough to be ignored in $\theta \leq \pi/2$, and (2) the array is not scanned closer than several beamwidths to endfire. Equation (4.16) is the one used in the program to calculate the directivity of a planar array. The following expression is used to calculate D_x and D_y (23:153):

$$D = \left[\sum_{m=1}^{M} A_m\right]^2 \Big/ \left[\sum_{m=1}^{M}\sum_{p=1}^{M} A_m A_p \left[\sin\left[(m-p)kd\right]/\left[(m-p)kd\right]\right]\right] \qquad (4.17)$$

which is valid for a broadside, equally spaced array.

Equation (4.16) is sufficient for dipoles up to approximately one wavelength in length. As the length of the dipole increases beyond one wavelength ($L>\lambda$), the number of lobes begin to increase and the main lobe becomes narrower, thus negating the assumption that the element pattern is broad.

Linear arrays can also be considered by the program, and code was added to calculate the directivity of a linear array scanned at some angle θ_0. The expression used for this calculation is (23:153):

$$D = \left[\sum_{m=1}^{M} A_m\right]^2$$

$$\div \sum_{m=1}^{M}\sum_{p=1}^{M} A_m A_p \exp[j(\alpha_m-\alpha_p)]\left[\sin[k(z_m-z_p)]/[k(z_m-z_p)]\right] \quad (4.18)$$

where $\alpha_i = -k(m-1)d_i\cos\theta_0$.

It is also possible to calculate the directivity and directive gain of a dipole at given angles θ,ϕ should the appropriate parameters be entered. The directivity of a dipole is calculated from (4:124-126):

$$D_0 = 2U_{dip}(\theta,\phi)\big|_{max}/Q \quad (4.19)$$

where:

$$Q = \gamma + \ln(kL) - C_i(kL) + \tfrac{1}{2}\sin(kL)\left[S_i(2kL) - 2S_i(kL)\right] + \tfrac{1}{2}\cos(kL)\left[\gamma + \ln(kL/2) + C_i(2kL) - 2C_i(kL)\right] \quad (4.20)$$

The maximum value of $U(\theta,\phi)$ varies and depends on the length of the dipole. The functions $C_i(x)$ and $S_i(x)$ are the cosine and sine integrals, respectively, and are defined by (4:744):

$$S_i(x) = \int_0^x (\sin\tau/\tau)\,d\tau \quad (4.21)$$

$$C_i(x) = -\int_x^{\infty} (\cos\tau, \quad 1\tau \quad (4.22)$$

$C_i(x)$ can also be found from (4:744):

$$C_i(x) = \gamma + \ln(x) - C_{in}(x) \quad (4.23)$$

where:

$$C_{in}(x) = \int_0^x \left[(1 - \cos\tau)/\tau\right]d\tau \quad (4.24)$$

The constant γ in the preceding equations is Euler's constant. The directive gain for a dipole is (23:36):

$$D(\theta,\phi) = D_0|U(\theta,\phi)|^2/|U(\theta_{max},\phi_{max})|^2 \qquad (4.25)$$

Equations (4.16) through (4.21), (4.23), and (4.24) are used in the code to calculate the required directivities. The directivity for the planar array (or linear array, or dipole) is calculated at the upper, center, and lower frequencies of the band in the routine DESDIR.FOR. The directivities for the planar array and linear array are computed directly in DESDIR.FOR. If the directivity for a dipole is called for, DESDIR.FOR calls DIPDIR.FOR. DIPDIR.FOR in turn calls the functions SI.FOR and CI.FOR to calculate the sine and cosine integrals. A Romberg integration routine (ROMBER.FOR) is used to calculate the sine and cosine integrals.

The change in directivity due to errors is calculated by the routine EXPDIR.FOR. EXPDIR.FOR employs equation (3.58), where the change in directivity is defined as:

$$\Delta D = \left[1 + (\epsilon^2/P)\right]^{-1} \qquad (4.25)$$

All directivities returned to PARRAY.FOR are in decibels.

<u>Part 5 - Output Routine and Recalculation.</u> All the data collected up to this point is sent to OUTPUT.FOR which in turn generates a file called OUTPUT.DAT. OUTPUT.DAT displays all the array specifications including the element weights. It also displays the beamwidths for the design and expected arrays at the upper, center, and lower frequencies

of the band, and the directivities of the design array and change in directivity for the expected array at the upper, center, and lower frequencies of the band. A sample of the output file is shown in Figure 18.

Besides the array specifications and standards, the program prints out the numerical error data from the beamwidth calculations. The "D" preceding the "FLAG" and "ITRM" terms indicates the design array. The "E" indicates the expected array. The number immediately following "FLAG" or "ITRM" indicates the frequency; 1 - center, 2 - upper, 3 - lower. The number in parentheses for the "FLAG" terms indicates the following:

(1) - Beamwidth in the Θ_h plane

(2) - Beamwidth in the Ψ_h plane

(3) - No pattern flag

What this means is, if "DFLAG2(1)=1" there is a 3-dB beamwidth in the Θ_h plane at the upper frequency for the design array. If "DFLAG2(1)=2" there is <u>not</u> a 3-dB beamwidth in the Θ_h plane. "DFLAG2(2)" has the same connotation as "DFLAG2(1)" except it is for Ψ_h. If "DFLAG2(3)=1", it means that there is a valid pattern to consider at the scan angles θ_0,ϕ_0. Conversely, if "DFLAG2(3)=2", it means, for whatever reason, the magnitude of the pattern factor in the direction θ_0,ϕ_0 is zero. The same logic applies to the "EFLAG" terms.

Before we discuss what the number in parentheses means for the "ITRM" terms, we need to discuss what is occurring

```
                    PARRAY SPECIFICATIONS AND DATA

 FREQUENCY OR WAVELENGTH SPECIFICATIONS:
      BANDWIDTH              FREQUENCY              WAVELENGTH
          UPPER:    29980.0000000 MHz          1.0000000 cms
         CENTER:    29980.0000000 MHz          1.0000000 cms
          LOWER:    29980.0000000 MHz          1.0000000 cms

                        ARRAY SPECIFICATIONS:
                          ARRAY ALONG X-AXIS   ARRAY ALONG Y-AXIS
 NUMBER OF ELEMENTS:          10 ELEMENTS          10 ELEMENTS
    ELEMENT SPACING:          .5000000 cms         .5000000 cms
          SYNTHESIS:            CHEBYSHEV            CHEBYSHEV
             DESIGN
    SIDE LOBE LEVEL:         -30.0000000 dB
             DESIGN
    SIDE LOBE LEVEL:                              -30.0000000 dB

 WEIGHTS:                        X-DIRECTION          Y-DIRECTION
        ELEMENT   1:               .2575323             .2575323
        ELEMENT   2:               .4299509             .4299509
        ELEMENT   3:               .6692189             .6692189
        ELEMENT   4:               .8780469             .8780469
        ELEMENT   5:              1.0000000            1.0000000
        ELEMENT   6:              1.0000000            1.0000000
        ELEMENT   7:               .8780469             .8780469
        ELEMENT   8:               .6692189             .6692189
        ELEMENT   9:               .4299509             .4299509
        ELEMENT  10:               .2575323             .2575323

  ELEMENT DATA:
       TYPE:    ISOTROPIC ELEMENTS

  ARRAY TOLERANCE DATA:
       ELEMENT RMS DRIVE AMPLITUDE ERROR:        .0020000 UNITS
                  ELEMENT RMS PHASE ERROR:     10.0000000 degree(s)
                 RMS ERROR IN X-PLACEMENT:       .0020000 cms
                 RMS ERROR IN Y-PLACEMENT:       .0020000 cms
                 RMS ERROR IN Z-PLACEMENT:       .0020000 cms
               RMS ELEMENT PATTERN ERROR:    -100.0000000 dB
          FRACTION OF ELEMENTS OPERATING:      1.0000000
 SCAN ANGLES:
   THETA0 =     .0000000 degrees      PHI0 =     .0000000 degrees

 BEAMWIDTHS FOR DESIGN ARRAY AT GIVEN SCAN ANGLES:
                          THETA sub H              PSI sub H
  UPPER FREQUENCY:    13.0375700 degrees     13.0375700 degrees
 CENTER FREQUENCY:    13.0375700 degrees     13.0375700 degrees
  LOWER FREQUENCY:    13.0375700 degrees     13.0375700 degrees

 BEAMWIDTHS FOR EXPECTED ARRAY AT GIVEN SCAN ANGLES:
                          THETA sub H              PSI sub H
  UPPER FREQUENCY:    13.0414800 degrees     13.0414800 degrees
 CENTER FREQUENCY:    13.0414800 degrees     13.0414800 degrees
  LOWER FREQUENCY:    13.0414800 degrees     13.0414800 degrees

 DIRECTIVITIES FOR DESIGN AND EXPECTED ARRAY AT GIVEN SCAN ANGLES:
                        DESIGN ARRAY       CHANGE DUE TO ERRORS
  UPPER FREQUENCY:     23.5317800 dB              -.1329967 dB
 CENTER FREQUENCY:     23.5317800 dB              -.1329967 dB
  LOWER FREQUENCY:     23.5317800 dB              -.1329967 dB
```

Figure 18. Sample output from PARRAY.EXE.

in the Regula Falsi root finding algorithms belonging to DBWDTH.FOR and EBWDTH.FOR. As mentioned in Part 3, DBWDTH.FOR passes two angles to the routine REGFAL.FOR to find the angle at which the pattern factor equals $(\frac{1}{2})^{\frac{1}{h}}$ to within a given tolerance. The REGFAL.FOR routine searches for this point until one of two things occur. The process terminates when either the maximum number of iterations is exceeded or when the desired tolerance is achieved. The maximum number of iterations for the REGFAL.FOR routine is set to 10. The tolerance is set to $1.0(10^{-7})$. This tolerance was selected since it was the maximum accuracy of the FORTRAN compiler used to compile the program. The maximum number of iterations was selected as a compromise between time and accuracy, such that, most often the tolerance will be achieved before the maximum number of iterations is exceeded. The ERGFAL.FOR routine is trying to locate the angle where the expected pattern factor equals $(\frac{1}{2})^{\frac{1}{h}}$. In this routine the tolerance is again set at $1.0(10^{-7})$ and the maximum number of iterations is set to 10. During the execution of DBWDTH.FOR and EBWDTH.FOR , four calls are made to REGFAL.FOR and ERGFAL.FOR, respectively. The number in parentheses indicates the side (left or right) of the beam and which plane it is considering, Θ_h or Ψ_h, as described

below:

(1) - theta left

(2) - theta right

(3) - psi left

(4) - psi right

Finally, if any "ITRM" term equals one, it means the tolerance was achieved. If "ITRM" equals two, it means the maximum number of iterations was exceeded before the tolerance was achieved.

The "Numerical Error Data From Beamwidths Calculations" section is set up so that with a quick glance one can tell if there is a problem. All "ones" indicates everything is satisfactory. If there is a "two" it means something happened and should be investigated further. There is a chance a zero (0) could occur in the "ITRM" terms. This would indicate that a particular REGFAL.FOR call was not made because the angle at which the pattern value equals $(\frac{1}{2})^{\frac{1}{2}}$ or $\frac{1}{2}$ was hit precisely and the ensuing call to the REGFAL.FOR routine wasn't needed.

Once control is returned to PARRAY.FOR, PARRAY.FOR prompts he user for instructions on how to proceed. The user may choose to terminate the program or recalculate the beamwidths and directivities for new scan angles. If the user wants to recalculate the data at new scan angles, the PARRAY.FOR returns to Part 3 where the user enters new scan angles. When OUTPUT.FOR is again reached, just the new scan

angles, data, and numerical error data is printed, not all the array specifications since they did not change. Then the process repeats again unless a termination order is given.

Summary

The information presented in this chapter detailed the specific development of the program. The program is broken down into five parts. Part 1 is the data entry section where the array specifications, element data, and error data are entered and the element weights are calculated. Part 2 is wnere the pattern data for the design and expected arrays are calculated. Part 3 contains the beamwidth calculation routines. Here, we showed how a coordinate translation was employed so the beamwidths of the design and expected arrays can be calculated for any general pattern shape. Part 4 contained the directivity calculation routines. The specific equations used to calculate the directivity were defined. We noted that the expressions were valid for certain conditions, but, none of which will affect the directivity calculation unless the element pattern is not broad. Part 5 contained the data output routine and the continue/terminate section of the program. Each item printed in the OUTPUT.DAT file was explained in detail. Finally, the user is given the opportunity to recalculate the beamwidths and directivities for new scan angles.

In Chapter V, the program is validated against known

results. First, the element weights calculated by the program for different excitation schemes are validated by generating their appropriate plots and comparing to what should be seen and against patterns in the literature. After confidence is gained that the excitation, array pattern, and element pattern routines are functioning properly, the beamwidth and directivity routines are validated against computed results found in the literature. Lastly, the error routines for the expected array will be validated against trends and assessments noted in the literature and specific problems, where possible.

V. Program Validation

The purpose of this chapter is to validate the code comprising the program PARRAY.FOR. In the first part of the chapter, the routines for generating the element weights and the data for the pattern plots for both the design and expected arrays are validated. If the element weights are calculated properly and the pattern factor routines function properly, then the program should generate the data points for the desired pattern. For example, if a Dolph-Chebyshev pattern with -30 dB side lobe suppression is desired then the element weights calculated by CHEBY.FOR together with the pattern routines should generate the data points necessary to give a pattern with one main lobe and equal side lobes at -30 dB. In the second part of the chapter, the routines that calculate the beamwidths and directivities of the array are validated against known results found in the literature. The remainder of the chapter is devoted to validating the error routines against trends identified during the literature review.

Validation of the Excitation and Pattern Routines

In this section the element weights produced by each of the routines CHEBY.FOR, TAYLOR.FOR, BINOML.FOR, UNIFRM.FOR, and USRDEF.FOR are validated by comparing calculated weights to numerical examples in the literature. At the same time, the pattern routines are validated by creating pattern plots

of the data output by these routines and verifying the plot matches the desired pattern or examples in the literature.

Let us assume we desire to design a planar array with 10 elements in the x-direction and 15 elements in the y-direction with $\lambda/2$ interelement spacing and a -26 dB side lobe level in the x-direction and a -36 dB side lobe level in the y-direction. The element weights calculated by CHEBY.FOR for the x- and y-directions are shown in Table I. The weights in the x-direction agree with a similar examples in Pozar (19:75) and Balanis (4:251). The pattern for the weights in the x-direction is shown in Figure 19. The pattern for the weights in the y-direction is shown in Figure 20. The pattern in Figure 19 is identical to the pattern in Pozar (18:74). For the y-direction, the desired pattern is to have a -36 dB side lobe level. The pattern in Figure 18 does show even side lobes at -36 dB, characteristic of a Dolph-Chebyshev array.

To validate the TAYLOR.FOR routine, let us assume we desire a planar array with 19 elements in the x-direction with 0.7 λ spacing, -20 dB side lobe suppression with $\bar{n}=6$ using the null matching weights. In the y-direction we want 19 elements with 0.7 λ spacing, -20 dB side lobe suppression with $\bar{n}=6$ using the aperture sampling weights. The element weights for this case are shown in Table II. The null matching weights in the x-direction agree with similar cases in Pozar (19:79) and Elliott (10:176). The aperture

Table I. Normalized currents for patterns of Figures 19-20

Element	I_n for Fig. 17 X-direction	I_n for Fig. 18 Y-direction
1	.3610756	.1597263
2	.4894356	.2471115
3	.7105761	.3973025
4	.8950094	.5654510
5	1.0000000	.7314007
6	1.0000000	.8722100
7	.8950094	.9667108
8	.7105761	1.0000000
9	.4894356	.9667108
10	.3610786	.8722100
11		.7314007
12		.5654510
13		.3973025
14		.2471115
15		.1597263

Table II. Normalized currents for patterns of Figures 21-22

Element	I_n for Fig. 19 X-direction Null Matching	I_n for Fig. 20 Y-direction Aperture Sampling
1	.7493064	.7432176
2	.6229094	.6262966
3	.5629416	.5699893
4	.6488633	.6502087
5	.7690658	.7666988
6	.8431128	.8427454
7	.9039928	.9043074
8	.9661377	.9646410
9	.9966137	.9954504
10	1.0000000	1.0000000
11	.9965672	.9954504
12	.9660780	.9646410
13	.9039486	.9043074
14	.8430912	.8427454
15	.7690604	.7666988
16	.6488639	.6502087
17	.5629424	.5699893
18	.6229098	.6262966
19	.7493064	.7432176

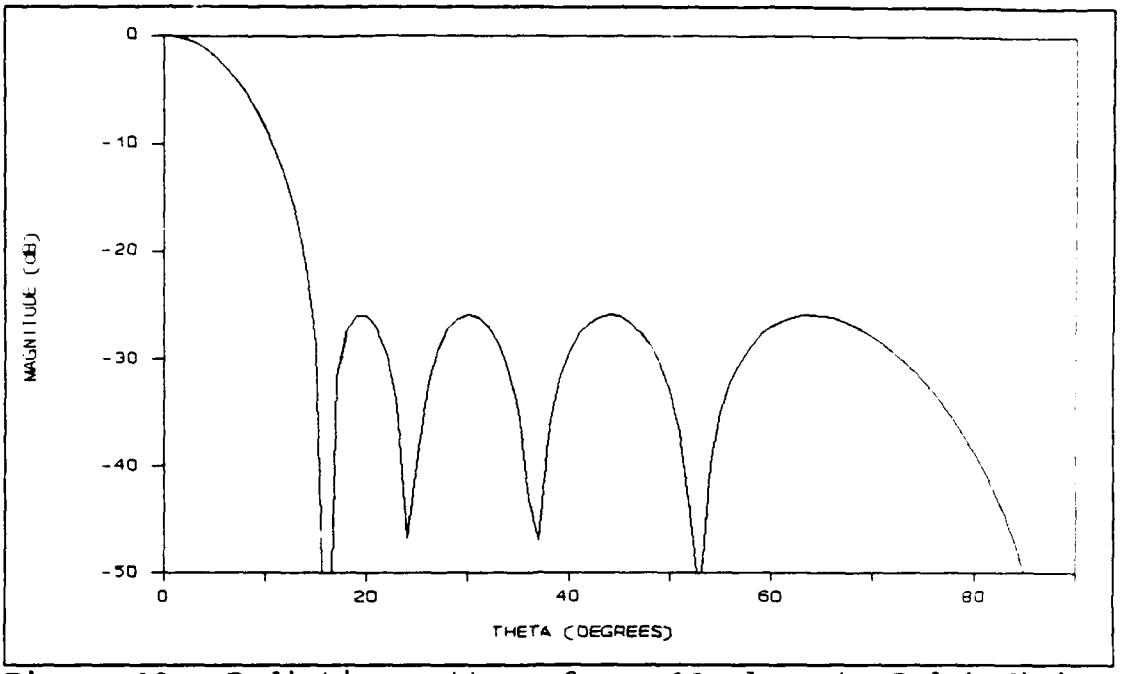

Figure 19. Radiation pattern for a 10 element, Dolph-Chebyshev synthesized array with ½ λ spacing showing a -26 dB side lobe level

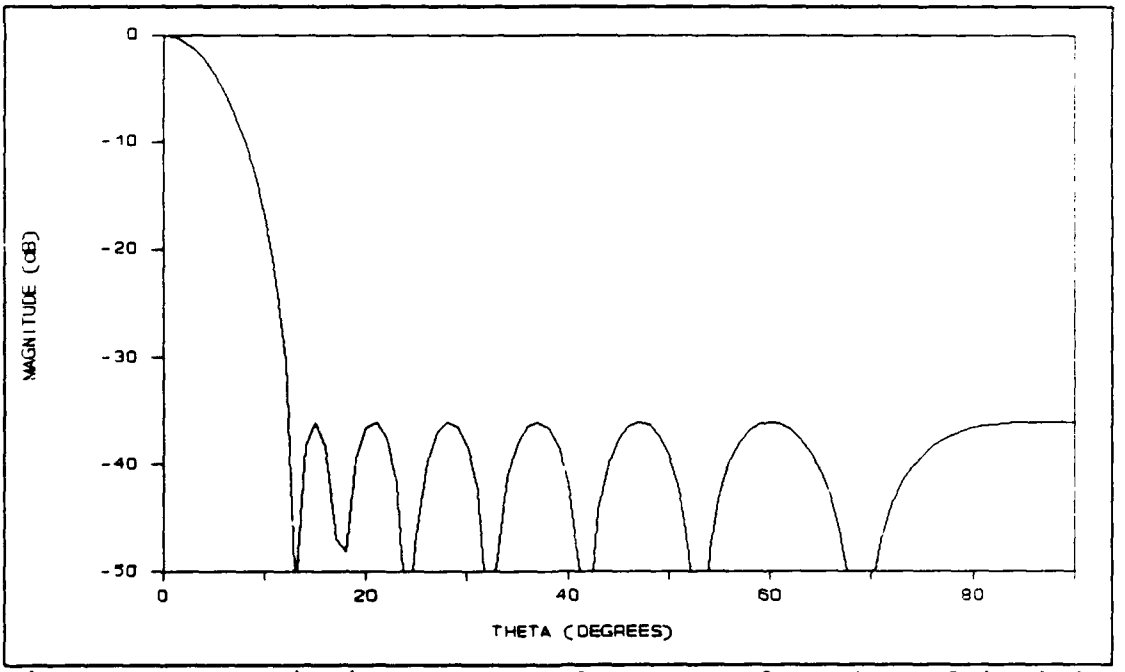

Figure 20. Radiation pattern for a 15 element, Dolph-Chebyshev synthesized array with ½ λ interelement spacing showing a -36 dB side lobe level

sampling weights in the y-direction agree with Pozar (19:79). The pattern for the null matching weights is shown in Figure 21. Notice how the six inner most side lobes in the pattern are very close to -20 dB as we desired. The pattern for the aperture sampling weights is shown in Figure 22. Again, the six inner most side lobes are at -20 dB as expected.

Before we leave the Taylor synthesis, let us test the routine for two new values of $\bar{n}$. Let us assume we have 21 elements in the x-direction and 22 elements in the y-direction with $\lambda/2$ interelement spacing. We want a -30 dB side lobe suppression in the x-direction and a -35 dB side lobe suppression in the y-direction. We will let $\bar{n} = 7$ in the x-direction and $\bar{n} = 8$ in the y-direction and we will use the null matching weights in both directions. The element weights produced by TAYLOR.FOR are shown in Table III. The pattern for the x-direction is shown in Figure 23. The pattern for the y-direction is shown in Figure 24. Looking at the pattern in Figure 23, we can see that the 7 inner-most side lobes are at -30 dB as desired. In Figure 24, the 8 inner-most side lobes are at -35 dB as desired.

To test the binomial current distribution routine (BINOML.FOR), we will assume a planar array with 10 elements in the x-direction with $\lambda/4$ spacing and 10 elements in the y-direction with $\lambda/2$ spacing. The weights for the array are shown in Table IV. The pattern for the weights in the

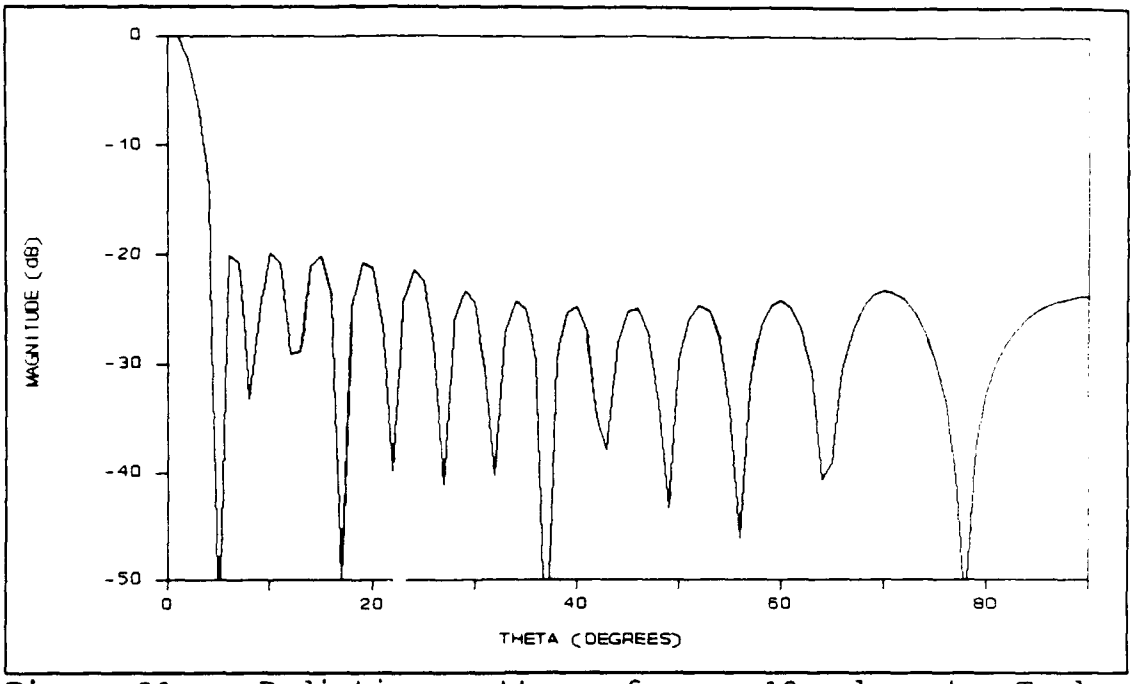

Figure 21. Radiation pattern for a 19 element, Taylor synthesized ($\bar{n}$=6) array with 0.7λ interelement spacing and a -20 dB side lobe level using null matching weights

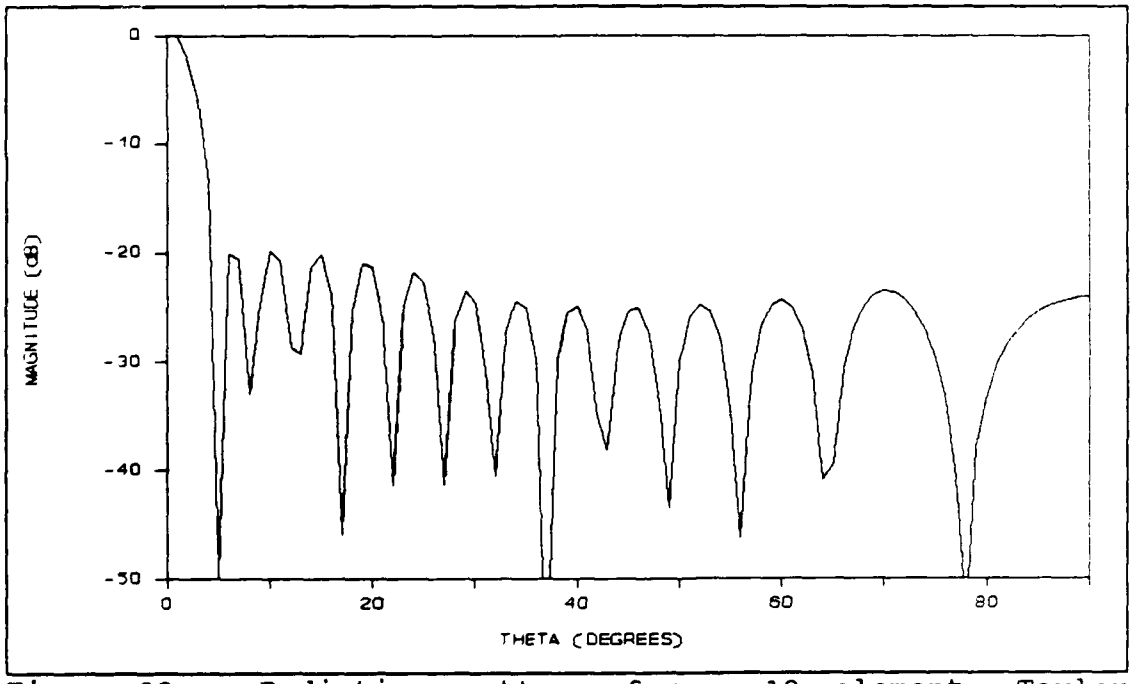

Figure 22. Radiation pattern for a 19 element, Taylor synthesized ($\bar{n}$=6) array with 0.7λ interelement spacing and a -20 dB side lobe level using aperture sampling weights

Table III. Normalized currents for patterns of Figures 23-24

Element	I_n for Fig. 21 X-direction	I_n for Fig. 22 Y-direction
1	.2816017	.1826574
2	.2983098	.2137403
3	.3638166	.2904074
4	.4736608	.3979462
5	.5889375	.5102512
6	.6939946	.6231356
7	.7938421	.7342620
8	.8805723	.8325624
9	.9439505	.9128824
10	.9847533	.9708424
11	1.0000000	1.0000000
12	.9848089	1.0000010
13	.9440464	.9708449
14	.8806777	.9128821
15	.7939240	.8325511
16	.6940391	.7342379
17	.5889544	.6231086
18	.4736658	.5102325
19	.3638179	.3979382
20	.2983101	.2904055
21	.2816017	.2137402
22		.1826574

Table IV. Normalized currents for patterns of Figures 25-26

ELEMENT	I_n for Fig. 21 X-direction	I_n for Fig. 22 Y-direction
1	.0079365	.0079365
2	.0714286	.0714286
3	.2857143	.2857143
4	.6666667	.6666667
5	1.0000000	1.0000000
6	1.0000000	1.0000000
7	.6666667	.6666667
8	.2857143	.2857143
9	.0714286	.0714286
10	.0079365	.0079365

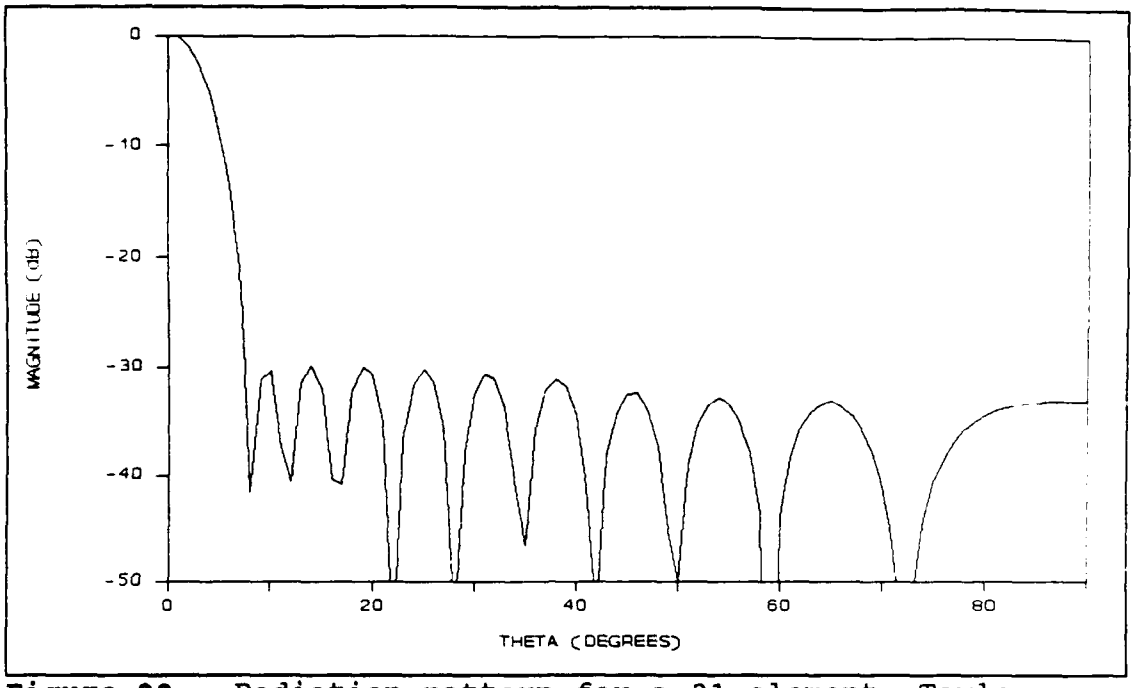

Figure 23. Radiation pattern for a 21 element, Taylor synthesized ($\bar{n}$=7) array with ½λ interelement spacing and a -30 dB side lobe level

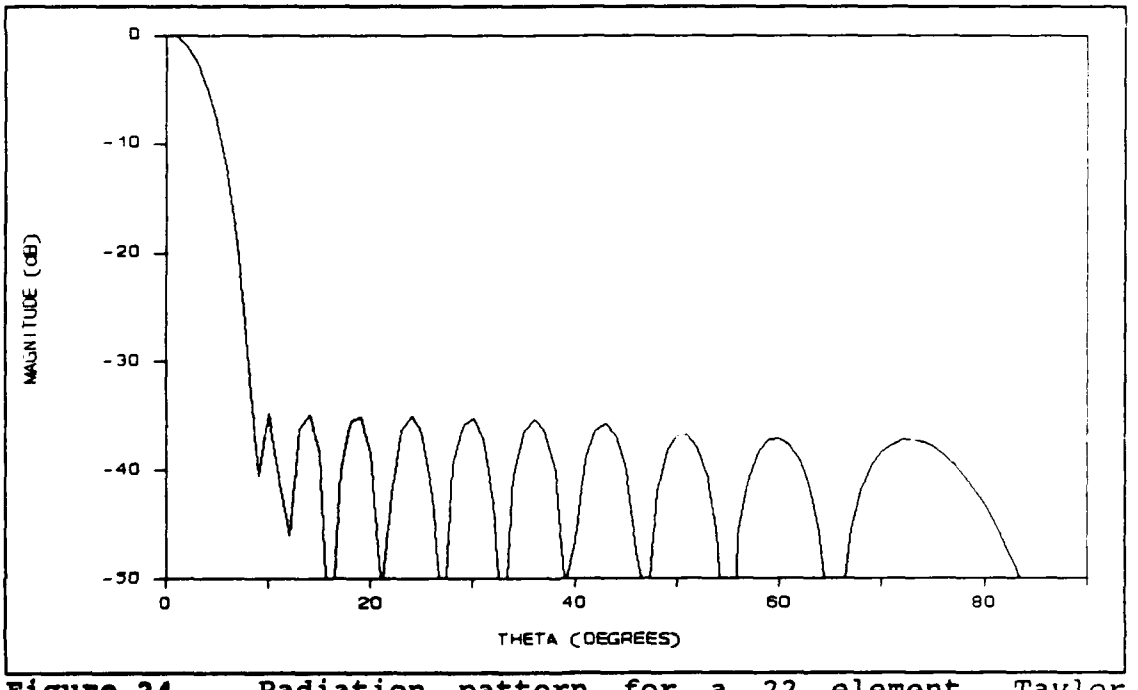

Figure 24. Radiation pattern for a 22 element, Taylor synthesized ($\bar{n}$=8) array with ½λ interelement spacing and a -35 dB side lobe level

x-direction is shown in Figure 25. The pattern for the weights in the y-direction is shown in Figure 26. Both patterns do not exhibit any side lobes as stated in Chapter 2, even though, the pattern in Figure 25 is very broad. Both patterns agree with the ones found in Balanis (4:245).

Next, the pattern functions are run for a uniform current distribution. For this case all element weights are set to one. We can show several items characteristic of a uniform array. First, as M (the number of elements in one direction) increases, the main lobe narrows. Second, there are M-2 minor lobes and one main lobe in the region $0° \leq \theta \leq 90°$ for $\phi=180°$ and $0° \leq \theta \leq 90°$ for $\phi=0°$. Finally, the first minor side lobe approaches -13.3 dB as M increases. We will assume our planar array has 10 elements in the x-direction and 16 elements in the y-direction. The array has $\lambda/2$ spacing in both directions. The pattern for the xz-plane is shown in Figure 27. In Figure 27, there would be 8 minor lobes and one main lobe as expected if the other half of the pattern were included. However, because the pattern is symmetric the other half of the pattern was not plotted. We can also see that the first minor lobe is at approximately -13.3 dB. The pattern for the yz-plane is shown in Figure 28. Here we see 7 minor lobes which means there are actually 14 if the entire pattern were plotted. The first minor lobe in Figure 28 is at approximately -13.3 dB. Comparing

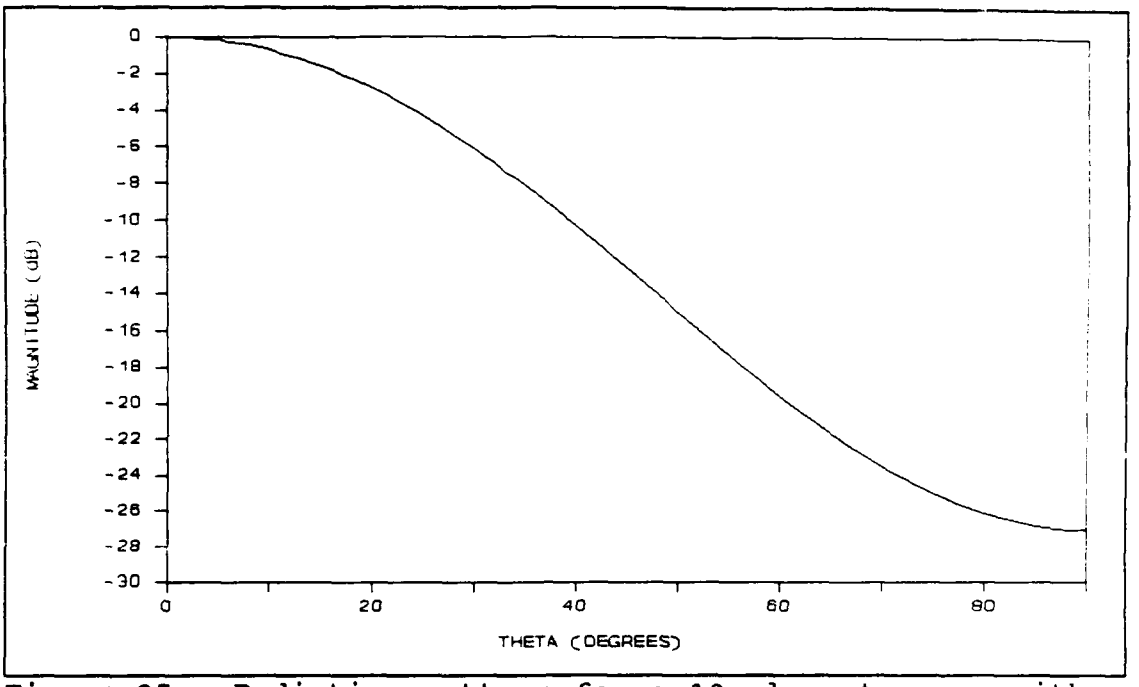

Figure 25. Radiation pattern for a 10 element array with a binomial current distribution and $\frac{1}{4}\lambda$ interelement spacing

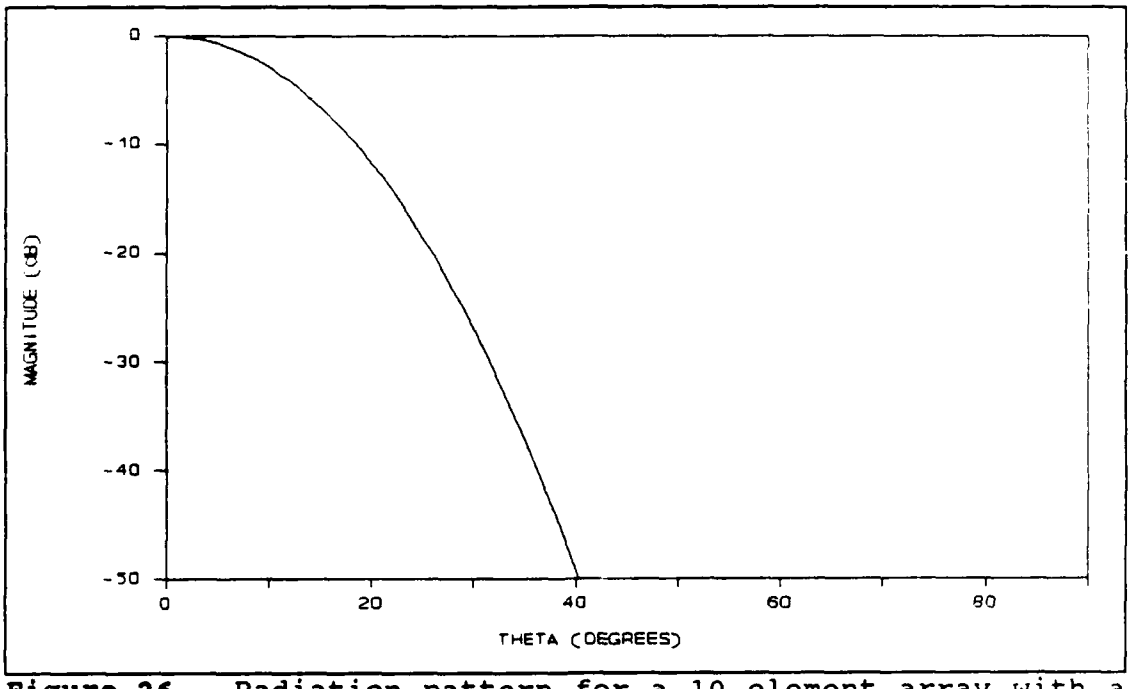

Figure 26. Radiation pattern for a 10 element array with a binomial current distribution and $\frac{1}{2}\lambda$ interelement spacing

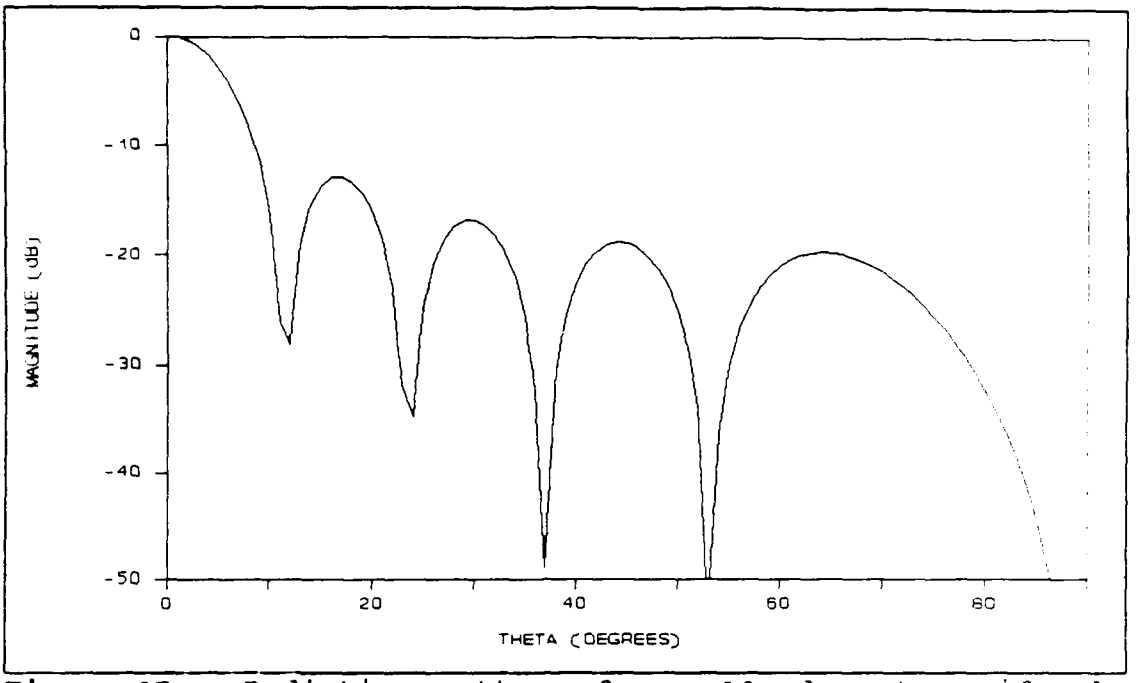

Figure 27. Radiation pattern for a 10 element, uniformly excited array with ½λ interelement spacing

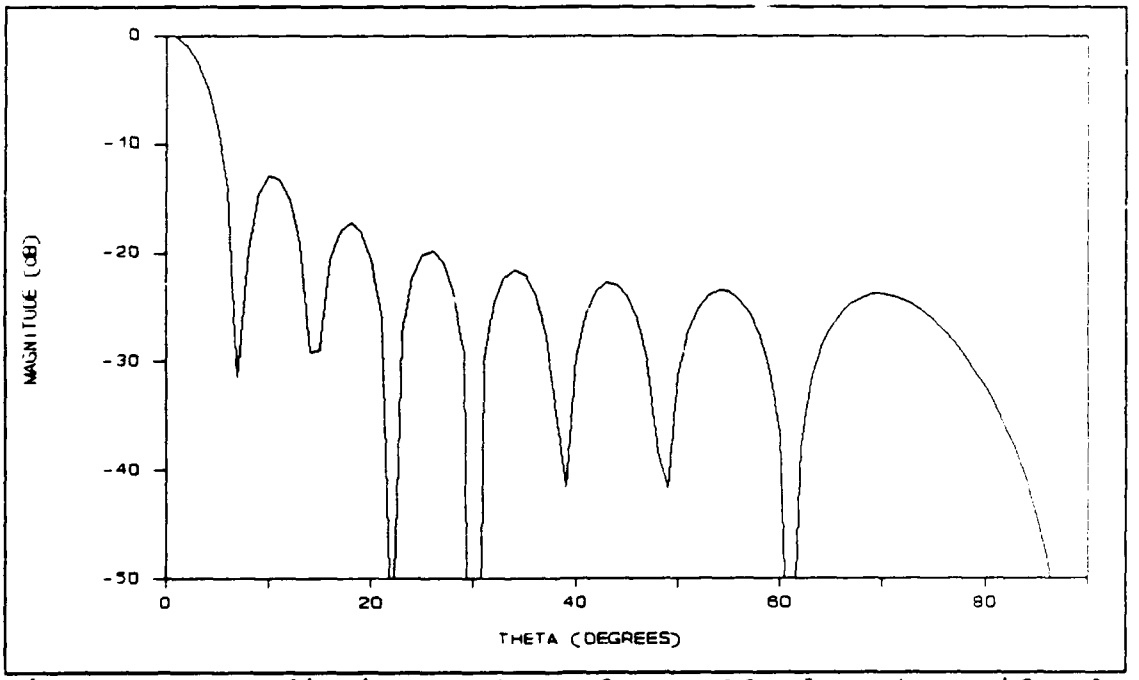

Figure 28. Radiation pattern for a 16 element, uniformly excited array with ½λ interelement spacing

Figures 27 and 28 we can see that the main lobe in Figure 28 is narrower than the main lobe in Figure 27 as expected.

As a last test of the pattern factor routines we will use an inverse triangular and triangular current distribution in the x- and y-directions, respectively. The element weights for these current distributions will be input by the user defined routine. We will assume 5 elements in each direction with $\lambda/2$ spacing so that we can compare the pattern plots with those in Stutzman and Thiele (23:148-152). The element weights for each direction are shown in Table V. Figure 29 shows the pattern due to the elements in the x-direction. Figure 30 shows the pattern due to the elements in the y-direction. The pattern in Figure 29 shows the main lobe at broadside and the two side lobes with the first lobe at a level of approximately -6.3 dB, the same as (23:152). The pattern in Figure 30 shows thc main lobe at broadside and the side lobe at 90° with a level of approximately -19.1 dB, the same as in Stutzman and Thiele (23:148).

Table V. Normalized currents for patterns in Figures 29-30

Element	I_n for Fig. 27 X-direction	I_n for Fig. 28 Y-direction
1	1.0000000	.3333333
2	.6666667	.6666667
3	.3333333	1.0000000
4	.6666667	.6666667
5	1.0000000	.3333333

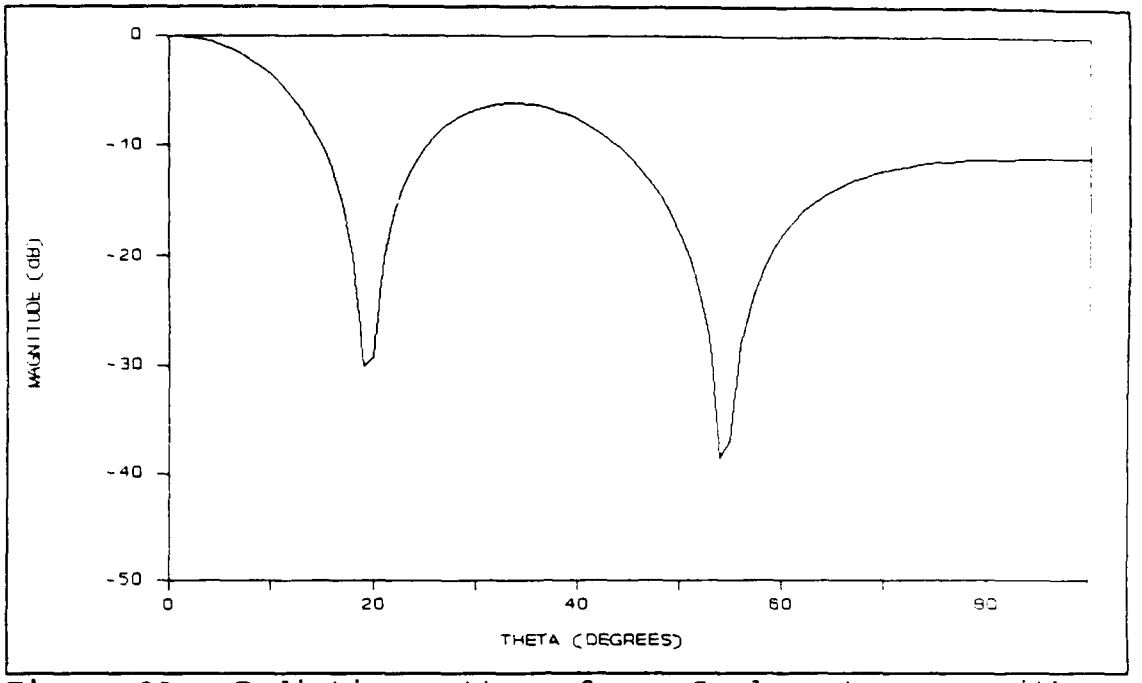

Figure 29. Radiation pattern for a 5 element array with an inverse triangular current distribution and ½λ spacing

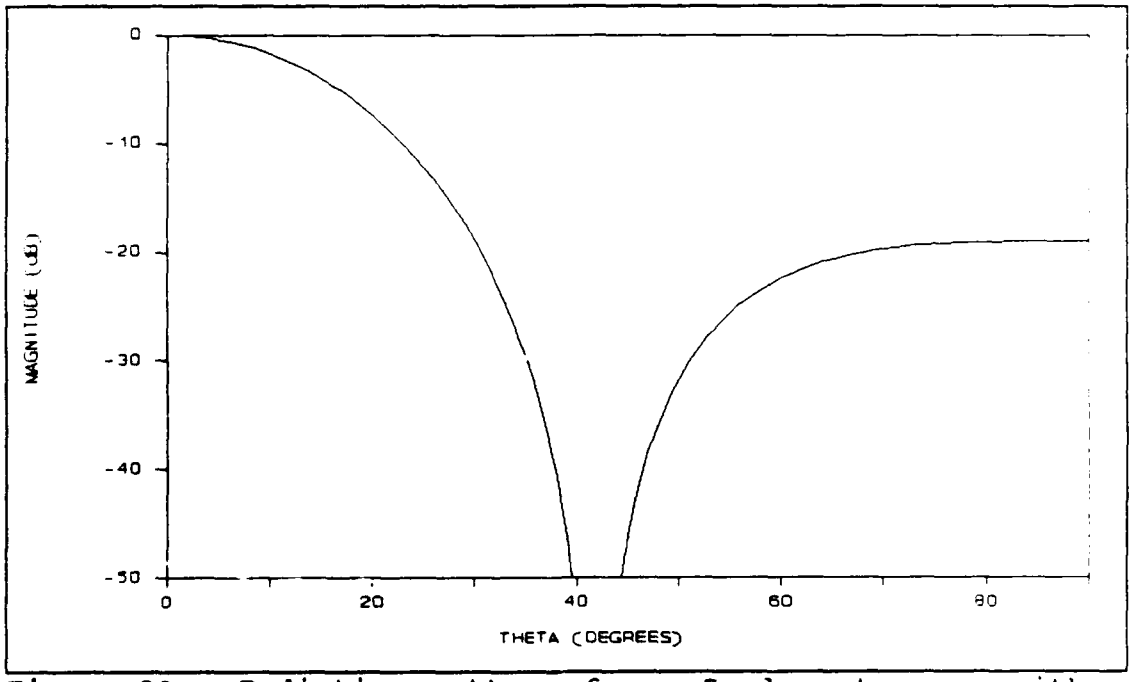

Figure 30. Radiation pattern for a 5 element array with a triangular current distribution with ½λ spacing

Up to this point, we have considered only isotropic elements, mainly because most of the examples in the literature consider isotropic elements. Now, let us look at the element patterns of a half and full wavelength dipoles to ensure the element factor routines are producing the proper values. Then, we will plot the pattern of a planar array of half and full wavelength dipoles to look at the effects of the dipole on the overall radiation pattern of the array. PARRAY.EXE was used to generate the plots for a $\lambda/2$ and a λ dipole and are shown in Figures 31 and 32, respectively. The program calculated the beamwidth for the $\lambda/2$ dipole as 78° and for the λ dipole as 47.8° in agreement with Balanis (4:122). The $\lambda/2$ dipole pattern is overlaid against a -25 dB Dolph-Chebyshev synthesized 10x10 array, with $\lambda/2$ inter-element spacing, pattern in Figure 33. The plots in Figure 33 depict the respective patterns in the xz-plane. As we can see from Figure 33, the dipole pattern would have negligible effect on the overall pattern. The pattern for the same 10x10 array, but, this time with x-aligned, $\lambda/2$ dipoles as the elements, is shown in Figure 34. Figure 34 shows that there is very little distortion in the pattern with only the outside side lobes slowly tapering off due to dipole pattern. Figure 35 shows the overlay of the same array as before, but, this time with a 1λ dipole pattern overlaying the array pattern. Obviously, the 1λ dipole will effect the pattern more than the $\lambda/2$ dipole. Indeed, in

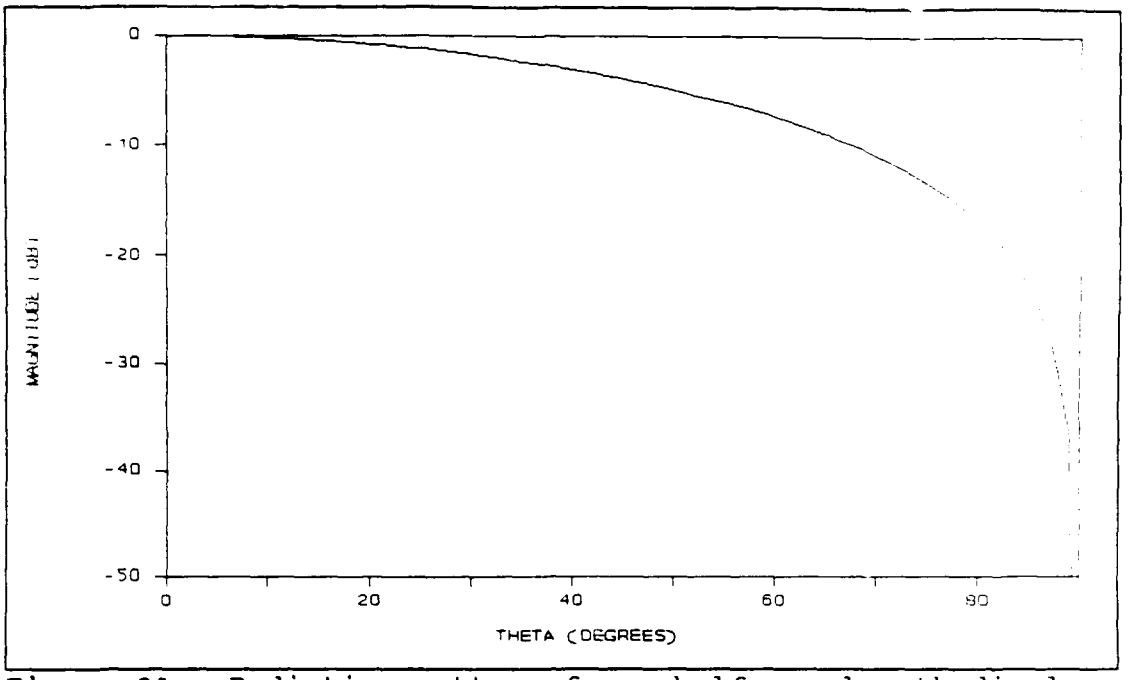

Figure 31. Radiation pattern for a half-wavelength dipole

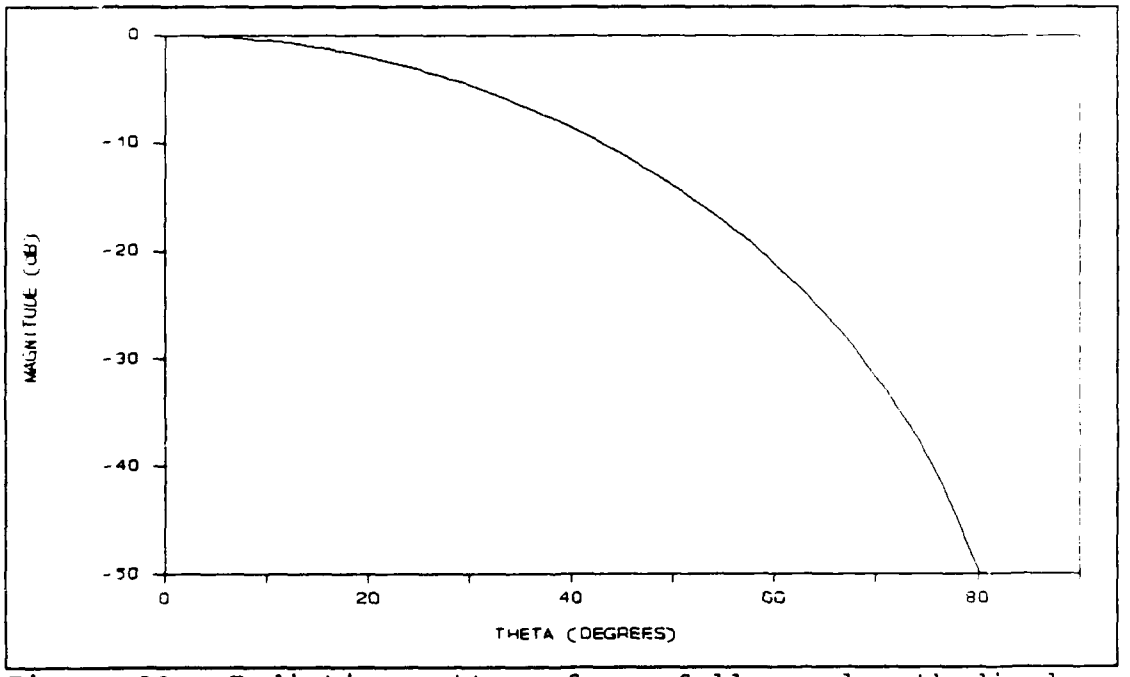

Figure 32. Radiation pattern for a full wavelength dipole

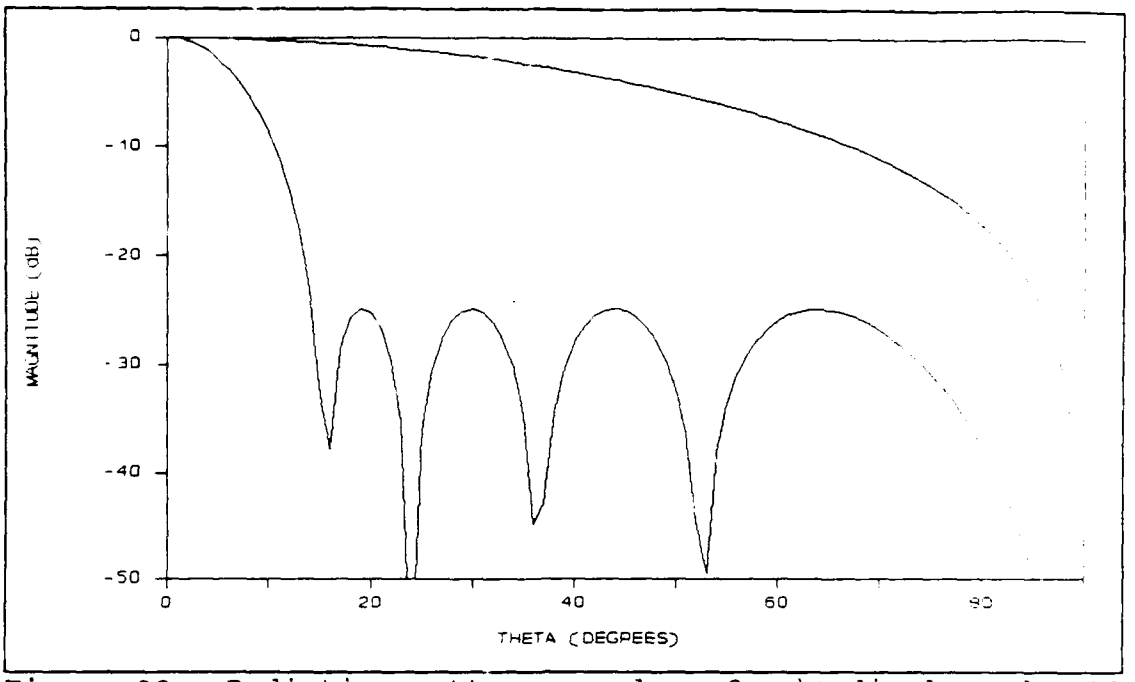

Figure 33. Radiation pattern overlay of a ½λ dipole and a 10 element, Dolph-Chebyshev synthesized array with ½λ inter-element spacing and -25 dB side lobe level

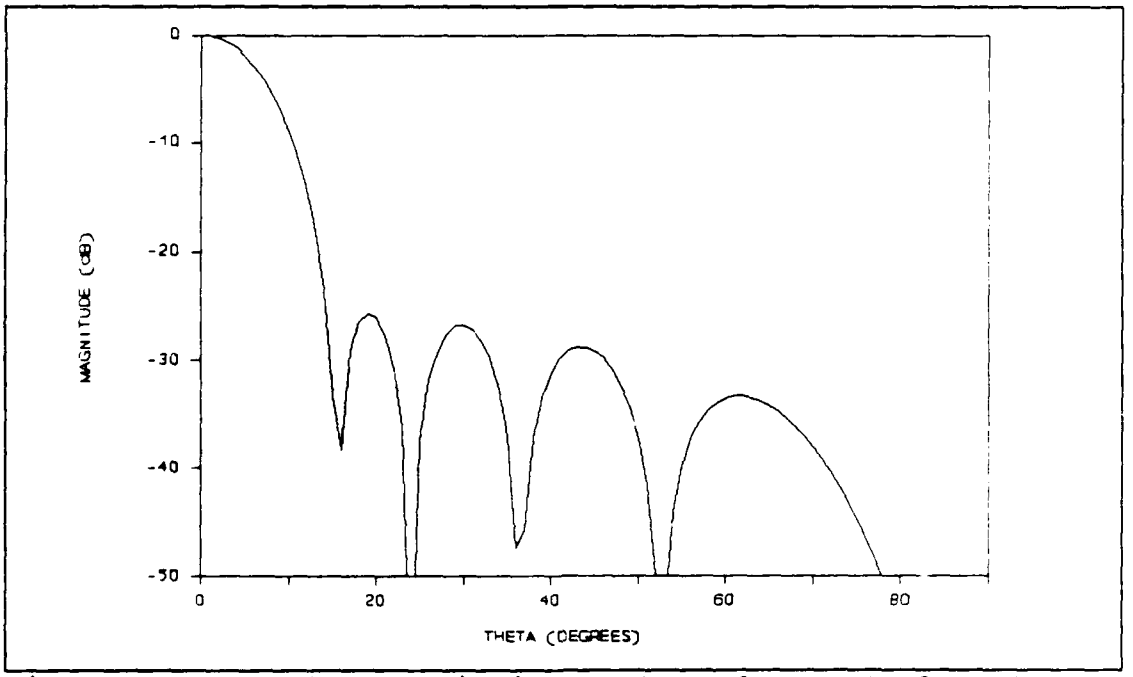

Figure 34. XZ-plane radiation pattern for a 10 element, -25 dB Dolph-Chebyshev synthesized array with ½λ spacing and x-aligned ½λ dipoles as elements

Figure 36 we can see the effect of an x-aligned, 1λ dipole as an element in the array. The outside side lobes are significantly reduced by the dipole pattern. Now let us see what happens when we scan the main beam off broadside with $\lambda/2$ and λ dipoles in the array.

Figure 37 shows an overlay of the radiation patterns of a 10x10, -25 dB Dolph-Chebyshev synthesized array, with $\lambda/2$ interelement spacing, scanned at 30° from broadside (θ_0=30°,ϕ_0=0°) and that of a $\lambda/2$ dipole. The "minus" theta on the scale signifies that ϕ=180° for that part of the x-axis. As we can see from Figure 37, the dipole pattern is beginning to impact the array pattern. Figure 38 shows the array's radiation pattern with the $\lambda/2$ dipole as an element. Indeed, the main beam is becoming broader as the array is scanned further from broadside.

Figure 39 shows the overlay of the radiation patterns for the same 10x10 array as before, scanned at 30° from broadside, with that of a 1λ dipole. The 1λ dipole significantly impacts the main beam. In Figure 40, we see the radiation pattern of the array with the 1λ dipole as an element. The main beam for Figure 40 is significantly broader than the main beam of the array in Figure 39.

The purpose of the preceding paragraphs was to show that the directivity expression used in the program may not yield accurate results for an array of x- or y-aligned dipoles for the main beam of the array scanned much beyond

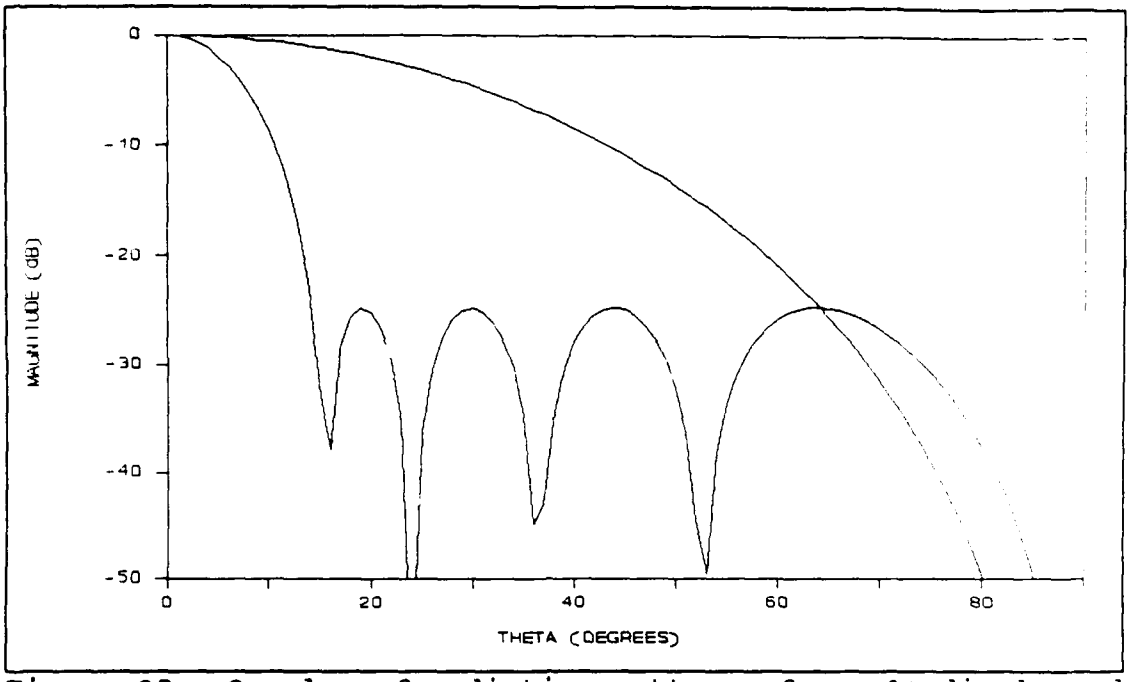

Figure 35. Overlay of radiation patterns for a 1λ dipole and a 10 element, -25 dB Dolph-Chebyshev synthesized array with ½λ interelement spacing

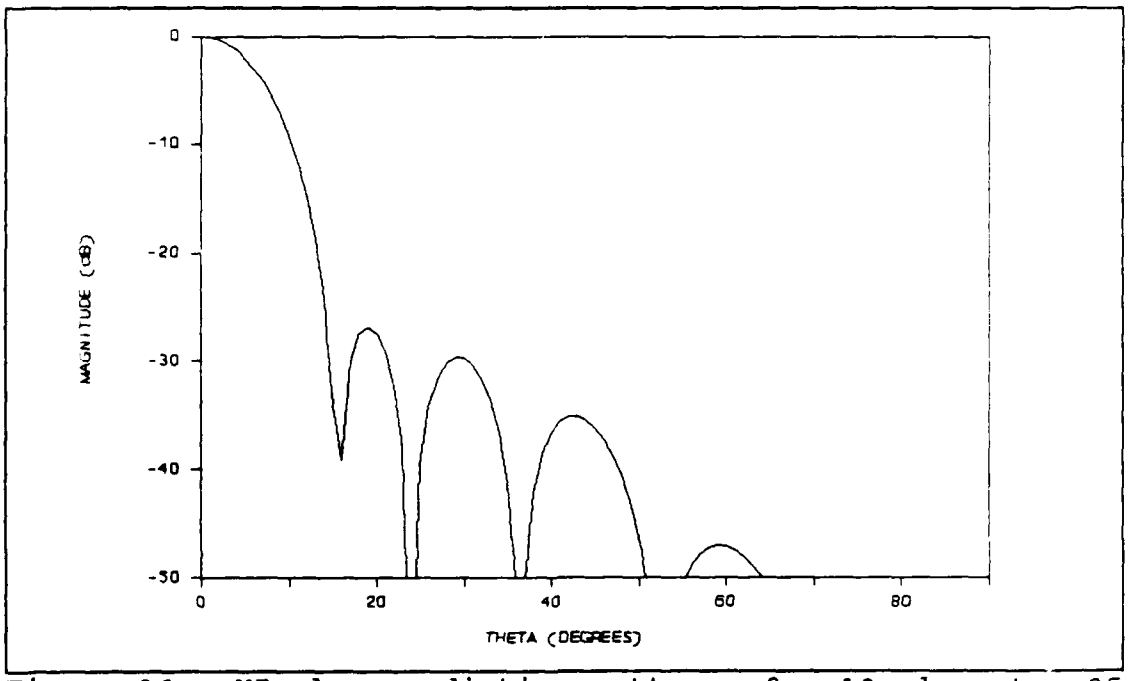

Figure 36. XZ-plane radiation pattern of a 10 element, -25 dB Dolph-Chebyshev synthesized array with ½λ interelement spacing and x-aligned 1λ dipoles as elements

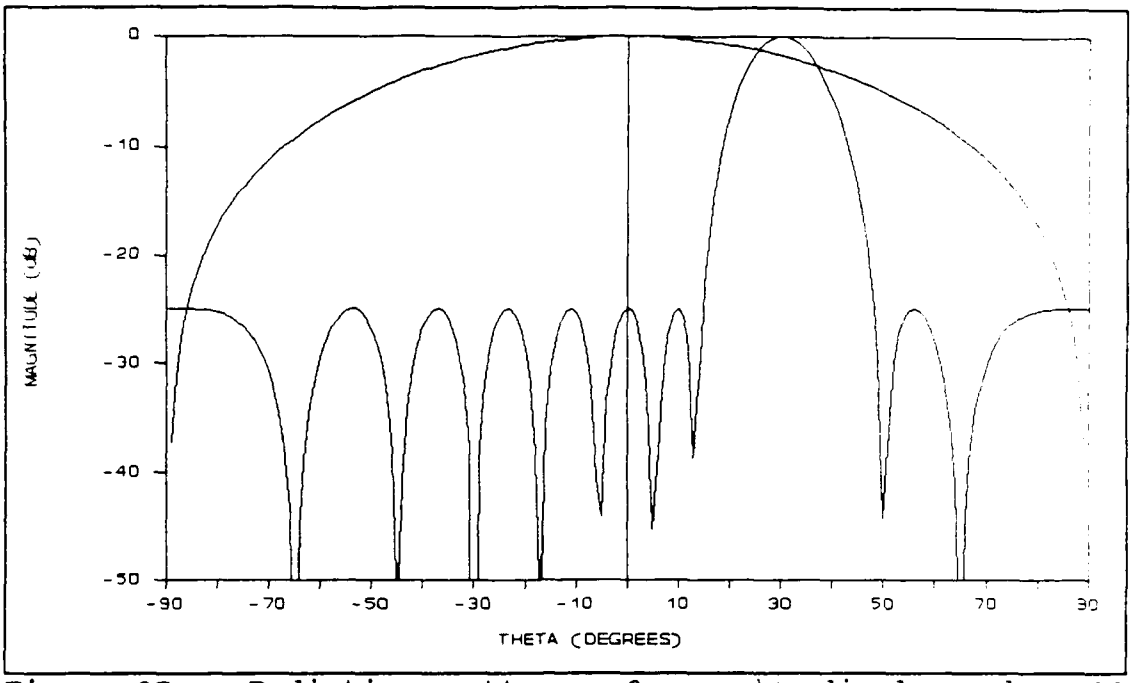

Figure 37. Radiation patterns for a ½λ dipole and a 10 element, Dolph-Chebyshev synthesized array with ½λ interelement spacing and a -25 dB design side lobe level scanned at 30° from broadside

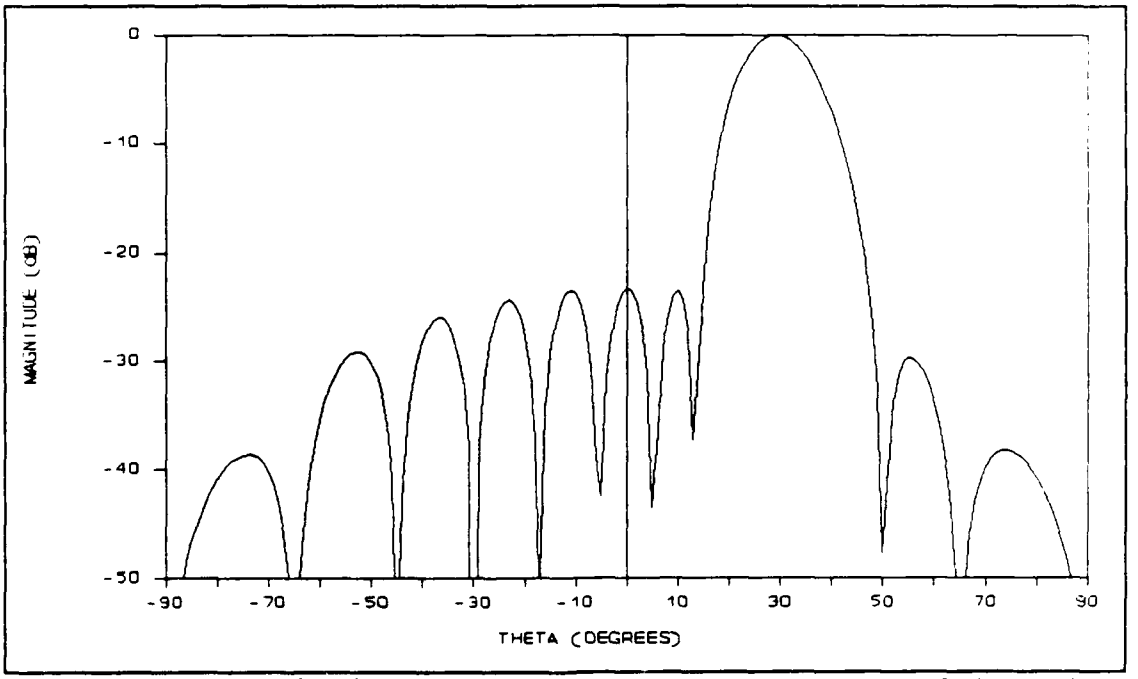

Figure 38. Radiation pattern of a 10 element, Dolph-Chebyshev synthesized array with ½λ interelement spacing showing a -25 dB side lobe level scanned at 30° off broadside with ½λ dipoles as elements

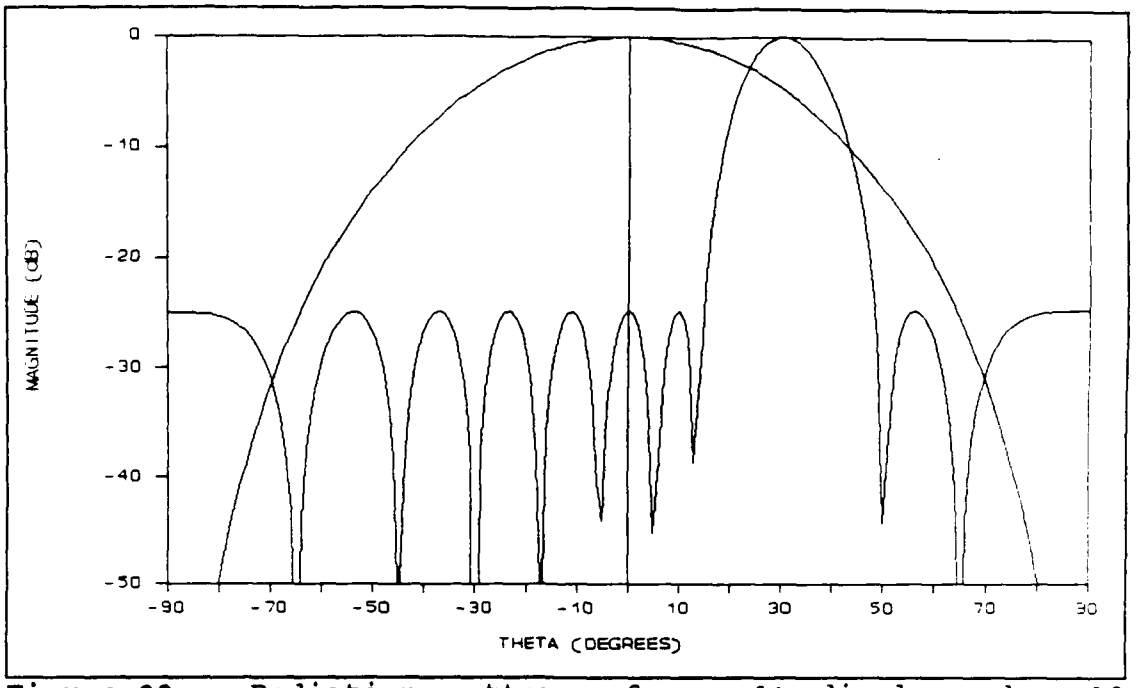

Figure 39. Radiation patterns for a 1λ dipole and a 10 element, Dolph-Chebyshev synthesized array with ½λ interelement spacing showing a -25 dB design side lobe level, scanned at 30° off broadside

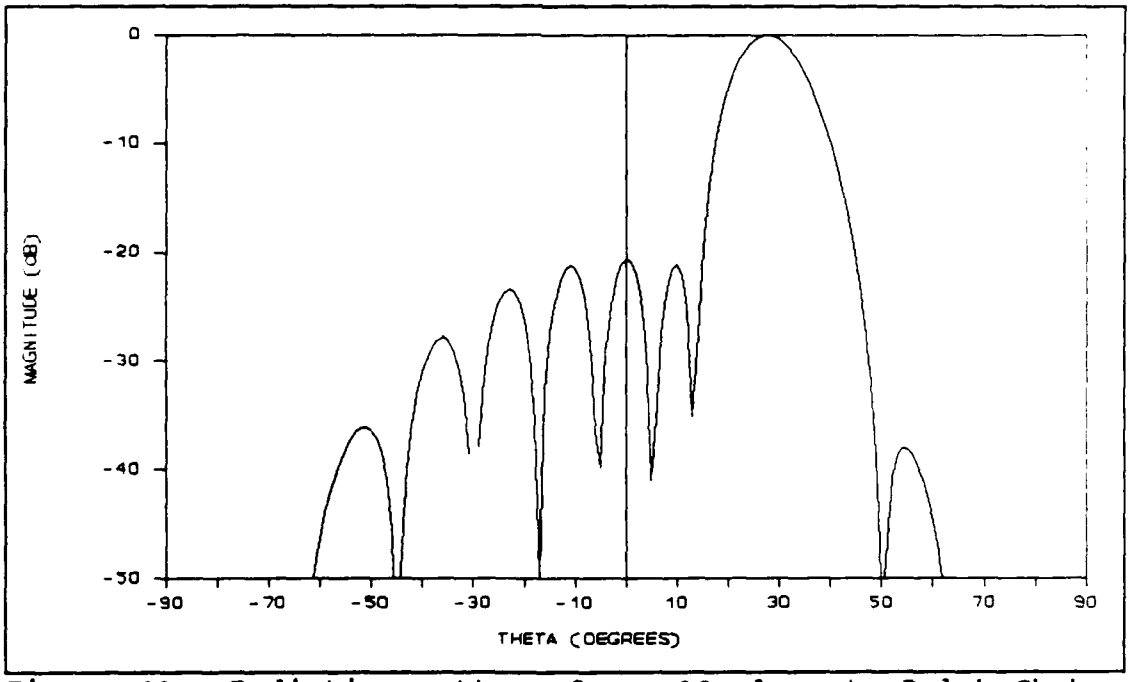

Figure 40. Radiation pattern for a 10 element, Dolph-Chebyshev synthesized array with ½λ interelement spacing and a -25 dB design side lobe level, and with 1λ dipoles as elements

30° from broadside or for an array of z-aligned dipoles for the main beam scanned much beyond 30° from endfire. If the beam is scanned past 30° from broadside with x- or y-aligned dipoles, another method of calculating the directivity is to use (10:206):

$$D_{PA} = 32{,}400/B_{areal} \tag{5.1}$$

where B_{areal} is the areal beamwidth given by:

$$B_{areal} = \theta_h \Psi_h \tag{5.2}$$

where θ_h and Ψ_h are in degrees. θ_h and Ψ_h are already computed by the program and can be used to calculate D_{PA} as will be seen shortly. The expression for the directivity in (5.1) is valid for planar arrays and most practical aperture distributions (10:206). If a linear array is being analyzed, then one could use the expression (10:157):

$$D_{LA} = 101.5°/\theta_h \tag{5.3}$$

where θ_h is the broadside half power beamwidth of a linear array and is expressed in degrees. Recall, in this program θ_h is associated with the x-axis and Ψ_h is associated with the y-axis for a broadside array. Therefore, when analyzing an array laying along the y-axis one would use Ψ_h in equation (5.3). Equations (5.1) and (5.3) provide a quick comparison with the other directivity values calculated in the program.

Now that we are assured that the excitation routines and the pattern factor routines are working properly, we can validate the beamwidth and directivity calculation routines.

To do this the program will be tested against several linear array and two planar array examples found in the literature.

Validation of the Beamwidth and Directivity Calculation Routines

The first part of this section deals with validating the beamwidth calculation routines in the program. First the program is validated against several linear array examples and then two planar array examples found in the literature. The last part of this section validates the directivity calculation routines against the same cases as for the beamwidth validation.

Beamwidth Validation. Eight different linear array cases found in the literature are used to validate the beamwidth routines. The eight linear cases are:

Case 1: Uniform current distribution, 5 elements, $\lambda/2$ spacing, $\theta_0=0°$, isotropic elements (23:149).

Case 2: Triangular current distribution, 5 elements, $\lambda/2$ spacing, $\theta_0=0°$, isotropic elements (23:149).

Case 3: Inverse triangular current distribution, 5 elements, $\lambda/2$, $\theta_0=0°$, isotropic elements (23:149).

Case 4: Binomial current distribution, 5 elements, $\lambda/2$ spacing, $\theta_0=0°$, isotropic elements (23:149).

Case 5: Dolph-Chebyshev synthesis, -20 dB design side lobe level, 5 elements, $\lambda/2$ spacing, $\theta_0=0°$, isotropic elements (23:150).

Case 6: Dolph-Chebyshev synthesis, -30 dB design side lobe level, 5 elements, $\lambda/2$, $\theta_0=0°$, isotropic elements (23:150).

Case 7: Dolph-Chebyshev synthesis, -26 dB design side lobe level, 10 elements, $\lambda/2$, $\theta_0=0°$, isotropic elements (4:257).

Case 8: Taylor $\bar{n}$-parameter synthesis ($\bar{n}=6$), -20 dB design side lobe level, null matching weights, 19 elements, 0.7λ spacing, $\theta_0=0°$, isotropic elements (19:79).

The beamwidths found in the literature and as calculated by the program are presented in Table VI for comparison. Comparing the beamwidths, we can see excellent agreement, except in Case 7. In Case 7, the beamwidths calculated by Balanis are calculated using certain approximations which may not be as accurate as the program.

Now, let us look at two cases for planar arrays and compare results. The two planar array cases are:

Case 9: A 10x10 array, Dolph-Chebyshev synthesis in both directions, -26 dB design side lobe level, $\lambda/2$ spacing both directions, $\theta_0=30°$, $\phi_0=45°$, isotropic elements (4:273).

Case 10: A 20x36 array, Dolph-Chebyshev synthesis both directions, -30 dB design side lobe level, 0.58λ spacing in the x-direction, 0.64λ spacing in the y-direction, $\theta_0=0°$, $\phi_0=0°$, isotropic elements (10:208-210).

The beamwidths for the planar array cases found in the literature and as calculated by the program are presented in Table VII for comparison. Again, there is good agreement between program results and the examples in the literature. Any discrepancies can be attributed to approximations used by the various authors.

Directivity Validation. The same ten cases used to validate the beamwidth calculations are used to validate the

directivity calculation routines. The directivities found in the literature and those calculated by the program are presented in Table VIII for comparison. Again we see excellent agreement with any discrepancies attributed to accuracy of element weights and approximations used by the various authors.

Error Validation

In this section, we will validate the error routines by confirming various trends in tolerance analysis noted in the literature. Unfortunately, specific examples for either the linear array or the planar array are not presented in the literature. If the following trends are confirmed, then, we will have reasonable confidence that the error routines are performing properly.

Before the trends are confirmed, we will run the program for a no-error situation to ensure the patterns and beamwidths of the no-error error routines match those of the design routines and to show that the change in directivity is 0 dB. We will rerun Case 7, page 112, to ensure the beamwidths and patterns of the no-error error routines match those of the design values. Table IX shows excerpts from the output file. We can see that the design and expected beamwidths match precisely and that the change in directivity is 0 dB. Figure 41 shows the no-error expected pattern and it matches Figure 19 precisely. Therefore, any differences we see between the design and expected values and the

Table VI. Linear array beamwidth comparisons

Case	Literature	Program
1	20.8°	20.7765°
2	26.0°	25.95161°
3	18.2°	18.23554°
4	30.3°	30.28262°
5	23.6°	23.70704°
6	26.4°	26.40292°
7	10.17°	12.34591°
8	4.1°	4.128539°

Table VII. Planar array beamwidth comparisons

Case	Literature		Program	
	Θ_h	Ψ_h	Θ_h	Ψ_h
9	12.67°	10.97°	14.60806°	12.60226°
10	5.0°	2.5°	5.4541°	2.69731°

Table VIII. Linear and planar array directivity comparisons

Case	Literature	Program
1	6.9897 dB	6.9897 dB
2	6.2941 dB	6.2973 dB
3	6.5128 dB	6.5142 dB
4	5.6348 dB	5.6314 dB
5	6.7025 dB	6.7078 dB
6	6.2531 dB	6.2590 dB
7	9.63 dB	9.5074 dB
8	13.90 dB	14.0468 dB
9	23.60 dB	23.3615 dB
10	34.1 dB	34.0463 dB

Table IX. Design versus no-error expected parameters

ARRAY TOLERANCE DATA:

ELEMENT RMS DRIVE AMPLITUDE ERROR:	.0000000 UNITS
ELEMENT RMS PHASE ERROR:	.0000000 degree(s)
RMS ERROR IN X-PLACEMENT:	.0000000 cms
RMS ERROR IN Y-PLACEMENT:	.0000000 cms
RMS ERROR IN Z-PLACEMENT:	.0000000 cms
RMS ELEMENT PATTERN ERROR:	-100.0000000 dB
FRACTION OF ELEMENTS OPERATING:	1.0000000

SCAN ANGLES:

THETA0 = .0000000 degrees PHI0 = .0000000 degrees

BEAMWIDTHS FOR DESIGN ARRAY AT GIVEN SCAN ANGLES:

	THETA sub H	PSI sub H
UPPER FREQUENCY:	11.7263900 degrees	7.6491070 degrees
CENTER FREQUENCY:	12.3459100 degrees	8.0523400 degrees
LOWER FREQUENCY:	12.9657800 degrees	8.4556710 degrees

BEAMWIDTHS FOR EXPECTED ARRAY AT GIVEN SCAN ANGLES:

	THETA sub H	PSI sub H
UPPER FREQUENCY:	11.7263900 degrees	7.6491070 degrees
CENTER FREQUENCY:	12.3459100 degrees	8.0523400 degrees
LOWER FREQUENCY:	12.9657800 degrees	8.4556710 degrees

DIRECTIVITIES FOR DESIGN AND EXPECTED ARRAY AT GIVEN SCAN ANGLES:

	DESIGN ARRAY	CHANGE DUE TO ERRORS
UPPER FREQUENCY:	26.2509700 dB	.0000000 dB
CENTER FREQUENCY:	25.8114200 dB	.0000000 dB
LOWER FREQUENCY:	25.3932600 dB	.0000000 dB

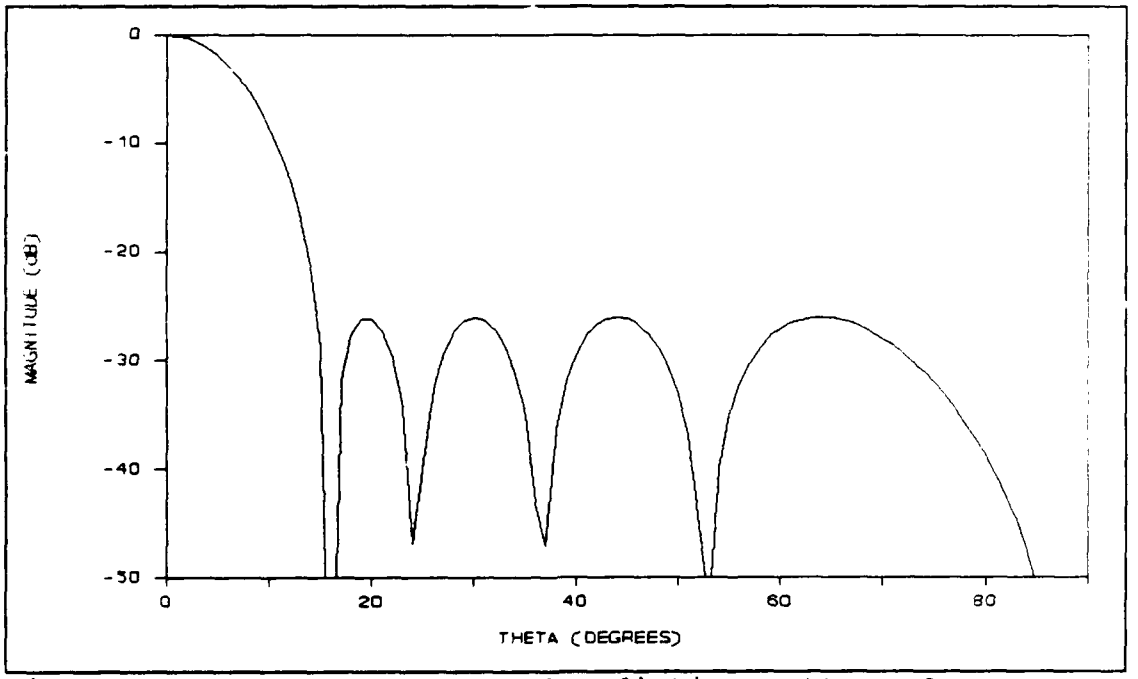

Figure 41. No-error expected radiation pattern for a 10x15 element, Dolph-Chebyshev synthesized array with $\lambda/2$ spacing and a -26 dB design side lobe level in both directions

patterns are due to errors in the design and not numerical errors caused by the program.

Five different trends were identified during the literature review and will be used to validate the error routines. The five trends are:

Trend 1: The rise in side lobe level due to random errors, for a given set of tolerances and number of elements, increases as the side lobe level is further suppressed (3:240; 11:120; 17:98).

Trend 2: For a given set of tolerances, pattern deterioration is found to decrease as the array is enlarged (11:120; 20:177).

Trend 3: For a given set of tolerances, pattern deterioration is less for a planar array of size L^2 than it is for a linear array of length L (11:120).

Trend 4: The side lobe level increase due to random errors does not depend on scan angle (11:120).

Trend 5: Translational errors in the positions of the elements are found to cause the dominant effect while amplitude errors in the radiating currents are of secondary importance (11:120).

When Elliott showed the fifth trend, he did not consider the fraction of elements operating. Therefore, when we confirm the fifth trend, we will set the fraction of elements operating to one and then proceed. The fraction of elements operating will overshadow any other errors in the design as we will show in confirming the fifth trend.

All five trends will be confirmed by using Dolph-Chebyshev synthesized arrays with isotropic elements. Dolph-Chebyshev patterns provide a good pattern for analyz-

ing these trends. Also, isotropic elements are used since dipoles tend to distort the pattern and what we really want to see are pattern distortions due to errors. Since we will be using isotropic elements, the RMS error in the element pattern will be set to -100 dB so as not to have any effect on the calculations.

To confirm the first trend, let us consider a 10x10 element planar array, with a Dolph-Chebyshev synthesized current distribution in both directions and $\lambda/2$ element spacing. Four runs of the program were made with a decrease of 5 dB in the side lobe level for each run beginning with a -25 dB design side lobe level. The following error data was used for each run:

RMS amplitude error:	0.002	units
RMS phase error:	10.0	degrees
RMS error in x-placement:	0.002	cms
RMS error in y-placement:	0.002	cms
RMS error in z-placement:	0.002	cms
RMS error in element pattern:	-100.0	dB
Fraction of elements operating:	1.0	

The plots of the expected radiation pattern overlaid on the design radiation pattern for each run are shown in Figures 42-45. Comparing these figures, we can see the side lobe level of the error pattern rising the further the design side lobe level is suppressed confirming the first trend. This trend can be explained by comparing the element weights for each run. As the side lobe level is further reduced, the end element weights begin to increase causing an abrupt change in the aperture distribution at the ends of the

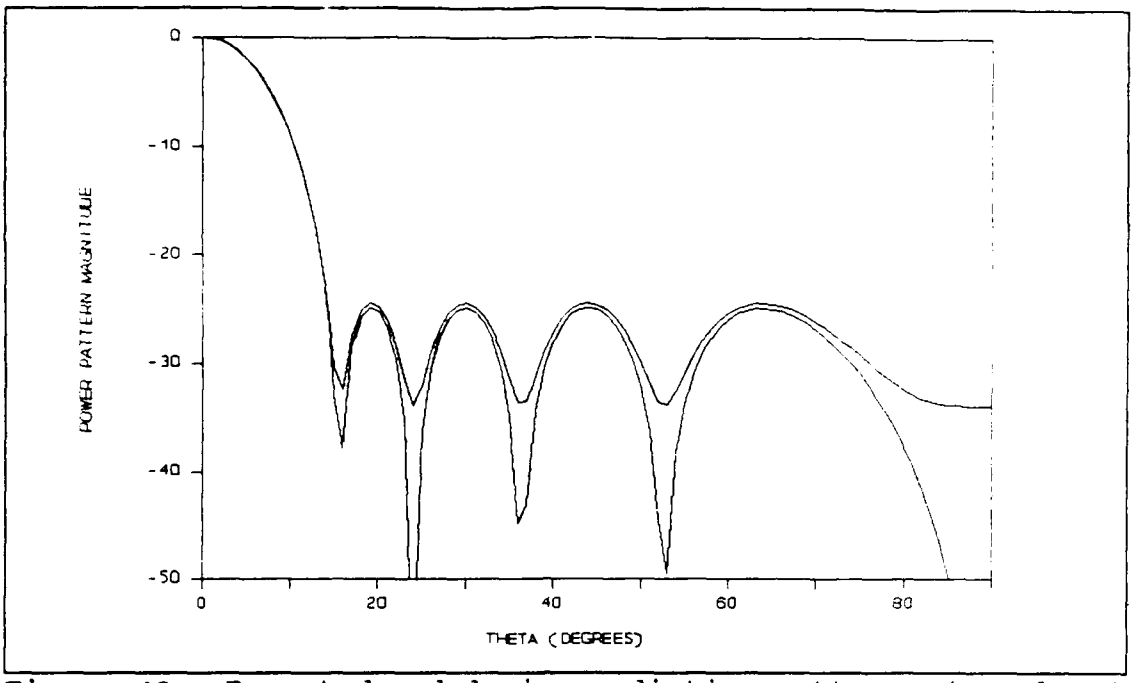

Figure 42. Expected and design radiation patterns (xz-plane) for a 10x10 element, Dolph-Chebyshev synthesized array with $\lambda/2$ spacing and a -25 dB design side lobe level

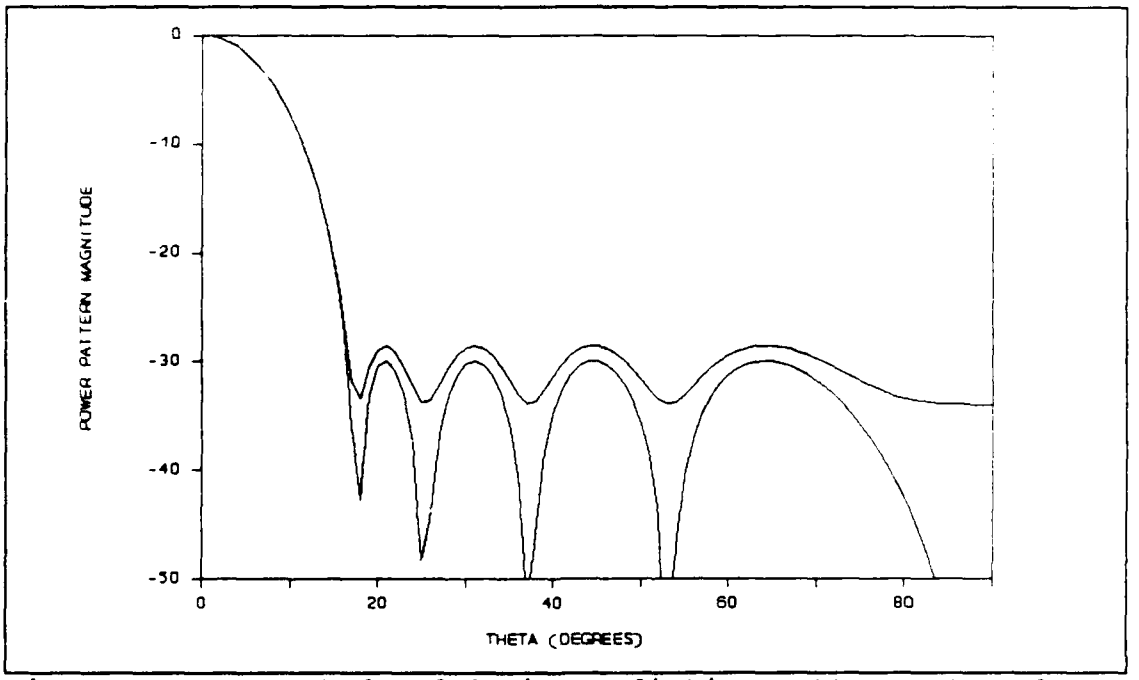

Figure 43. Expected and design radiation patterns (xz-plane) for a 10x10 element, Dolph-Chebyshev synthesized array with $\lambda/2$ spacing and a -30 dB design side lobe level

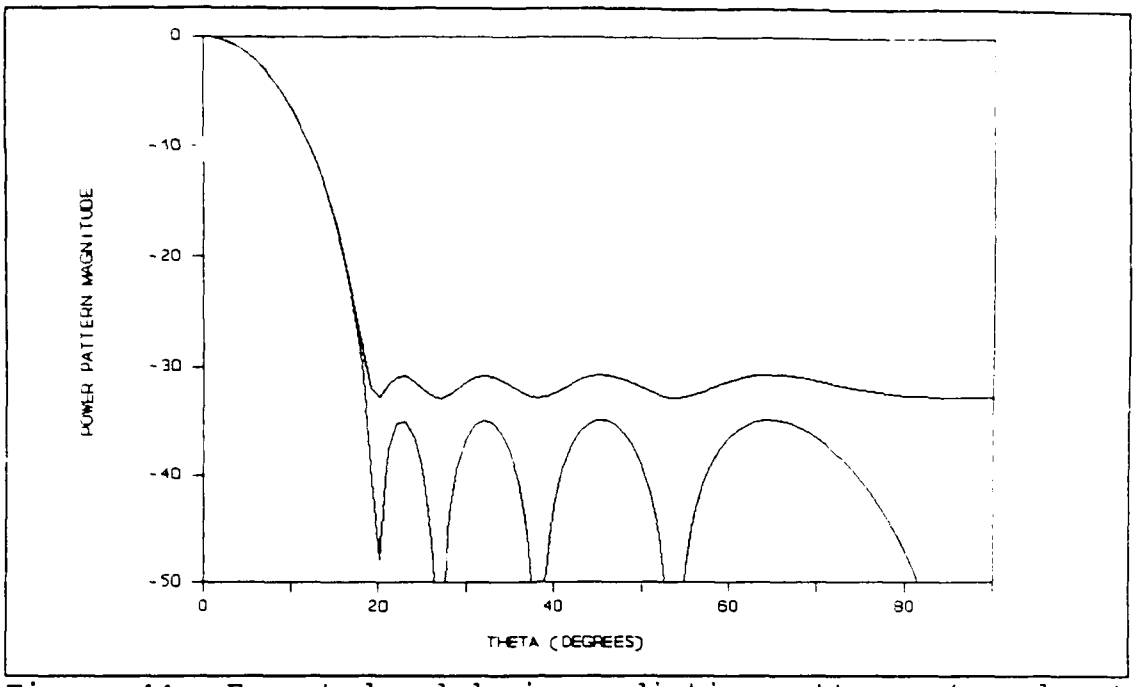

Figure 44. Expected and design radiation patterns (xz-plane) for a 10x10 element, Dolph-Chebyshev synthesized array with $\lambda/2$ spacing and a -35 dB design side lobe level

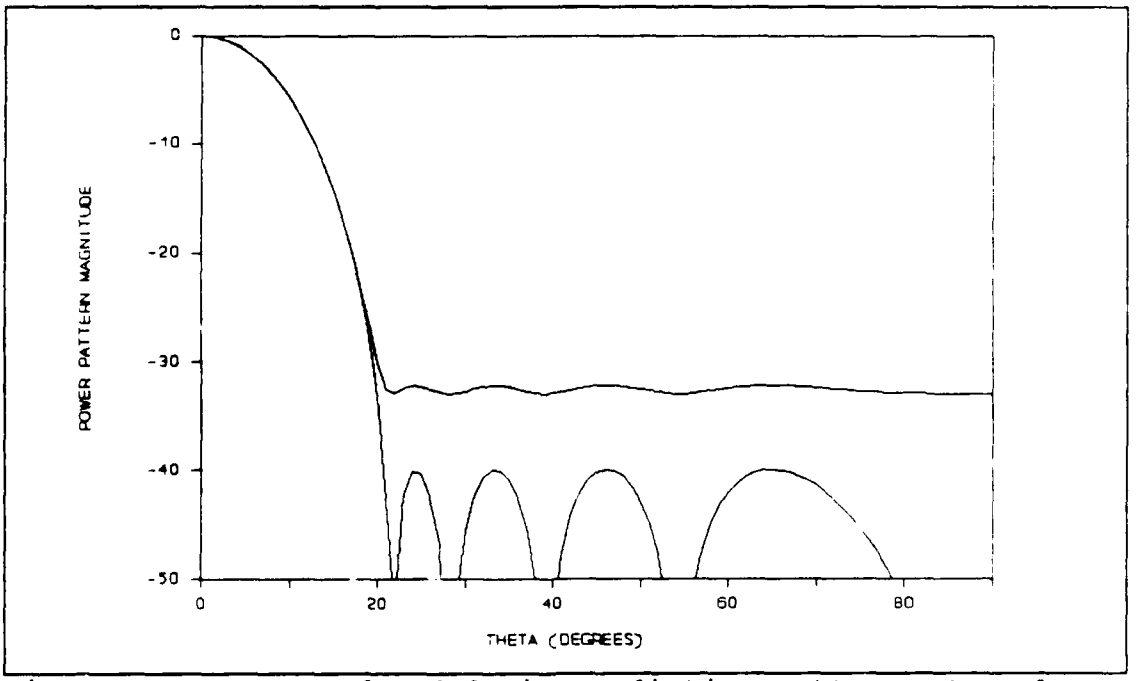

Figure 45. Expected and design radiation patterns (xz-plane) for a 10x10 element, Dolph-Chebyshev synthesized array with $\lambda/2$ spacing and a -40 dB design side lobe level

array. This abrupt change at the ends of the array coupled with the errors in the design cause the side lobe level to increase.

The second trend is confirmed by considering four different sizes of planar arrays. Each array will have a Dolph-Chebyshev synthesized current distribution with a design side lobe level of -30 dB and the same errors presented earlier. Figures 46-49 show the expected radiation pattern overlaid on the design radiation pattern for a 10x10, 12x12, 15x15, and 20x20 element planar array, respectively. By comparing these figures, we see the pattern distortion decreasing as the size of the array increases confirming the second trend. The reason this trend is occurring is because as the array becomes larger (more elements) the sum of all the errors tends to the mean of the design thus reducing the overall effects of the errors.

For the third trend, we will consider a 20x20 element planar array and a 20 element linear array. Each array will have a Dolph-Chebyshev synthesized current distribution giving a -30 dB design side lobe level, $\lambda/2$ element spacing, and the same set of tolerances used earlier. The expected radiation pattern overlaid on the design radiation pattern is shown in Figure 50 for the planar array. The expected radiation pattern overlaid on the design radiation pattern for the linear array is shown in Figure 51. Comparing Figures 50 and 51 we can see that the expected pattern in

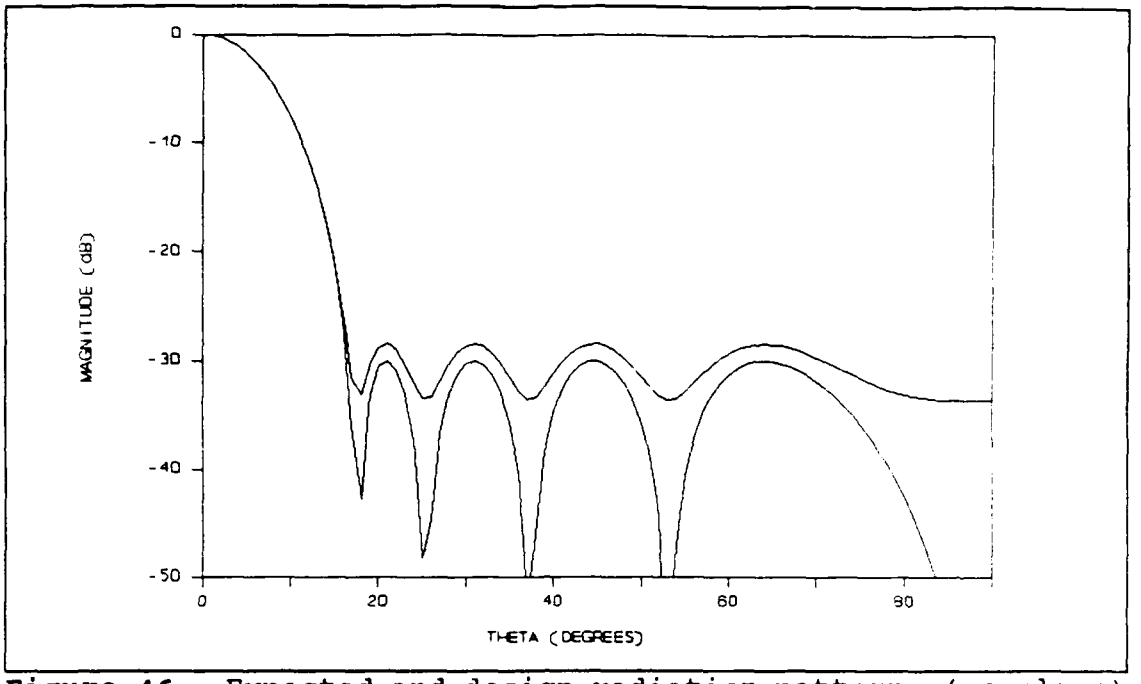

Figure 46. Expected and design radiation patterns (xz-plane) for a 10x10 element, Dolph-Chebyshev synthesized array with $\lambda/2$ spacing and a -30 dB design side lobe level

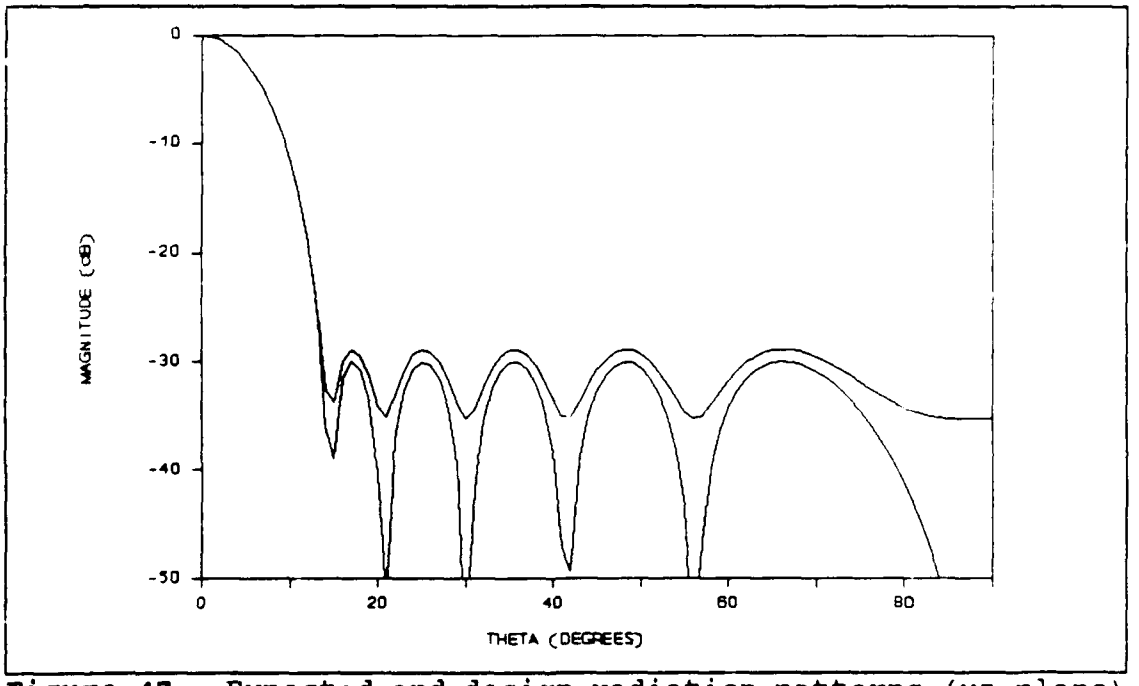

Figure 47. Expected and design radiation patterns (xz-plane) for a 12x12 element, Dolph-Chebyshev synthesized array with $\lambda/2$ spacing and a -30 dB design side lobe level

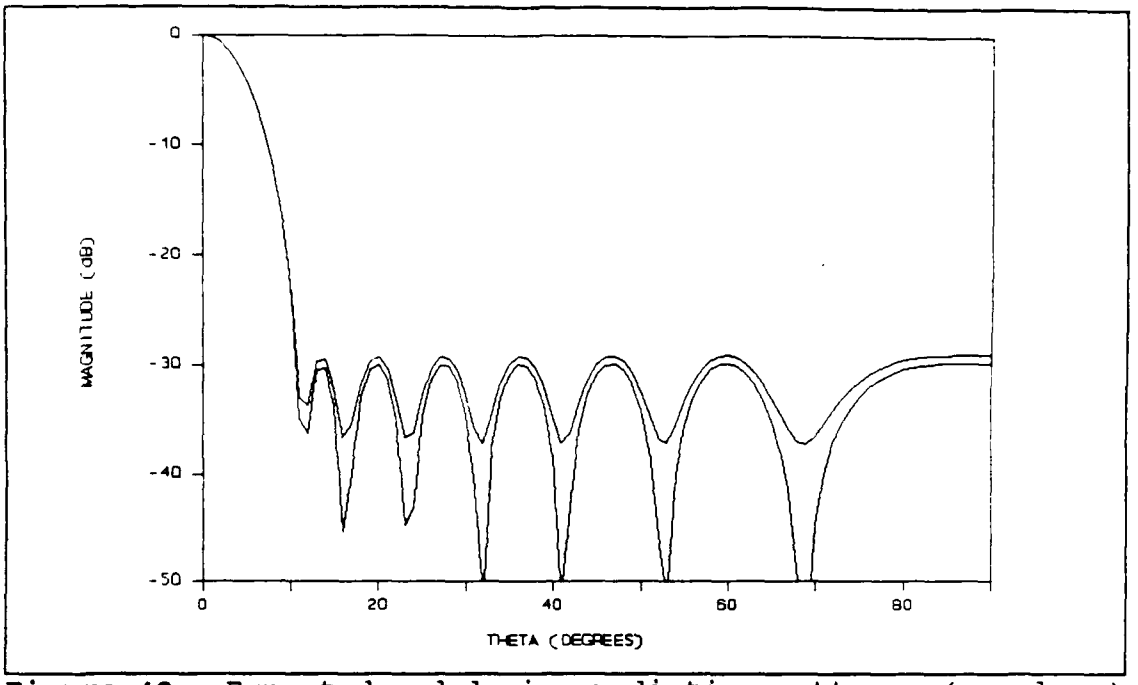

Figure 48. Expected and design radiation patterns (xz-plane) for a 15x15 element, Dolph-Chebyshev synthesized array with $\lambda/2$ spacing and a -30 dB design side lobe level

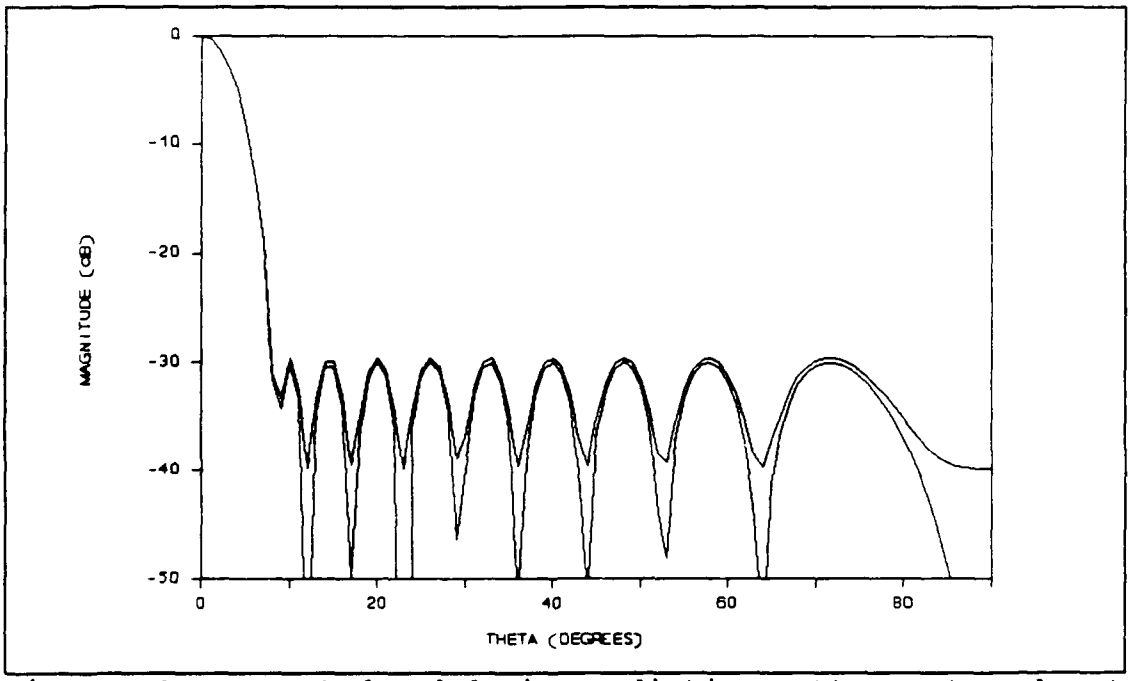

Figure 49. Expected and design radiation patterns (xz-plane) for a 20x20 element, Dolph-Chebyshev synthesized array with $\lambda/2$ spacing and a -30 dB design side lobe level

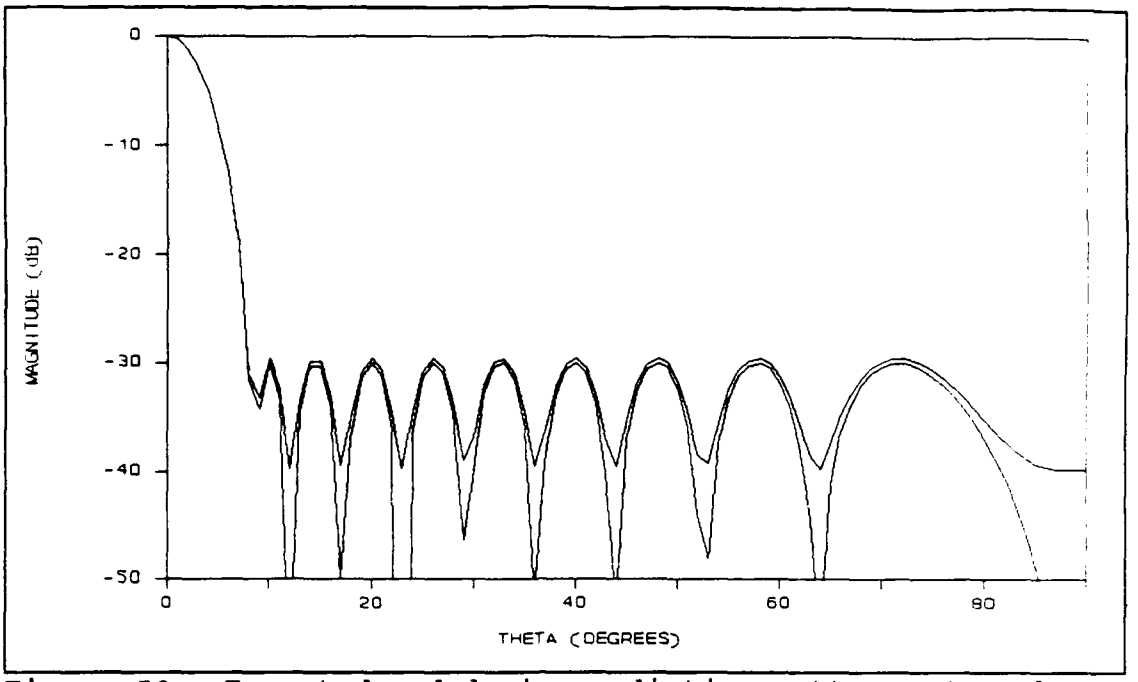

Figure 50. Expected and design radiation patterns (xz-plane) for a 20x20 element, Dolph-Chebyshev synthesized array with $\lambda/2$ spacing and a -30 dB design side lobe level

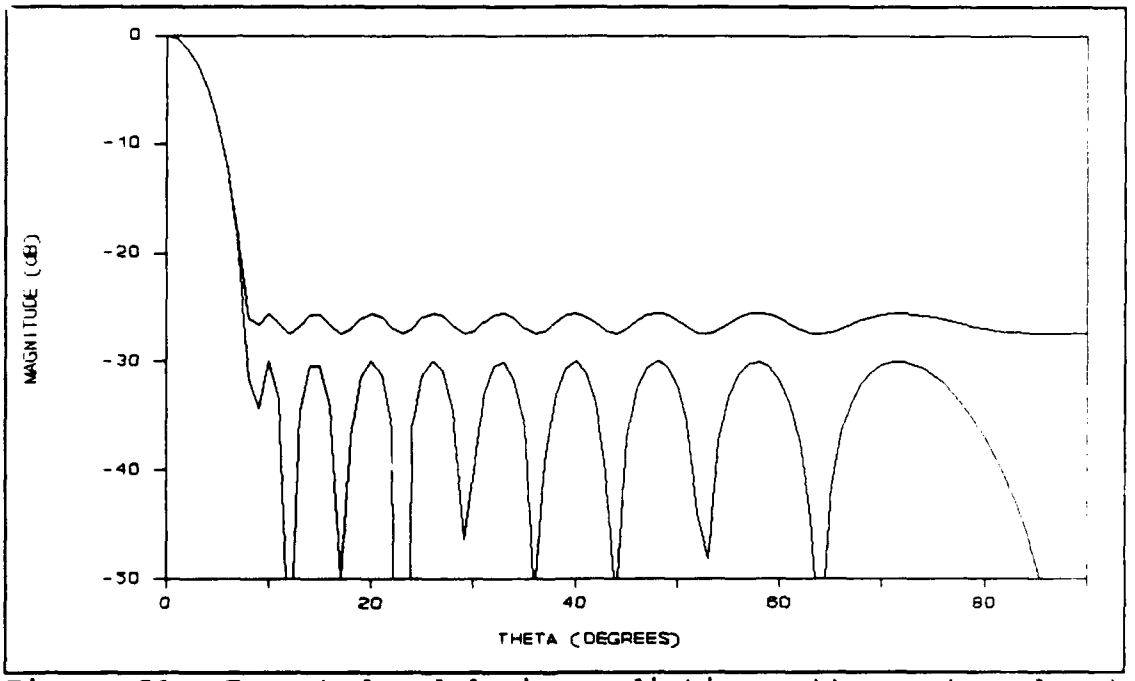

Figure 51. Expected and design radiation patterns (xz-plane) for a 20 element, Dolph-Chebyshev synthesized array with $\lambda/2$ spacing and a -30 dB design side lobe level

Figure 50 is considerably less distorted than the expected pattern in Figure 51. Again, the reason this trend occurs can be attributed to the increased number of elements and the fact that the errors tend to their mean value as the population (of elements) grows.

The fourth trend is confirmed by considering five different scan angles in the same array. The scan angle is varied in 10° increments beginning at 0° and scanning through 40° for a 15x15 element planar array with a Dolph-Chebyshev synthesized current distribution giving a -30 dB design side lobe level, with $\lambda/2$ element spacing. The case for the array scanned at broadside (0°) is shown in Figure 48. The cases for the array scanned at 10°, 20°, 30°, and 40° are shown in Figures 52-55, respectively. Each figure shows the expected radiation pattern overlaid on the design radiation pattern. By comparing all five figures, we can see that the side lobe level due to errors remains constant as the array is scanned through 40° confirming this trend. This trend is best explained by considering equation (3.39) and the same reasoning used in deriving the change in directivity due to errors. In Chapter III we showed that $\epsilon^2(\theta,\phi)$ was only weakly angle dependent and, this being the case, the second term in equation (3.39) becomes that of an omni-directional type pattern. This adds a constant term to the overall pattern that does not increase or decrease with scan angle.

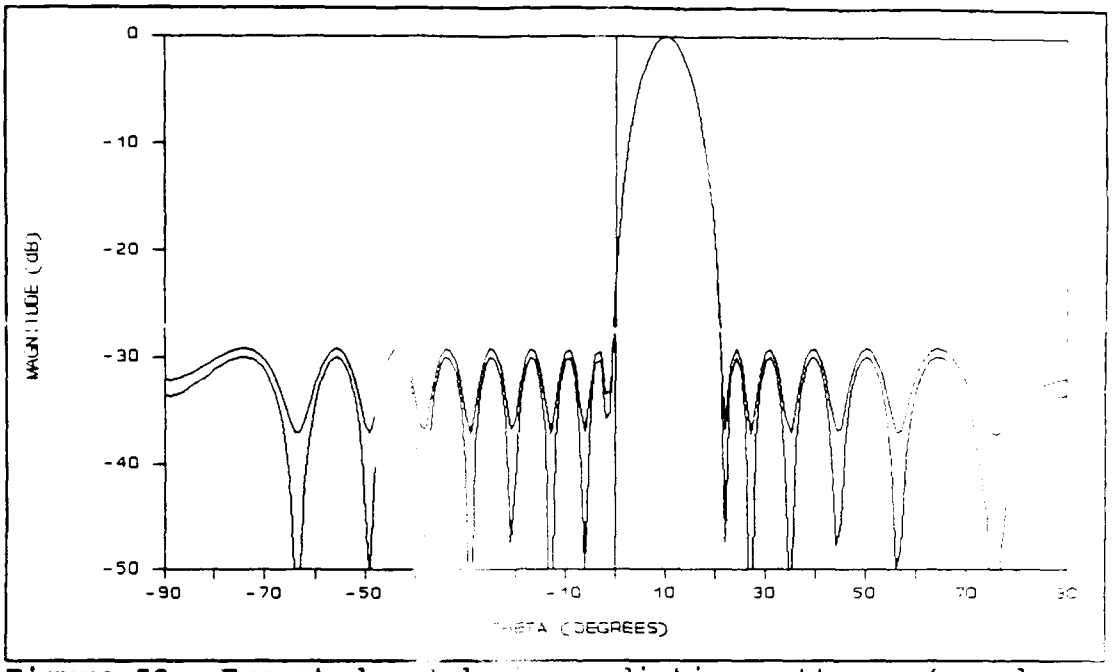

Figure 52. Expected and design radiation patterns (xz-plane) for a 15x15 element, Dolph-Chebyshev synthesized array with $\lambda/2$ spacing and a -30 dB design side lobe level scanned at 20° from broadside

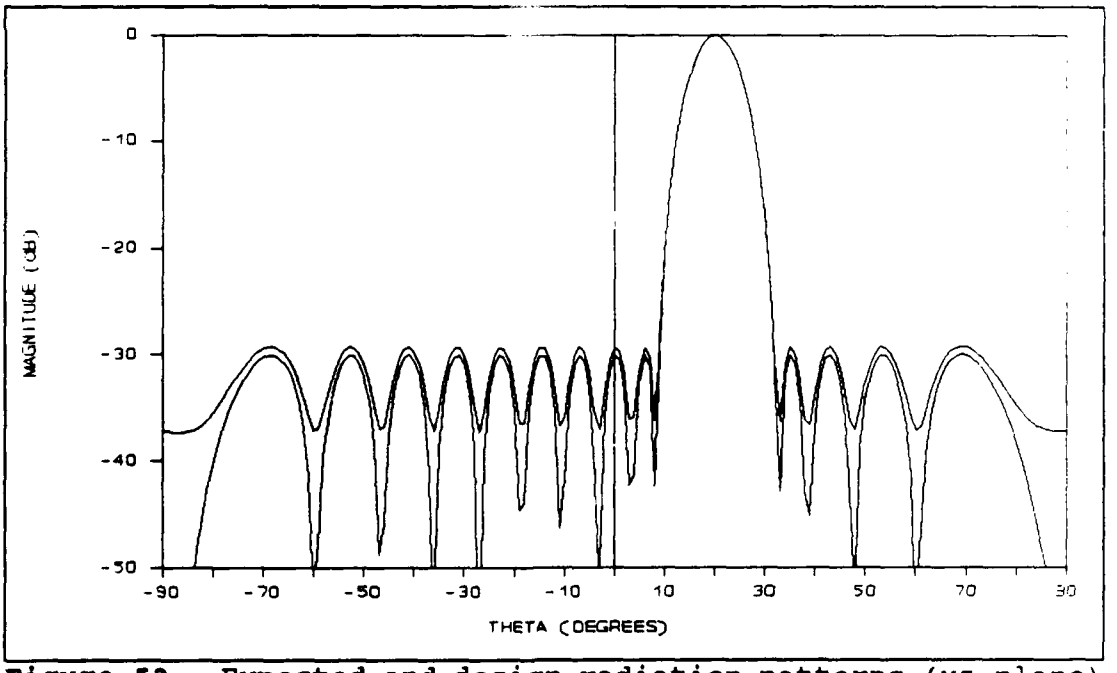

Figure 53. Expected and design radiation patterns (xz-plane) for a 15x15 element, Dolph-Chebyshev synthesized array with $\lambda/2$ spacing and a -30 dB design side lobe level scanned at 20° from broadside

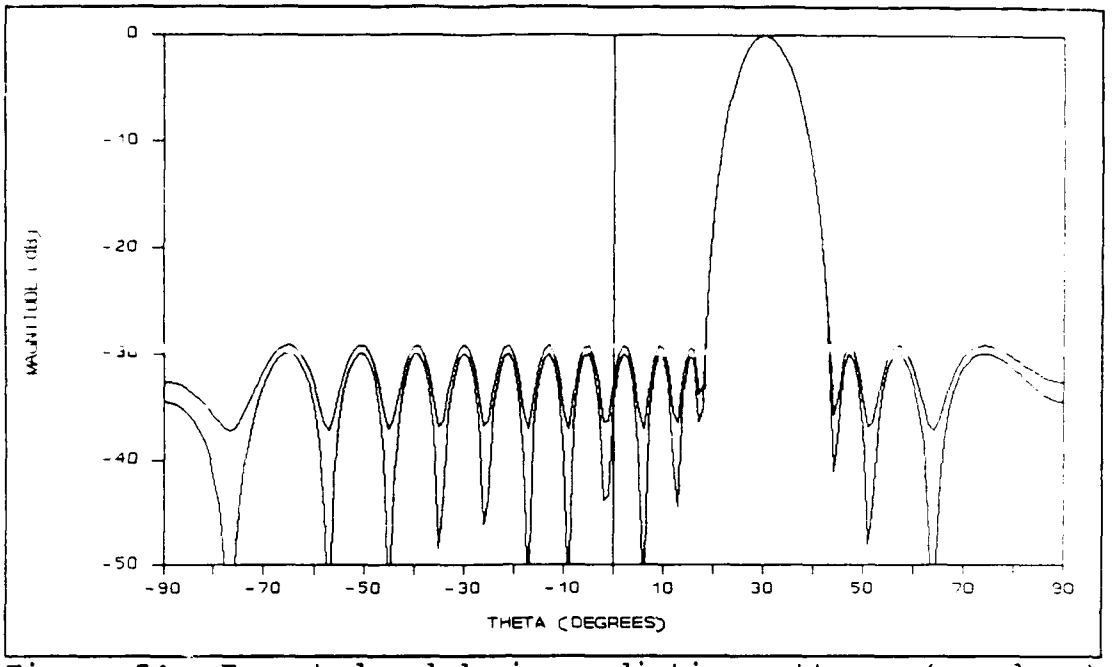

Figure 54. Expected and design radiation patterns (xz-plane) for a 15x15 element, Dolph-Chebyshev synthesized array with $\lambda/2$ spacing and a -30 dB design side lobe level scanned at 30° from broadside

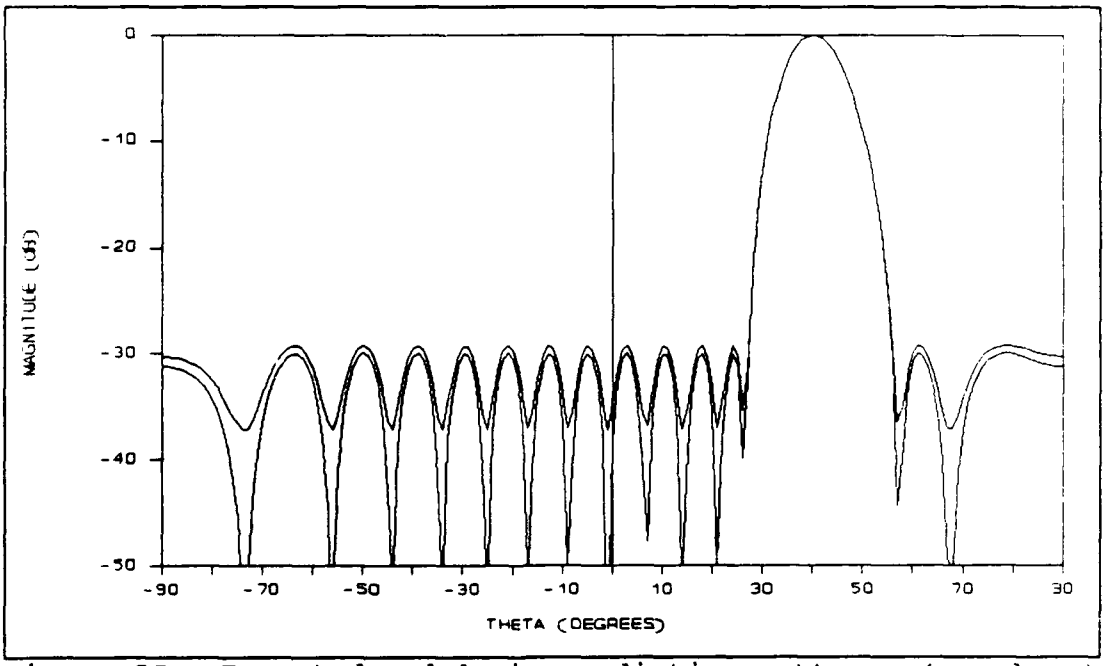

Figure 55. Expected and design radiation patterns (xz-plane) for a 15x15 element, Dolph-Chebyshev synthesized array with $\lambda/2$ spacing and a -30 dB design side lobe level scanned at 40° from broadside

In order to validate the fifth trend an extensive sensitivity analysis would have to be undertaken which is not within the purview of this paper. Instead, we will take a qualitative look at which errors are the most dominant by examining equation (3.39), and by looking at a pattern with typical errors, and removing them one-at-a-time until the design pattern is obtained.

For this analysis, the absolute value of $\overline{|U(\theta,\phi)|^2}$ is immaterial so we can divide equation (3.39) by $P^2\Psi_{AP}(\theta,\phi)$ and look at the term preceding the double summation of the second term in equation (3.39). Calling this term the error term (E.T.) we have:

$$E.T. = \left[\left[1 + \sigma_A^2(\theta,\phi)\right]/P\Psi_{AP}(\theta,\phi)\right] - 1 \qquad (5.4)$$

If the variances in the term $\Psi_{AP}(\theta,\phi)$ as given by equation (3.37) are roughly equal, we can rewrite equation (5.4) as:

$$E.T. = \left[\left[1 + \sigma_A^2\right]\exp(\overline{\delta^2})\exp(k^2\overline{\gamma_x^2})/P\right] - 1 \qquad (5.5)$$

In equation (5.5) we see that the error term is inversely proportional to the fraction of elements operating. P clearly has the potential for causing the dominant effect if element reliability is not very high. Assuming for now that P is approximately one the next dominant effect will come from the translational errors in the positions of the elements. Since the variance in the element position is multiplied by the factor k^2 in the exponential, it clearly has the leading effect on the overall pattern. It is purely

conjecture as to which of the remaining two factors, variance in the phase error or the amplitude error, would be the more dominant of the two. Elliott claims that errors in the radiating currents are of secondary importance (11:120).

To illustrate which errors are most dominant and the least dominant, let us consider a case with realistic errors. Consider a 10x10 planar array with a Dolph-Chebyshev synthesized current distribution giving a -30 dB design side lobe level and $\lambda/2$ element spacing. The center operating frequency is 18 GHz. For the errors, we will assume the radiating elements are tolerably matched to the feed structure such that the RMS amplitude and phase errors are 0.1 and 5°, respectively. We will assume the array is manufactured with a 0.05 centimeter RMS error in the (x,y,z) placement of the individual radiating elements. Finally, for the mission being considered, we can expect no more than 10 elements will fail. The resulting total error pattern overlaid with the design pattern is shown in Figure 56. Now let us remove the errors one-at-a-time until we get the design radiation pattern back. With the phase error set to zero, the resulting pattern is shown in Figure 57. Comparing Figures 56 and 57 we see very little change in the expected pattern. The expected pattern with both the amplitude and phase errors set to zero and all other errors remaining is shown in Figure 58. Again, there is very

little change in the expected pattern. The expected pattern with the fraction of elements set to one and the amplitude and phase errors set to zero and just the translational errors remaining is shown in Figure 59. We can see a significant change in the expected patterns between Figures 58 and 59. Setting the translational errors to zero so that all errors are zero or one in the case of the fraction of elements operating, we obtain the design pattern as shown in Figure 60. Though not conclusive, we can infer that the translational errors, as small as they were, caused the largest degradation in the pattern as evidenced by comparing the transition of the expected pattern from Figure 58 to 59 and then from Figure 59 to 60. Of secondary importance is the fraction of elements operating followed by the amplitude error.

Summary

In this chapter the program PARRAY.EXE was validated to ensure each routine functioned properly. The routines for generating the element weights were validated against examples found in the literature. The pattern factor routines were validated by using the element weights and other specific array parameters to produce data points whereby patterns could be plotted and compared to patterns in the literature or by knowing how the pattern should appear. The program was used to produce Dolph-Chebyshev and Taylor synthesized current distributions and patterns, uniform and binomial

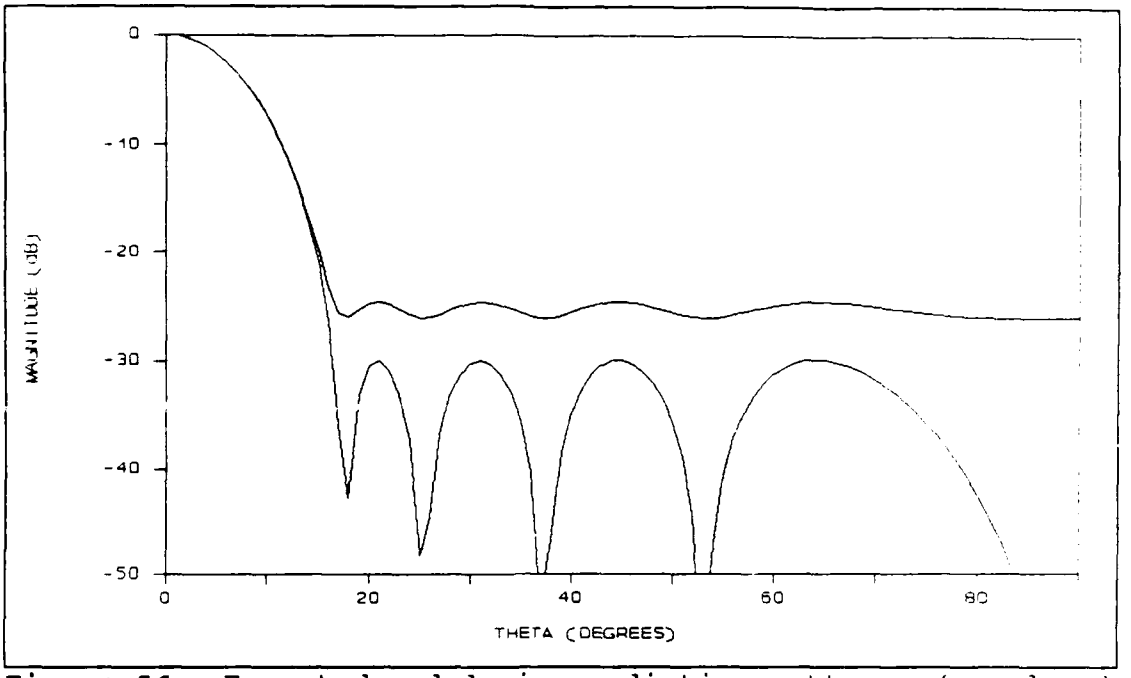

Figure 56. Expected and design radiation patterns (xz-plane) for a 10x10 element, Dolph-Chebyshev synthesized array with $\lambda/2$ spacing and a -30 dB design side lobe level (all errors present)

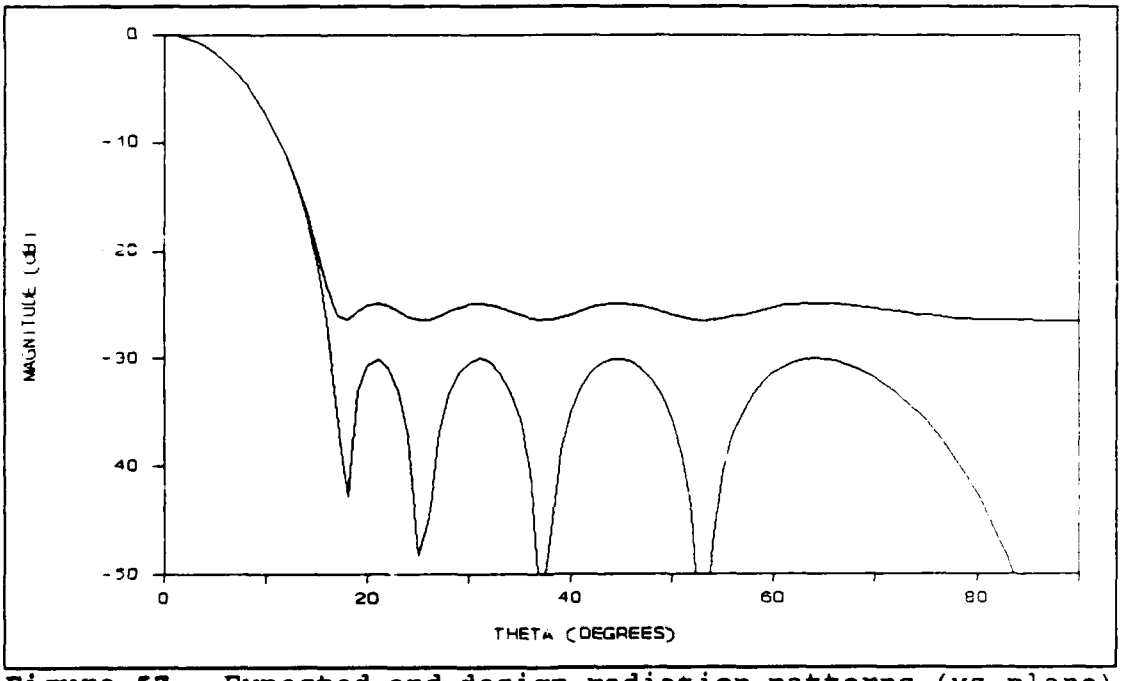

Figure 57. Expected and design radiation patterns (xz-plane) for a 10x10 element, Dolph-Chebyshev synthesized array with $\lambda/2$ spacing and a -30 dB design side lobe level (phase error set to 0)

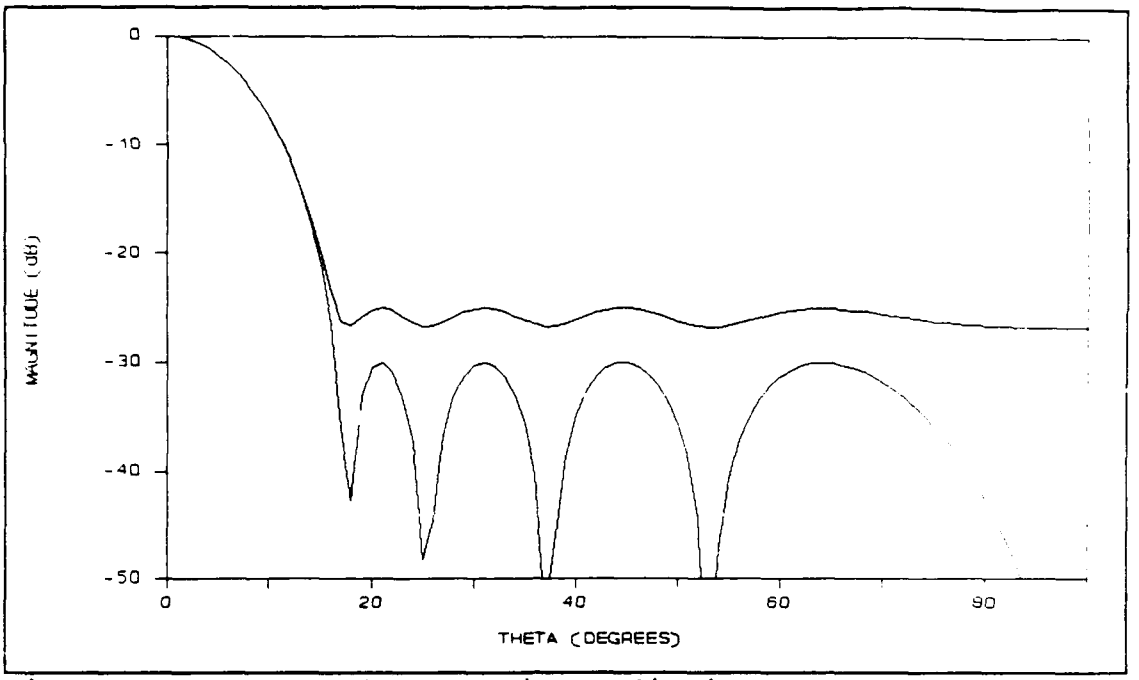

Figure 58. Expected and design radiation patterns (xz-plane) for a 10x10 element, Dolph-Chebyshev synthesized array with $\lambda/2$ spacing and a -30 dB design side lobe level (phase and amplitude errors set to 0)

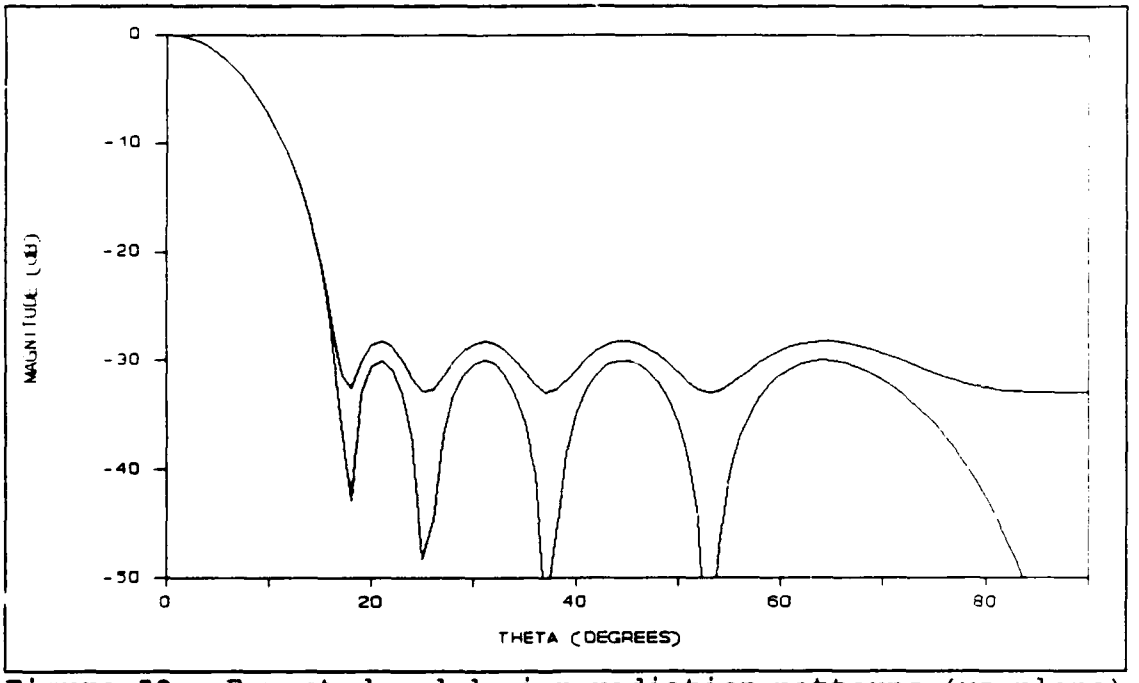

Figure 59. Expected and design radiation patterns (xz-plane) for a 10x10 element, Dolph-Chebyshev synthesized array with $\lambda/2$ spacing and a -30 dB design side lobe level (amplitude and phase errors set to 0; P = 1)

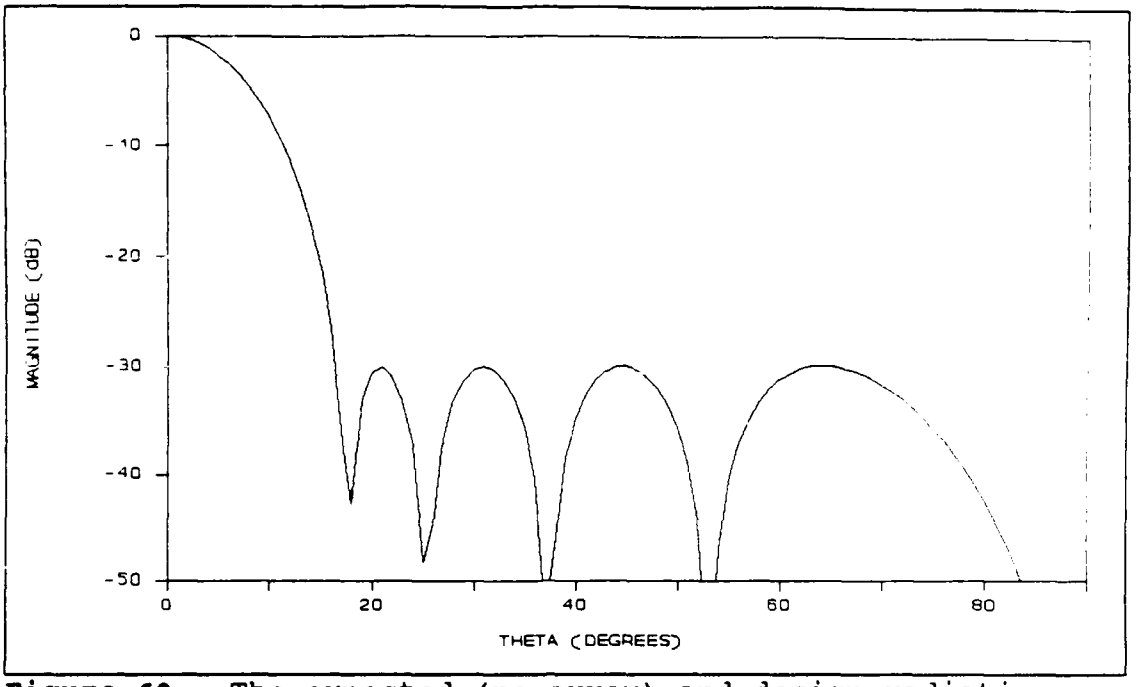

Figure 60. The expected (no-error) and design radiation patterns (xz-plane) for a 10x10 element, Dolph-Chebyshev synthesized array with $\lambda/2$ spacing and a -30 dB design side lobe level

current distributions and patterns, and the user-defined routine was used to produce triangular and inverse-triangular current distributions and patterns.

Next, the beamwidth and directivity calculation routines were validated against examples in the literature for linear and planar arrays. The beamwidth routines performed properly as did the directivity routines, however, it was shown that the directivity routines may not be as accurate when long dipoles (in terms of wavelength) are considered as elements in the array or when the array is scanned past 40° from broadside for dipoles much longer than one-half wavelength. These problems arise because of the restrictions placed on the directivity expression used in the program.

An alternate method of quickly computing the directivity was given in equation (5.1). The directivity calculated by (5.1) can be compared to the directivity calculated by the program to establish a bound on the true directivity.

Finally, the error routines were validated by comparing patterns plotted from data calculated by the error routines to five trends noted in the literature. Also, the error routines were run for a no-error case to show that the beamwidths matched those of the design beamwidths and that there was no change in directivity due to errors. This ensures the integrity of the program in determining the differences between the design array and the expected arrays. The specific case used to validate the error routines was not the only one used for this purpose. Several cases were run, but, only this one was presented as being representative of all the cases that were run, in confirming the error routines.

VI. Conclusions and Recommendations

A program was developed to analyze the effects of perturbations in an array's design parameters on the overall performance of the array. An expression relating these perturbations to the planar array's radiation pattern was derived and used in developing the tolerance analysis routines used in the program. Tolerances considered by the program include amplitude and phase errors in the element's drive current, errors in the element positions within the array, and errors between an element's actual pattern and the average element pattern, as well as the fraction of elements operating. The program user can input an array's design parameters and tolerances and assess the impact of the tolerances on the array's side lobe level, beamwidth, and directivity for a specified bandwidth and scan angle.

Several trends were evident as confirmed by the program. First, the rise in side lobe level due to random errors, for a given set of tolerances and number of elements, increases (relative to the design side lobe level) as further design side lobe level suppression is attempted. Second, for a given set of tolerances, pattern deterioration was found to decrease as the array was enlarged. Third, for a given set of tolerances, pattern deterioration is less for a planar array of size L^2 than it is for a linear array of length L. Fourth, the side lobe level increase due to random errors does not depend on scan angle or is, at most,

weakly dependent on scan angle. Finally, translational errors in the positions of the elements were found, qualitatively, to cause the dominant effect in pattern deterioration provided the fraction of elements operating is high.

The array antenna engineer or program manager now has a useful tool for assessing the effects of tolerances, at least to a first order, on the performance of an array. Two avenues are now evident for the user in designing an array in the presence of errors. The user can specify the tolerances in a specification or the user can over-design the array by designing for an M dB side lobe level when an N dB side lobe level is desired. The user can use this program to determine the amount of over-design needed to produce the desired side lobe level.

There are several logical steps that can be taken in continuing the work presented in this paper. The element weights in the program could be modified to be complex, thereby, becoming more general. The user could then enter weights in the form $|I|e^{j\phi}$ and, therefore, the program could consider a wider variety of array excitations and patterns. However, along with this generalization, a more general means of calculating the directivity would have to be developed and used in the program. A routine could be added for investigations of deliberate element omission, where the variable P becomes a function of position. Additional element types could be added to the program making it more

comprehensive, provided a new, general means of calculating the directivity is developed, as mentioned earlier. Designated errors could also be made completely random in the program by using a random number generator to create errors within a certain standard deviation bound. That is, for a specified root-mean-square error, 68% of the error values would be within one standard deviation of the mean, 95% within two standard deviations of the mean, and 99% within three standard deviations of the mean while conforming to the magnitude restrictions set forth in Chapter I. Finally, a sensitivity analysis could be performed and a nomograph made giving the antenna designer a priority of which errors to reduce first, and to what level, before reducing other errors.

Two additional routines could be added to the program. One routine would calculate the probability of a side lobe level exceeding the design side lobe level in different regions of the pattern. This would be of particular interest since most antenna designers are interested in this quantity. A second beneficial routine would determine the change in pointing direction of the main beam due to errors. These two routines, along with the other aforementioned changes would greatly enhance the overall effectiveness of this program.

Appendix A: Development of the Finite Length Dipole Element Factor

In this appendix, the element factors for a finite length dipole oriented along the x-, y-, or z-axis are developed (23:195-196).

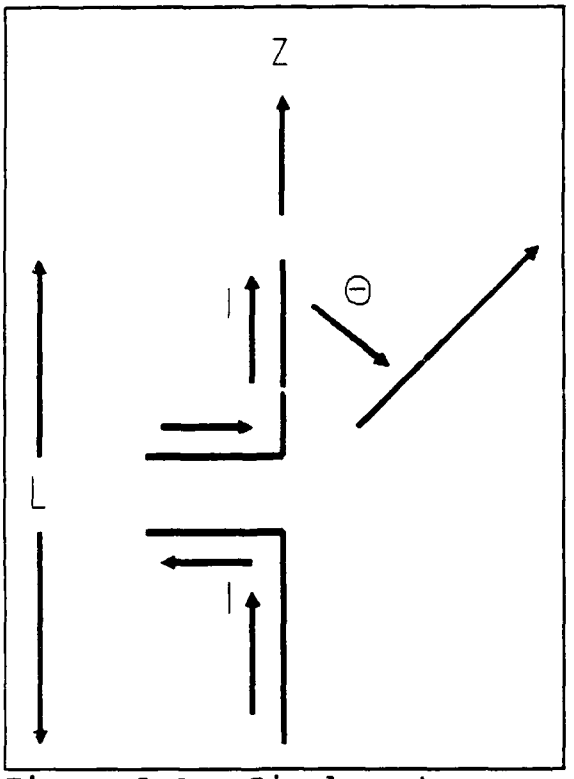

Figure A.1. Dipole antenna along z-axis

Consider a dipole of length L aligned along the z-axis as shown in Figure A.1. We assume a sinusoidal current distribution along the dipole such that:

$$I(z) = I_m \sin\left[k\left[(L/2)-|z|\right]\right] \quad (A.1)$$

for $|z| \leq (L/2)$. To find the dipole radiation pattern we must apply equation (2.27) substituting in our expression for the current distribution. Equation (2.27) becomes:

$$U_\theta(\theta,\phi) = I_m \sin\theta \left[\int_{-L/2}^{0} \sin\left[k\left[(L/2)+z'\right]\right] \exp(jkz'\cos\theta)\,dz' + \int_{0}^{L/2} \sin\left[k\left[(L/2)-z'\right]\right] \exp(jkz'\cos\theta)\,dz' \right] \quad (A.2)$$

We can evaluate these integrals using:

$$\int e^{\alpha x}\sin(\beta x+\gamma)\,dx = \left[e^{\alpha x}/(\alpha^2+\beta^2)\right] \times \left[\alpha\sin(\beta x+\gamma)-\beta\cos(\beta x+\gamma)\right] \qquad (A.3)$$

where for our problem; $\alpha = jk\cos\vartheta$ $\beta = \pm k$, and $\gamma = kL/2$. After some mathematical manipulations we find:

$$U_\theta(\theta,\phi) = (2I_m/k) \times \left[\left[\cos\left[(kL/2)\cos\theta\right]-\cos(kL/2)\right]/\sin\theta\right] \qquad (A.4)$$

and from equation (2.26) we find:

$$P_{r,\theta}(\theta,\phi) = \tfrac{1}{2}\left[\eta I_m^2/(2\pi r)^2\right] \times \left[\left[\cos\left[(kL/2)\cos\theta\right] - \cos(kL/2)\right]/\sin\theta\right]^2 \qquad (A.5)$$

The θ-variation of this function determines the far field pattern. Thus, from equation (A.5), we will use:

$$U_{\theta,e}(\theta,\phi) = \left[\cos\left[(kL/2)\cos\theta\right]-\cos(kL/2)\right]/\sin\theta \qquad (A.6)$$

as the element factor for a z-aligned dipole of length L.

Now let us suppose we have several dipoles positioned parallel to each other along the z-axis, but, with currents that are x-directed as shown in Figure A.2. We will let γ be the spherical polar angle from the x-axis, such that, $0°\le\gamma\le180°$. We can find the element factor from the expression:

$$U_\gamma(\gamma) = \sin\gamma \int_{-L/2}^{L/2} J(x')\exp(jkx'\cos\gamma)\,dx' \qquad (A.7)$$

which is analogous to equation (A.2). We note that:

$$\cos\gamma = \hat{\mathbf{x}} \cdot \hat{\mathbf{r}} \qquad (A.8)$$

so:

$$\cos\gamma = \sin\theta\cos\phi \qquad (A.9)$$

and:

$$\sin\gamma = (1-\sin^2\theta\cos^2\phi)^{1/2} \qquad (A.10)$$

Solving the integral in equation (A.7), we find the element pattern for the dipole of length L to be:

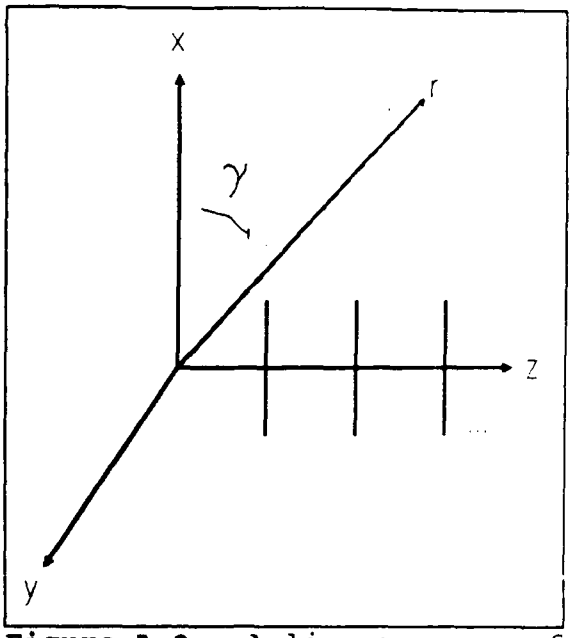

Figure A.2. A linear array of x-directed dipoles

$$U_{\gamma,e}(\gamma) = \left[\cos\left[(kL/2)\cos\gamma\right] - \cos(kL/2)\right]/\sin\gamma \qquad (A.11)$$

In order to find the element factor in terms of θ and ϕ, we substitute in equations (A.9) and (A.10) for $\cos\gamma$ and $\sin\gamma$ and equation (A.11), for an x-directed dipole, becomes:

$$U_{\theta,e}(\theta,\phi) = \left[\cos\left[(kL/2)\sin\theta\cos\phi\right] - \cos(kL/2)\right] \times (1 - \sin^2\theta\cos^2\phi)^{-1/2} \qquad (A.12)$$

Now let us assume we have several dipoles lying along the z-axis, but, with y-directed currents. Following a similar procedure to that of the x-directed dipoles with:

$$\cos\gamma = \hat{\mathbf{y}} \cdot \hat{\mathbf{r}} = \sin\theta\cos\phi \qquad (A.13)$$

and

$$\sin\gamma = (1 - \sin^2\theta\cos^2\phi)^{1/2} \qquad (A.14)$$

we find:

$$U_{\theta,e} = \left[\cos\left[(kL/2)\sin\theta\sin\phi\right] - \cos(kL/2)\right]$$

$$X\ (1 - \sin^2\theta\sin^2\phi)^{-1/2} \qquad \text{(A.15)}$$

Equation (A.15) is the element factor for a y-directed dipole of length L.

Appendix B: Program Listings

This appendix lists the names of the main program and subprograms comprising the program PARRAY.EXE. The actual code is contained in Volume II and may be requested by writing:

AFIT/ENG
Wright Patterson Air Force Base, OH 45433
Attn: Major H. H. Barksdale

or:

ASD/RWZI
Wright Patterson Air Force Base, OH 45433
Attn: Major D. J. Haskell

and specifying the "Planar Array Antenna Design Analysis Code."

Program Name	Program Name
PARRAY.FOR	AVERP.FOR
BINOML.FOR	CHEBY.FOR
CI.FOR	DBWDTH.FOR
DESDIR.FOR	DESRP.FOR
DIPDIR.FOR	EBWDTH.FOR
ELDATA.FOR	ELEFEA.FOR
ELFAC.FOR	ERDATA.FOR
ERGFAL.FOR	ERPFEA.FOR
EXPDIR.FOR	EXPRPF.FOR
FACTRL.FOR	OUTPUT.FOR
PARFAC.FOR	PARFEA.FOR
REGFAL.FOR	ROMBER.FOR
SI.FOR	TAYLOR.FOR
UNIFRM.FOR	USRDEF.FOR

Appendix C: Planar Array Design Analysis Program User's Guide

This appendix contains instructions on how to use the Planar Array Design Analysis Program. Specific design parameters required by the program are listed in preparation for running the program. Then, step-by-step instructions are provided to guide you through the program. It is assumed that you have read Chapter 4, so that you have a basic understanding of how the program operates.

Before running the program you will need to know the following data:

(1) The center operating frequency or wavelength.

(2) The operating bandwidth as a percentage of the frequency (upper minus lower) divided by the center frequency of the bandwidth multiplied by 100. The program will also let you enter a bandwidth in terms of wavelengths. You must realize that a wavelength specified bandwidth is not the same as a frequency bandwidth. Also, the upper wavelength gives the lower frequency and the lower wavelength gives the upper frequency because of the inverse relationship between frequency and wavelength.

(3) Number of elements in the x-direction and their spacing in centimeters.

(4) The type of current distribution or synthesis in the x-direction. If you are using a Dolph-Chebyshev synthesis and you want the program to calculate the weights,

you'll need to know the design side lobe level. If you are using a discretized Taylor distribution and you want the program to calculate the weights, you will need to know the parameter $\bar{n}$ and the side lobe level.

(5) Number of elements in the y-direction and their spacing in centimeters.

(6) The type of current distribution or synthesis in the y-direction. The same comments apply here as they did for the x-direction.

(7) The type of element you want to use in the array. In the program, you may choose between a dipole oriented in the x-, y-, or z-direction or an isotropic element. If you choose a dipole, you'll need to know its length in centimeters.

(8) The tolerances for your expected array. This information can probably be found in a design specification or obtained directly from the design authority. You will need to know the Root Mean Square (RMS) errors in the amplitude and phase drive current at the elements, the RMS translational errors in the x, y, and z placement of the elements, the RMS error between the average element pattern and the actual element pattern in the array, and the fraction of elements expected to be operating during a given mission. If you don't have every tolerance item readily available, you can simply set that tolerance to zero in the program, except the RMS element pattern error which should be set to

a value of -100 dB. The program is looking for the element pattern error in decibels.

(9) Pointing angles where you want to calculate the beamwidths and directivities.

A Word of Caution: All data entered to the program, is entered as either an "integer" or a "real" number. For the purpose of this program, an integer is defined as a number that does not have a decimal point. Conversely, a real number is defined as a number that does have a decimal point. If you enter a real number where an integer is asked for, a DOS run error will occur and the program terminates. If you enter an integer for a real number, then you will not end up with the number you entered. For example, if you enter a "1" for a real number response, you will end up with a value like 0.000001. In the program, this situation is correctable since you will be able to verify the data you just entered. One last item, when you verify a response, the program will ask you;

"Is this correct? [1]Yes [2]No"

Respond with the integer "1" or "2". All other questions asked by the program will specify whether an integer or a real number is wanted.

Now that you have all the information you need to run the program you may begin by typing "PARRAY" followed by a [RETURN]. You should get a brief introduction statement. Now follow these steps to proceed through the program.

STEP	ACTION REQUESTED
1	The program is asking you if you want to enter the center operating frequency or wavelength. Enter a "1" for frequency or a "2" for wavelength. Notice the numbers for each are integers. If you choose frequency the bandwidth will be in frequency. If you choose wavelength the bandwidth will be in wavelengths.
2	No matter if you choose frequency of wavelength, you will now enter the center operating frequency in hertz or the wavelength in centimeters. Type your value followed by a [RETURN].
3	Now the program is asking you to verify your input. Respond appropriately. If you respond with a "2" for "No" the program backs up to the last step to get your new value. Otherwise the program continues.
4	The program wants to know the bandwidth. If you are working in wavelengths simply use: $\frac{\text{(upper wavelength- lower wavelength) X 100}}{\text{center wavelength}}$ to calculate the bandwidth as a percentage. Enter the bandwidth as a percentage.
5	Now the program asks you to verify the upper and lower frequencies or wavelengths it has calculated based on your bandwidth specification. Enter the appropriate response. If you enter a "1" the program continues. If you enter a "2" the program will ask you for a new bandwidth.
6	The program asks for the number of elements in the x-direction. You may enter any value from 1 to 500. If you enter a large number, be prepared to spend some time waiting for the program to calculate patterns, beamwidths, and directivities. The program was written to be efficient, however, there are some things in array theory that take time to calculate especially for large arrays. If you enter a "1" at this point, the program automatically skips to the uniform current distribution routine. Enter the number of elements in the x-direction. Note, the program is asking for an integer.

Step	Action Requested
7	Verify the number of elements in the x-direction. If you have only one element in the x-direction, go to step 22.
8	Enter the distance between elements in the x-direction in centimeters.
9	Verify the spacing. If you have two elements in the x-direction go to step 22 as all element weights are set to unity by the uniform current distribution routine.
10	Now you need to decide what type of current distribution or synthesis procedure you want to use in the x-direction. The binomial and uniform current distributions are automatically calculated. If you choose Dolph-Chebyshev synthesis then you will need to know the design side lobe level. If you choose the Taylor $\bar{n}$-parameter synthesis you'll need to know the $\bar{n}$ parameter and the design side lobe level. If you choose the user defined current distribution you'll need to know the currents for each element in the x-direction. Make your selection.
11	Verify your selection. If you chose Dolph-Chebyshev synthesis go to step 12. If you chose Taylor $\bar{n}$-parameter synthesis go to step 14. If you chose user defined current distribution go to step 20. If you chose uniform or binomial current distributions go to step 22.
12	Enter the desired side lobe level in decibels. Note that the program is asking for a positive value and it will not let you proceed until it gets a positive quantity. For example, if you know that the design side lobe level is -25 dB then enter 25.
13	Verify your side lobe level. After you verify your response, you will see the element weights scroll across your screen. Go to step 22.
14	Now you see the guidelines for selecting the $\bar{n}$-parameter. You also see the range of the $\bar{n}$-parameter the program has calculated based on the array specifications and the center operating frequency or wavelength. Choose the appropriate value of $\bar{n}$ for the design side lobe level. There may be a conflict arise at this point. The array may not

Step	Action Requested
	be able to support the specific side lobe level you want based on the specifications you entered. For example, if you want a -40 dB side lobe level, but, the largest value of $\bar{n}$ you're able to enter is 5, you have a problem. $\bar{n}$ must be at least 6 for a -40 dB side lobe level. If this conflict does arise, you may need to investigate the details of the design with the design authority. Enter the value of $\bar{n}$ you need.
15	Verify your value of $\bar{n}$.
16	Enter the desired side lobe level in decibels. Note that the program is asking for a positive value and it will not proceed until it gets a positive value. For example, if you know that the design side lobe level is -25 dB, then enter 25.
17	Verify your side lobe level.
18	Now you must decide on whether to use the aperture sampling or null matching weights. Some guidelines are given for selecting the appropriate weights for your application. Make your choice.
19	Verify your choice. These are the element weights the program will use for the x-direction. Go to step 22.
20	Enter the weight of the first element in the x-direction. The first element is the one at the origin in Figure 13, Chapter 3. The second element is the next element in the positive x-direction, and so on.
21	Verify your element weight. Steps 20 and 21 are repeated as many times as the number of elements in the x-direction. As soon as you enter the weight for the last element go to step 22.
22	Repeat steps 6 through 21, as required, for the y-direction. The procedure is exactly the same. When you are finished with the y-direction continue with step 23.
23	Now you need to decide what type of element you want to use in your array. If you choose a dipole you will need to know its length.

Step	Action Requested
24	Verify your element selection. If you choose an isotropic element go to step 27.
25	Enter the length of your dipole in centimeters.
26	Verify's your dipole's length.
27	Now the program wants to know the errors in the expected array. The first error it wants is the RMS amplitude error. Enter this error as a fraction of the total amplitude. Enter the RMS amplitude term.
28	Verify your response.
29	Enter the RMS phase error in degrees.
30	Verify your response.
31	Enter the standard deviation (RMS error) in centimeters in the x-translational error of a typical element in the array.
32	Verify your response.
33	Enter the standard deviation (RMS error) in centimeters of the y-translational error of a typical element in the array.
34	Verify your response.
35	Enter the standard deviation (RMS error) in centimeters of the z-translational error of a typical element in the array.
36	Verify your response.
37	Enter the RMS error between the average element pattern and the actual element pattern in the array environment in decibels. If data is not available for this error then enter -100 (dB) since this will essentially set this term to zero in the program.
38	Verify your response.
39	Enter the fraction of elements operating. The program wants a number between zero and one. Also, be reasonable with your response. If you have, for example, a 25 element array, it doesn't

Step	Action Requested
	make sense to specify 0.98 as the fraction of elements operating since this would mean that 24½ elements are operating.
40	Verify your response.
41	Decide now if you want the program to calculate the data points for the design and expected radiation patterns in the xz- and yz-planes at the center wavelength or frequency. Four sets of data are generated in this run.
42	Verify your response. If the data points for these pattern plots are not wanted, then proceed to step 49.
43	The program lets you specify a scan angle in the θ direction (as defined in Figure 13, Chapter 3) along the positive x-axis (ϕ=0°). If you want a broadside pattern, simple enter 0.0(°). The scan angle you enter will be for the design array in the xz-plane. Enter your scan angle.
44	Verify your response. The program begins calculating the data points.
45	Now enter the scan angle in the θ direction for the design array in the yz-plane. This time the θ direction will be along the positive y-axis (ϕ=90°). Enter your scan angle.
46	Verify your response. The program begins calculating the data points.
47	This time, enter the scan angle in the θ direction for the expected array in the xz-plane. Again the θ direction will be along the positive x-axis (ϕ=0°). Enter your scan angle.
48	Verify your response. The program begins calculating the data points.
49	Decide now if you want the program to calculate the data points for the design and expected radiation patterns in the xz-and yz-planes at the lower wavelength or upper frequency. Four sets of data are generated in this run.

Step	Action Requested
50	Verify your response. If the data points for this pattern plot are not wanted, then proceed to step 57.
51	The program lets you specify a scan angle in the θ direction (as defined in Figure 13, Chapter 3) along the positive x-axis (ϕ=0°). If you want a broadside pattern, simple enter 0.0(°). The scan angle you enter will be for the design array in the xz-plane. Enter your scan angle.
52	Verify your response. The program begins calculating the data points.
53	Now enter the scan angle in the θ direction for the design array in the yz-plane. This time the θ direction will be along the positive y-axis (ϕ=90°). Enter your scan angle.
54	Verify your response. The program begins calculating the data points.
55	This time, enter the scan angle in the θ direction for the expected array in the xz-plane. Again the θ direction will be along the positive x-axis (ϕ=0°). Enter your scan angle.
56	Verify your response. The program begins calculating the data points.
57	Decide now if you want the program to calculate the data points for the design and expected radiation patterns in the xz-and yz-planes at the upper wavelength or lower frequency.
58	Verify your response. If the data points for this pattern plot are not wanted, then proceed to step 65.
59	The program lets you specify a scan angle in the θ direction (as defined in Figure 13, Chapter 3) along the positive x-axis (ϕ=0°). If you want a broadside pattern, simple enter 0.0(°). The scan angle you enter will be for the design array in the xz-plane. Enter your scan angle.
60	Verify your response. The program begins calculating the data points.

Step	Action Requested
61	Now enter the scan angle in the θ direction for the design array in the yz-plane. This time the θ direction will be along the positive y-axis (ϕ=90°). Enter your scan angle.
62	Verify your response. The program begins calculating the data points.
63	This time, enter the scan angle in the θ direction for the expected array in the xz-plane. Again the θ direction will be along the positive x-axis (ϕ=0°). Enter your scan angle.
64	Verify your response. The program begins calculating the data points.
[NOTE:	If you had data points calculated for pattern plots refer to pages 68-69, Chapter 4, for the names of the files generated by the program for a particular pattern.]
65	For the calculations that follow from this point on, the program needs to know the scan angles in the θ and ϕ directions as defined in Figure 13. You will be able to vary these angle later in the program. Enter the scan angle in the θ direction.
66	Verify your response.
67	Enter the scan angle in the phi direction.
68	Verify your response. Now sit back for a few minutes and watch the program calculate the beamwidths and directivities at the center and both extremes of your specified bandwidth for the design and expected arrays.
69	Your data was just sent to an output file. Now you have the option of varying the scan angles, in which case the program returns to step 65, or terminating your run. All the data compiled up to this point was sent to the file "OUTPUT.DAT". If you select new scan angles, the program will not over-write your earlier data with the new data. It simply extends the length of the output file with the new scan angles and data. Make your selection.
70	Verify your response. If you chose to recalculate for new scan angles go to step 65. Otherwise you are finished. [Please read next page.]

[NOTE: Your data is contained in a file called "OUTPUT.DAT". This is an ASCII text file and you should be able to read this file in to any word processor for viewing. You will notice a numerical error data for the beamwidth calculations section at the end of each run for a given scan angle. Each item listed in this section is defined on pages 81 through 83, Chapter 4.]

Bibliography

1. Allen, J.L. et al. Phased Array Radar Studies: Technical Report No. 236, 1 July 1960 - 1 July 1961. Lexington MA: Massachusetts Institute of Technology, Lincoln Laboratory, 13 November 1961 (AD-271724).

2. Ashmead, D. "Optimum Design of Linear Arrays in the Presence of Random Errors," I.R.E. Transactions on Antennas and Propagation, AP-4: 81-92 (December 1952).

3. Bailin, L.L. and M.J. Ehrlich. "Factors Affecting the Performance of Linear Arrays," Proceeding of the I.R.E., 41: 235-241 (February 1953).

4. Balanis, Constatine A. Antenna Theory Analysis and Design. New York: Harper & Row, Publishers, 1982.

5. Bresler, A.D. "A New Algorithm for Calculating the Current Distributions of Dolph-Chebyshev Arrays," I.E.E.E. Transactions on Antennas and Propagation, AP-28: 951-952 (November 1980).

6. Burns, M.A., S.R. Laxpati, and J.P. Shelton, Jr. "A Comparitive Study of Linear Array Synthesis Technique Using a Personal Computer," I.E.E.E. Transactions on Antennas and Propagation, AP-32: 884-887 (August 1987).

7. Cheng, D.K. "Effect of Arbitrary Phase Errors on the Gain and Beamwidth Characteristics of Radiation Pattern," I.R.E. Transactions on Antennas and Propagation, AP-3: 145-147 (July 1955).

8. Dwight, H.B. Tables of Integrals and Other Mathematical Data. New York: The Macmillan Company, 1947.

9. Dolph, C.L. "A Current Distribution for Broadside Arrays which Optimizes the Relationships Between Beamwidth and Side-Lobe Level," Proceedings of the I.R.E., 34: 335-348 (June 1946).

10. Elliott, Robert S. Antenna Theory and Design. Englewood Cliffs NJ: Prentice-Hall, Inc., 1981.

11. Elliott, Robert S. "Mechanical and Electrical Tolerances for Two Dimensional Scanning Antenna Arrays," I.R.E. Transactions on Antennas and Propagation, AP-6: 114-120 (January 1958).

12. Elliott, Robert S. "On Discretizing Continuous Aperture Distributions," I.E.E.E. Transactions on Antennas and Propagation, AP-25: 617-621 (September 1977).

13. Elliott, Robert S. "The Theory of Antenna Arrays," Microwave Scanning Antennas, Volume 2, edited by R.C. Hansen. New York: Academic Press, 1966.

14. Gilbert, E.N. and S.P. Morgan. "Optimum Design of Directive Antenna Arrays Subject to Random Variations," Bell Systems Technical Journal, 34: 637-663 (May 1955).

15. Goldstein, H. Classical Mechanics. Reading, MA: Addison-Wesly, 1950.

16. Leichter, M. "Beam Pointing Errors of Long Line Sources," I.R.E. Transactions on Antennas and Propagation, AP-8: 268-275 (May 1960).

17. Parsons, Robert. Statistical Analysis: A Decision-Making Approach (Second Edition). New York: Harper and Row, Publishers, 1978.

18. O'Neill, H.F. and Bailin, L.L. "Further Effects of Manufacturing Tolerances on the Performance of Linear Shunt Arrays," I.R.E. Transactions on Antennas and Propagation, AP-4: 93-102 (December 1952).

19. Pozar, David M. Antenna Design Using Personal Computers. Dedham MA: Artech House, Inc., 1985.

20. Rondinelli, L.A. "Effects of Random Errors on the Performance of Antenna Arrays of Many Elements," I.R.E. National Convention Record, Part 1: 174-189 (1959).

21. Ruze, J. "The Effect of Aperture Errors on the Antenna Radiation Pattern ," Nuovo Cimento, 9, Supplement 3: 364-380 (1952).

22. Skolnik, Merrill I. "Nonuniform Arrays," Antenna Theory, Part 1, edited by R.E. Collin and F.J. Zucker. New York: McGraw Hill Book Company, 1969.

23. Stutzman, Warren L. and Gary A. Thiele. Antenna Theory and Design. New York: John Wiley & Sons, 1981.

24. Taylor, T.T. "Design of Line-Source Antennas for Narrow Beamwidth and Low Sidelobes," I.R.E. Transactions on Antennas and Propagation, AP-3, No. 1: 16-28 (January 1955).

25. The Ballistic Missile Defense Advanced Technology Center, U.S. Army. Contract DASG60-77-C-0078 with Department of Industrial and Management Systems Engineering, Pennsylvania State University. Huntsville AL, 11 June 1979.

26. Villaneuve, A.T. "Taylor Patterns for Discrete Arrays," I.E.E.E. Transactions on Antennas and Propagation, AP-32: 1089-1093 (October 1984).

Vita

Captain Bradley P. Chrisman [redacted] He graduated from high school in Tahlequah, Oklahoma, in 1974 and attended Northeastern Oklahoma State University, from which he received the degree of Bachelor of Science in Engineering Physics in July 1979. He received a commission in the USAF through OTS in December 1979. His first assignment was as a Systems Safety Manager in the Aeronautical Systems Division, Deputy for Tactical Systems, Fighter/Attack Systems Program Office until August 1982 when he was accepted into the Electrical Engineering conversion program at the School of Engineering, Air Force Institute of Technology. He graduated from AFIT with a Bachelors of Science degree in Electrical Engineering in March 1984. Captain Chrisman served four years on the Stragic Air Command Headquarters staff as a Defensive Avionics Engineer until entering the School of Engineering, AFIT, in May 1988.

[redacted]

REPORT DOCUMENTATION PAGE

Form Approved
OMB No. 0704-0188

1a. REPORT SECURITY CLASSIFICATION UNCLASSIFIED	1b. RESTRICTIVE MARKINGS
2a. SECURITY CLASSIFICATION AUTHORITY	3. DISTRIBUTION/AVAILABILITY OF REPORT
2b. DECLASSIFICATION/DOWNGRADING SCHEDULE	
4. PERFORMING ORGANIZATION REPORT NUMBER(S) AFIT GE ENG 89D-4	5. MONITORING ORGANIZATION REPORT NUMBER(S)
6a. NAME OF PERFORMING ORGANIZATION School of Engineering 6b. OFFICE SYMBOL (If applicable) AFIT ENG	7a. NAME OF MONITORING ORGANIZATION
6c. ADDRESS (City, State, and ZIP Code) Air Force Institute of Technology Wright Patterson AFB OH 45433-6583	7b. ADDRESS (City, State, and ZIP Code)
8a. NAME OF FUNDING/SPONSORING ORGANIZATION ASD 8b. OFFICE SYMBOL (If applicable) RWZI	9. PROCUREMENT INSTRUMENT IDENTIFICATION NUMBER
8c. ADDRESS (City, State, and ZIP Code) Wright-Patterson AFB OH 45433	10. SOURCE OF FUNDING NUMBERS PROGRAM ELEMENT NO. / PROJECT NO. / TASK NO / WORK UNIT ACCESSION NO.

11. TITLE (Include Security Classification)

Planar Array Antenna Design Analysis

12. PERSONAL AUTHOR(S)
Bradley P. Chrisman, M.S., Captain, USAF

13a. TYPE OF REPORT	13b. TIME COVERED	14. DATE OF REPORT (Year, Month, Day)	15. PAGE COUNT
MS Thesis	FROM _____ TO _____	1989 December	175

16. SUPPLEMENTARY NOTATION

17. COSATI CODES			18. SUBJECT TERMS (Continue on reverse if necessary and identify by block number)
FIELD	GROUP	SUB-GROUP	Antennas, Phased Arrays, Arrays, Linear Arrays, Planar Array, Directional Antennas
09	01		

19. ABSTRACT (Continue on reverse if necessary and identify by block number)

Thesis Advisor: Major Harry H. Barksdale, Jr.
Associate Professor
Department of Electrical Engineering

20. DISTRIBUTION/AVAILABILITY OF ABSTRACT ☒ UNCLASSIFIED/UNLIMITED ☐ SAME AS RPT. ☐ DTIC USERS	21. ABSTRACT SECURITY CLASSIFICATION UNCLASSIFIED
22a. NAME OF RESPONSIBLE INDIVIDUAL Maj. Harry H. Barksdale, Assoc. Prof.	22b. TELEPHONE (Include Area Code) 255-6027 22c. OFFICE SYMBOL AFIT ENG

DD Form 1473, JUN 86 *Previous editions are obsolete.*

UNCLASSIFIED

The purpose of this study wac to develop a computer program that can assess the impact of small design perturbations on the performance of a planar array antenna of dipoles. The antenna designer can compare an array's theoretical performance standards with those of the pertrubed array.

In the course of this study, an expression for the expected, or average, radiation pattern for the perturbed planar array was developed and used in the program. Translational errors in the positions of the elements, errors in the element's drive amplitude and phase, non-identical element patterns, and missing elements were accounted for in the expected radiation pattern.

The designer specifies the array design parameters and the tolerance data, then the program calculates the radiation pattern data, half-power beamwidths, and directivities for specified scan angles and frequency bandwidth for the design and perturbed arrays. The radiation pattern data can be plotted allowing side lobe comparison between the expected and design arrays.

This study confirmed five trends noted in earlier studies: (1) The rise in side lobe level due to random errors, for a given set of tolerances and number of elements, increased as the side lobe level was further suppressed. (2) For a given set of tolerances, pattern deterioration was found to decrease as the array was enlarged. (3) For a given set of tolerances, pattern deterioration was less for a planar array of size L-squared than it was for a linear array of length L. (4) The side lobe level increase due to random errors did not depend on the scan angle. (5) Although not shown conclusively, but, qualitatively, translational errors were found to cause the dominant effect provided element reliability was high.

The antenna designer can use the program to assess the effects of certain tolerances in designing the array. The program can be used as a tool for establishing a bound on the tolerances to achieve a certain side lobe level. Or, given the tolerances, the designer can adjust the size of the array until the desired side lobe level is achieved.